



Saeed Mashdour

**Resource allocation techniques for cell-free
massive MIMO networks**

Tese de Doutorado

Thesis presented to the Programa de Pós-graduação em Engenharia Elétrica of PUC-Rio in partial fulfillment of the requirements for the degree of Doutor em Engenharia Elétrica.

Advisor: Prof. Rodrigo Caiado de Lamare

Rio de Janeiro
November 2024



Saeed Mashdour

**Resource allocation techniques for cell-free
massive MIMO networks**

Thesis presented to the Programa de Pós-graduação em Engenharia Elétrica of PUC-Rio in partial fulfillment of the requirements for the degree of Doutor em Engenharia Elétrica. Approved by the Examination Committee.

Prof. Rodrigo Caiado de Lamare

Advisor

Departamento de Engenharia Elétrica – PUC-Rio

Prof. Lukas Tobias Nepomuk Landau

Departamento de Engenharia Elétrica – PUC-Rio

Prof. Marco Antonio Grivet Mattoso Maia

Departamento de Engenharia Elétrica – PUC-Rio

Prof. Anke Schmeink

– RWTH Aachen University

Prof. Kanapathippillai Cumanan

– University of York

Prof. Elena Veronica Belmega

– Université Gustave Eiffel

Prof. Paulo Ricardo Branco da Silva

Centro de Pesquisa e Desenvolvimento em Telecomunicações –
CPqD

Rio de Janeiro, November the 29th, 2024

All rights reserved. Reproduction in whole or in part of the work without authorization from the university, the author and the supervisor is prohibited.

Saeed Mashdour

The author received the B.Sc. and M.Sc. degrees in Telecommunications Engineering both from Shiraz University, Shiraz, Iran in 2007 and 2011, respectively.

Bibliographic data

Mashdour, Saeed

Resource allocation techniques for cell-free massive MIMO networks / Saeed Mashdour; advisor: Rodrigo Caiado de Lamare. – Rio de Janeiro: PUC-Rio, Departamento de Engenharia Elétrica, 2024.

116 f: il. color. ; 30 cm

Tese (doutorado) - Pontifícia Universidade Católica do Rio de Janeiro, Departamento de Engenharia Elétrica.

Inclui bibliografia

1. Engenharia Elétrica – Teses. 2. Processamento de Sinais, Automação e Robótica – Teses. 3. MIMO massivo sem células. 4. Agrupamento. 5. Programação de usuários. 6. Alocação de potência. 7. Informação do estado do canal. I. de Lamare, Rodrigo Caiado. II. Pontifícia Universidade Católica do Rio de Janeiro. Departamento de Engenharia Elétrica. III. Título.

CDD: 621.3

This thesis is dedicated to my parents
for their endless love, support and encouragement.

Acknowledgments

I wish to acknowledge the support accorded to me by my parents, Mr. Ghader Pourhashemi and Mrs. Shahrbanoo Panahandeh ever since they brought me upon earth. May God bless you for all you have done. Special consideration to my brothers and sisters.

I would like to thank the administration of CETUC and PUC-Rio for their efforts to provide a distinctive model research university.

Special thanks go to my advisor Prof. Rodrigo Caiado. de Lamare, for his continuous encouragement, support, patience, discussions, valuable comments, and excellent suggestions to improve the quality of my research work.

Last but not least, I would like to show my sincere appreciation and gratitude to my colleagues and friends who have provided me with guidance and critical help.

This study was financed in part by the Coordenação de Aperfeiçoamento de Pessoal de Nível Superior - Brasil (CAPES) - Finance Code 001.

Finally, the author is supported by a scholarship from the Conselho Nacional de Desenvolvimento Científico e Tecnológico (CNPq). I would like to thank CAPES and CNPq for funding my research and PhD Education.

Abstract

Mashdour, Saeed; de Lamare, Rodrigo Caiado (Advisor). **Resource allocation techniques for cell-free massive MIMO networks**. Rio de Janeiro, 2024. 116p. Tese de Doutorado – Departamento de Engenharia Elétrica, Pontifícia Universidade Católica do Rio de Janeiro.

Cell-Free Massive Multiple-Input Multiple-Output (CF-mMIMO) networks are a promising evolution in wireless communications, offering notable improvements in user experience and network performance by eliminating traditional cell boundaries. These networks employ a large number of distributed access points (APs) to serve a smaller number of user equipments (UEs), forming a unique wireless network architecture that ensures solid coverage and service delivery. A primary concern in the context of CF-mMIMO networks is the efficient allocation of resources, particularly user scheduling and power allocation. The aim of this thesis is to investigate these tasks in the downlink of a CF-mMIMO network, considering both perfect and imperfect channel state information (CSI).

In user scheduling, the objective is to select a subset of UEs to be served at any given time. This process is inherently complex as it must cater for numerous factors such as the priority of UEs, varying channel conditions, and physical UE locations. Effective user scheduling is instrumental in optimizing the utilization of network resources, enhancing UE satisfaction, and managing network traffic efficiently. Power allocation also plays a key role in the distribution of transmission power among APs and the selected UEs. In CF-mMIMO systems, an effective power allocation strategy can help mitigate inter-user interference and optimize energy efficiency, while enforcing the total available power and hardware constraints.

This thesis further considers the context of clustered cell-free (CLCF) networks, as non-overlapping network clustering and also user-centric cell-free (UCCF). These networks present their own unique challenges and opportunities in terms of user scheduling and power allocation. An in-depth exploration and comparison of different techniques within this settings could offer valuable insights into the development of more efficient resource allocation strategies. The thesis aims to provide a comprehensive study of resource allocation, focusing on user scheduling and power allocation in the downlink of CF-mMIMO networks, taking into account both perfect and imperfect CSI and exploring the implications of these techniques in CLCF and UCCF network contexts, and indicate some topics for further investigation in the future works.

Keywords

Cell-Free Massive MIMO; Clustering; User scheduling; Power allocation; Channel state information;

Resumo

Mashdour, Saeed; de Lamare, Rodrigo Caiado. **Técnicas de alocação de recursos em redes de múltiplas antenas massivas livres de células**. Rio de Janeiro, 2024. 116p. Tese de Doutorado – Departamento de Engenharia Elétrica, Pontifícia Universidade Católica do Rio de Janeiro.

As redes multi-input multi-output massivas livres de células (CF-mMIMO) são uma evolução promissora nas comunicações sem fio, oferecendo melhorias notáveis na experiência do usuário e no desempenho da rede ao eliminar as fronteiras tradicionais das células. Essas redes empregam um grande número de pontos de acesso (APs) distribuídos para servir um número menor de equipamentos de usuário (UEs), formando uma arquitetura de rede sem fio única que garante uma cobertura sólida e entrega de serviço. Uma preocupação primária no contexto das redes CF-mMIMO é a alocação eficiente de recursos, particularmente o agendamento de usuários e a alocação de potência. O objetivo desta dissertação é investigar essas tarefas na transmissão downlink de uma rede CF-mMIMO, considerando tanto a informação perfeita quanto a imperfeita do estado do canal (CSI).

No agendamento de usuários, o objetivo é selecionar um subconjunto de UEs para serem atendidos em um determinado momento. Esse processo é inerentemente complexo, pois deve levar em consideração diversos fatores, como a prioridade dos UEs, as condições variáveis do canal e as localizações físicas dos UEs. O agendamento eficaz de usuários é fundamental para otimizar a utilização dos recursos da rede, melhorar a satisfação dos UEs e gerenciar o tráfego da rede de forma eficiente. A alocação de potência também desempenha um papel crucial na distribuição da potência de transmissão entre os APs e os UEs selecionados. Nos sistemas CF-mMIMO, uma estratégia eficaz de alocação de potência pode ajudar a mitigar a interferência entre usuários e otimizar a eficiência energética, enquanto impõe as restrições de potência total disponível e de hardware.

Esta dissertação também considera o contexto das redes livres de células agrupadas (CLCF), como o agrupamento de rede não sobreposto e também o livres de células centrado no usuário (UCCF). Essas redes apresentam seus próprios desafios e oportunidades únicos em termos de agendamento de usuários e alocação de potência. Uma exploração e comparação aprofundada de diferentes técnicas dentro desses contextos poderia oferecer insights valiosos para o desenvolvimento de estratégias de alocação de recursos mais eficientes. A dissertação visa fornecer um estudo abrangente da alocação de recursos, focando no agendamento de usuários e na alocação de potência na transmissão

downlink de redes CF-mMIMO, levando em consideração tanto a CSI perfeita quanto a imperfeita e explorando as implicações dessas técnicas nos contextos das redes CLCF e UCCF, além de indicar alguns tópicos para investigação futura.

Palavras-chave

MIMO massivo sem células; Agrupamento; Programação de usuários; Alocação de potência; Informação do estado do canal;

Table of contents

1	Introduction	16
1.1	Motivation and Prior Works	16
1.2	Contributions	17
1.3	List of the Abbreviations and Variables	18
1.4	Notation and Outline	19
1.5	Publication List	21
2	Architectures and Models for Cellular and Cell-Free Networks	23
2.1	Cellular Networks	24
2.2	CF Networks	25
2.3	UCCF Networks	25
2.4	CLCF Networks	26
2.5	Multicell and CF-mMIMO System Models	26
2.5.1	Multicell Channel and Signal Model	26
2.5.2	Cell-Free Channel and Signal Model	28
2.5.3	Network-Centric Cell-Free	30
2.6	ZFS User Scheduling and the Proposed Enhanced Scheduling Algorithm	30
2.6.1	ZFS Algorithm	31
2.6.2	Enhanced Greedy Algorithm	32
2.7	Numerical Results	33
2.8	Summary	38
3	Sequential Multiuser Scheduling and Power Allocation in CF-mMIMO Networks	39
3.1	SMSPA Overview	40
3.2	Proposed Clustered Enhanced Subset Greedy Algorithm	40
3.3	Analysis of the Proposed C-ESG Algorithm	43
3.4	Impact of Clustering on Signaling Load and Scheduling Cost	45
3.5	C-ESG Assessment	46
3.6	GD Power Allocation in the SMSPA Scheme	48
3.6.1	GD Power Allocation Formulation	51
3.6.2	Simulation Results for SMSPA with GD	55
3.7	GA Power Allocation in the SMSPA Scheme	56
3.7.1	GA Power Allocation Formulation	56
3.7.2	Simulation Results for SMSPA with GA	59
3.8	Summary	61
4	Clustering Strategies based on Information Rates and Fair Resource Distribution in CF-mMIMO Networks	63
4.1	Network Model	64
4.1.1	Multi-Antenna CF-mMIMO Network Model	64
4.1.2	UCCF-mMIMO Network Model	65
4.2	AP Clustering Strategies	65
4.2.1	LSF-Based Clustering	66

4.2.2	Proposed Information Rate-Based Clustering	66
4.2.3	Analysis of the Proposed BSR Technique	68
4.3	Resource Allocation with Fairness	70
4.3.1	Proposed Resource Allocation Problem	70
4.3.2	Proposed F-Gr Algorithm	71
4.4	Simulation Results	72
4.5	Summary	78
5	Robust Resource Allocation in CF-mMIMO Networks	79
5.1	Network Model	81
5.1.1	Resource Allocation in UCCF Networks	81
5.2	Robust Resource Allocation	82
5.2.1	Robust multiuser scheduling	83
5.2.2	Robust Power Allocation	88
5.2.2.1	RGDPA approach	88
5.2.2.2	WRGDPA approach	91
5.3	Analysis	96
5.3.1	Analysis and Proposed Solutions to REOP Problems	97
5.3.1.1	Convexity analysis of the objective function J with respect to the channel estimation error	97
5.3.1.2	Convexity analysis of the objective function with respect to CSI imperfection parameter	99
5.3.1.3	Problem Solution	100
5.3.2	Convexity Analysis of the Conditioned Error Expectation	102
5.3.3	Analysis of the error with respect to $\tilde{\mathbf{G}}_a$	102
5.3.4	Computational complexity	103
5.4	Simulation Results	103
5.5	Summary	105
6	Conclusions and Future Works	108

List of figures

Figure 2.1	Presentation of different networks.	23
Figure 2.2	Network-centric CF Model.	31
Figure 2.3	Performance comparison of cell-free and multicell networks considering all UEs.	35
Figure 2.4	Performance of cell-free network with different scheduling methods	36
Figure 2.5	Performance of multicell network with different scheduling methods	36
Figure 2.6	Performance comparison using enhanced greedy algorithm, cell-free and multicell networks	37
Figure 2.7	Performance comparison using enhanced greedy algorithm, cell-free network using sum-rate and channel-correlation criteria	38
Figure 3.1	Block diagram of the proposed SMSPA resource allocation.	41
Figure 3.2	Performance of scheduling schemes for CLCF and CF, $M = 64$, $K = 256$ and $n = 64$	47
Figure 3.3	Performance of scheduling schemes for CLCF and CF, $M = 64$, $K = 16$ and $n = 8$ and exhaustive search scheduling included.	48
Figure 3.4	Computational complexity for the CF and the CLCF networks, (a): Number of required FLOPs for scheduling the UEs by C-ESG and WSR methods, (b): Signaling load.	49
Figure 3.5	Comparison of the proposed SMSPA technique in CF and CLCF networks with the system that uses the proposed C-ESG scheme and EPL for ZF and MMSE precoders, ($M = 64$, $K = 128$, $n = 24$)	57
Figure 3.6	Comparison of different resource allocation techniques considering a GD power allocation algorithm in CF and CLCF networks when an MMSE precoder is used, ($M = 64$, $K = 16$, $n = 8$)	57
Figure 3.7	Comparison of the proposed SMSPA resource allocation technique in CF networks for ZF and MMSE precoders with the system which has implemented the proposed C-ESG algorithm and EPL ($M = 64$, $K = 128$, $n = 24$)	60
Figure 3.8	Comparison of the different resource allocation techniques in CF and CLCF networks adapting GA power allocation when MMSE precoder is used ($M = 64$, $K = 16$, $n = 8$).	61
Figure 4.1	User-centric cell-free network.	65
Figure 4.2	Sum-rate for UCCF with different clustering criteria and CF network with no user scheduling, $L = 16$, $N = 4$, $K = 128$	73
Figure 4.3	BER of UCCF networks with different clustering criteria and the CF network with no user scheduling, $L = 16$, $N = 4$, $K = 128$.	74
Figure 4.4	Performance of F-Gr resource allocation sum-rate in CF and UCCF networks, $L = 16$, $N = 4$, $K = 128$ and $n = 20$.	74

Figure 4.5	Median Rate Distribution for CF network using Gr scheduling for $K = 32$, $n = 16$ and 100 channel realizations.	75
Figure 4.6	Median Rate Distribution for CF network using F-Gr scheduling for $K = 32$, $n = 16$ and 100 channel realizations.	76
Figure 4.7	Complexity of F-Gr resource allocation for CF and UCCF networks when $n = LN$ UEs are scheduled.	76
Figure 4.8	Scheduling times for each UE in CF network using Gr and F-Gr scheduling methods for $K = 128$, $n = 20$ and 100 channel realizations.	77
Figure 5.1	Block diagram of the proposed robust resource allocation.	83
Figure 5.2	Boundary extremum illustration, convex case	94
Figure 5.3	Boundary extremum illustration, concave case.	101
Figure 5.4	Comparison of the C-ESG multiuser scheduling in perfect CSI and imperfect CSI UCCF networks and the RC-ESG for MMSE precoder and EPL power loading, when $\alpha = 0.15$ for imperfect CSI case, $L = 16$, $N = 4$, $K = 32$ and $n = 16$.	104
Figure 5.5	Comparison of the RGDPA power allocation, GDPA with ICSI and GDPA with PSCI, when $\alpha = 0.15$ for imperfect CSI case, $L = 16$, $N = 4$, $K = 32$, $n = 16$ and MMSE precoder.	105
Figure 5.6	Comparison of WRGDPA and RGDPA power allocation, GDPA with ICSI and GDPA with PSCI, when $\alpha = 0.15$ for imperfect CSI case, $L = 16$, $N = 4$, $K = 32$, $n = 16$ and ZF precoder.	106
Figure 5.7	Performance of the proposed resource allocation technique, when $\alpha = 0.1$ for imperfect CSI case, $L = 16$, $N = 4$, $K = 32$, $n = 16$ and MMSE precoder.	106

List of tables

Table 1.1	List of Abbreviations	18
Table 1.2	List of Variables	19
Table 1.3	Notation	20
Table 2.1	Characteristics of the simulated systems	34
Table 2.2	Computational complexity in flops	38
Table 3.1	Computational complexity of different methods, $M = 64$, $K = 16$, and $n = 8$.	49
Table 3.2	Simulation parameters	56
Table 3.3	Computational complexity of the proposed resource al- location algorithm and the signaling load for CF and CLCF networks	58
Table 3.4	Computational complexity of the proposed SMSPA scheme in floating point operations and the signaling load in parameters for CF and CLCF networks when $M = 64$, $K = 128$ and $n = 64$.	61
Table 4.1	Computational complexity and signaling load of the pro- posed resource allocation algorithm	77

1 Introduction

Cell-free Massive multi-input multi-output (CF-mMIMO) is a novel network architecture initially suggested in [1], that utilizes a large number of access points (APs) dispersed across a geographic region. These APs serve all user equipment (UEs) using the same time-frequency resources. This represents a departure from conventional multicell multi-input multi-output (MIMO) systems, where UEs are served by a single base station per cell. This new structure offers consistent high-quality service for all UEs and leads to an improvement in network coverage [2]. Additionally, CF-mMIMO networks provide higher throughput than traditional small cell networks, representing a significant advancement in wireless communication systems.

1.1 Motivation and Prior Works

The introduction of CF-mMIMO networks has significantly reshaped the communication landscape [1]. However, these distributed networks, comprising several APs to serve UEs, present certain challenges, including an enormous computational load and heightened costs due to concurrent processing of all channels and signals [1, 2]. This has called for the adoption of clustering techniques, both user-centric and network-centric, to mitigate signaling and computational expenses [2]. Notably, resource allocation strategies like power allocation and multiuser scheduling are vital for enhancing system performance in these CF networks, attracting a great deal of interest in these topics [3–8].

Previous research has highlighted the importance of multiuser scheduling, which minimizes interference and optimizes system performance [5, 7]. Furthermore, power allocation is essential to support the large number of receivers, making the entire process more efficient [6, 9, 10]. Different techniques have been investigated, including maximization of a weighted sum-rate problem, joint optimization of UE scheduling, power allocation, pilot length, and the minimization of the total grid power consumption [9–11]. These studies have set the stage for further research to address various performance and efficiency concerns associated with CF networks.

Although various precoding techniques like linear minimum mean square

error (MMSE) and zero-forcing (ZF) have been discussed in several studies [4–6], there is a clear need for more research on resource allocation in Clustered Cell-Free (CLCF) networks, considered as non-overlapping networks, and user-centric cell-free (UCCF) massive MIMO networks, especially regarding multiuser scheduling and power allocation. The challenge here lies in creating a balance between high performance and manageable computational cost. In view of this, we aim to look into more efficient strategies. In our work, we propose using enhanced greedy and stochastic gradient techniques, in CLCF network and UCCF network incorporating different clustering criteria. Moreover, we introduce robust resource allocation techniques for UCCF networks. These approaches aim to address existing challenges and drive advancements in the field.

1.2 Contributions

The primary objective of this thesis is to improve understanding and application of resource allocation strategies in CF, CLCF and UCCF massive MIMO networks. To achieve this, our research first explores the use of linear precoding techniques, particularly ZF and MMSE, in the broader context of multicell, CF and CLCF networks. These techniques have been instrumental in addressing interference and enhancing overall network performance. We also derive and analyze sum-rate expressions for these diverse network models, providing an in-depth comparison that is anticipated to illuminate the performance characteristics of each network type and guide future strategies for their improvement.

In terms of resource allocation, our focus then turns to two critical components: user scheduling and power allocation. For user scheduling, we propose a novel approach based on the enhanced greedy technique, optimizing it for the CLCF context. This refined version of the greedy user scheduling technique is projected to significantly boost the performance of user scheduling. Power allocation is also thoroughly analyzed. We propose and examine two techniques, gradient ascent and gradient descent, in the context of the CLCF network. By implementing these approaches, we aim to augment the performance of power allocation in CF-mMIMO networks. Afterwards, we explore UCCF networks with multiple-antenna APs, evaluating network performance under different AP clustering criteria and propose an AP clustering technique for these networks. We also present a fair resource allocation strategy aimed at equitably distributing network resources among the UEs.

To develop more robust resource allocation techniques against CSI imper-

fections, we propose a robust user scheduling technique alongside two robust resource allocation methods. These methods are designed to significantly enhance network performance by addressing the challenges posed by imperfect CSI, ensuring more reliable and efficient resource management. Taken together, these efforts are expected to significantly contribute to the understanding and practical applications of resource allocation in CF, CLCF and UCCF massive MIMO networks.

1.3

List of the Abbreviations and Variables

In this thesis, the lists of abbreviations and variables used throughout the work are provided below, detailing their respective meanings and descriptions for clarity and consistency.

List of Abbreviations

Abbreviation	Description
CF-mMIMO	Cell-Free Massive Multiple-Input Multiple-Output
AP	Access Point
UE	User Equipment
CLCF	Clustered Cell-Free
UCCF	User-Centric Cell-Free
CSI	Channel State Information
MMSE	Minimum Mean Square Error
ZF	Zero-Forcing
ICI	Inter-Cell Interference
SNR	Signal-to-Noise Ratio
ZFS	Zero-Forcing with Selection
LSF	Large-Scale Fading
SR	Sum Rate
BER	Bit Error Rate
FLOPs	Floating-Point Operations
EPL	Equal Power Loading
GD	Gradient Descent
GA	Gradient Ascent
PCSI	Perfect Channel State Information
ICSI	Imperfect Channel State Information
REOP	Robust Extremum Optimization Problem
RGDPA	Robust Gradient Descent Power Allocation
WRGDPA	Worst-Case Robust Gradient Descent Power Allocation
6G	Sixth Generation Wireless Networks

Table 1.1: List of Abbreviations

List of Variables

Variable	Description
M	Total antenna number of APs
L	Number of APs in multiple antenna APs
L_t	Number of cells in cellular network
N	Number of antenna per AP
N_t	Number of Base Station antennas
K	Total number of UEs
n	Number of UEs scheduled in the network or timeslot
M_c	Number of APs in cluster c
K_c	Number of UEs in cluster or cell c
n_c	Number of UEs scheduled in the cluster c
n_s	Number of UEs scheduled in the cell s
C	Number of clusters
\mathbf{H}	Channel matrix in cellular network
\mathbf{G}	Cell-free channel matrix
$\hat{\mathbf{G}}$	Estimated channel matrix
$\tilde{\mathbf{G}}$	Channel estimation error matrix
\mathbf{P}	Precoding matrix
\mathbf{x}	Transmitted symbol vector
\mathbf{w}	Additive noise vector
R_{CF}	Sum-rate of the cell-free network
R_{UC}	Sum-rate of the user-centric cell-free network
R_c	Sum-rate of cluster c
β_{mk}	Large-scale fading coefficient between AP m and UE k
\mathcal{S}_n	Subset of n UEs scheduled in the timeslot
SR_{Av}	Average sum-rate across all timeslots
\mathbf{R}	Covariance matrix
g_{mk}	Channel coefficient between AP m and UE k
σ_w^2	Variance of the additive noise
PL_{mk}	Path loss between AP m and UE k
d_{mk}	Distance between AP m and UE k
R_t	Total sum-rate
ρ_f	Downlink power normalization factor
P	Total power constraint
\mathbf{D}	Power allocation matrix
\mathbf{d}	Power allocation vector

Table 1.2: List of Variables

1.4

Notation and Outline

Throughout this report, the notations in table 1.3 are adopted. The rest of this thesis is organized as follows:

Table 1.3: Notation

Small letters	Scalar, e.g., x
Bold small letters	Vector, e.g., \mathbf{x}
Bold capital letters	Matrix, e.g., \mathbf{X}
$(\cdot)^T$	Transposition
$(\cdot)^*$	Complex Conjugate
$(\cdot)^H$	Complex Conjugate transpose (Hermitian)
$\ \cdot\ _F$	Frobenius norm
\mathbf{I}_N	denotes the $\mathbb{C}^{N \times N}$ identity matrix
$\mathcal{CN}(\cdot, \cdot)$	Complex normal distribution
$\mathcal{A} \cup \mathcal{B}$	Union of sets \mathcal{A} and \mathcal{B}
$\mathcal{A} \setminus \mathcal{B}$	Exclusion of set \mathcal{B} from set \mathcal{A}
$\text{Tr}(\cdot)$	Trace of a matrix
$\text{diag}\{\dots\}$	Creates a diagonal matrix with $\{\dots\}$ on its diagonal entries

- Chapter 2 reviews network topologies and system models that are fundamental to modern wireless communications. We then analyze four main types of networks: traditional cellular, cell-free (CF), user-centric cell-free (UCCF), and clustered cell-free (CLCF) networks. The chapter also introduces system models and downlink communication techniques, focusing on linear precoding and multiuser scheduling for optimizing multicell and CF-mMIMO systems.
- Chapter 3 presents the Sequential Multiuser Scheduling and Power Allocation (SMSPA) approach to enhance performance in CF and CLCF networks. We develop the Clustered Enhanced Subset Greedy (C-ESG) user scheduling method and employ gradient-based optimization for power allocation, providing analytical and simulation-based validation of this resource allocation framework.
- Chapter 4 deals with clustering and fair resource allocation in UCCF networks using information rates as the AP clustering criterion. Providing a detailed analysis of the proposed clustering technique and examination of network performance under various conditions, its effectiveness in achieving equitable resource distribution among UEs is demonstrated.
- Chapter 5 investigates robust resource allocation techniques and proposes a robust user scheduling algorithm and two distinct power allocation methods to enhance network performance against CSI imperfections. It

includes a detailed analysis and performance assessment, showcasing the improvements brought by the proposed robust techniques.

- Finally, Chapter 6 concludes the study by providing a summary of the findings, outlining the implications of this research, and suggesting directions for future work in this area. By exploring these key areas in-depth, this thesis seeks to contribute significantly to the understanding and optimization of resource allocation in CF-mMIMO networks.

1.5

Publication List

This work so far has resulted in a number of published papers as follows:

- Journal Papers
 - Mashdour, S., de Lamare, R. C., Lima, P. S. H., **Enhanced Subset Greedy Multiuser Scheduling in Clustered Cell-Free Massive MIMO Systems**, IEEE Commun. Lett., 2022, doi: 10.1109/LCOMM.2022.3230641.
 - Mashdour, S., Salehi, S., de Lamare, R. C., and Schmeink, A., Lima, P. S. H., **Clustering and Scheduling With Fairness Based On Information Rates for Cell-Free MIMO Networks**, IEEE Wireless. Commun. Lett., 2024, doi: 10.1109/LWC.2024.3388318.
- Conference Papers
 - Mashdour, S., de Lamare, R. C., Lima, P. S. H., **Multiuser Scheduling with Enhanced Greedy Techniques for Multicell and Cell-Free Massive MIMO Systems**, presented at the IEEE 95th VTC, Helsinki, Finland, June. 19-22, 2022, pp. 1–5.
 - Mashdour, S., de Lamare, R. C., Schmeink, A., Lima, P. S. H., **MMSE-Based Resource Allocation for Clustered Cell-Free Massive MIMO Networks**, presented at the 26th International ITG Workshop on Smart Antennas and 13th Conference on Systems, Communications and Coding, Germany, Braunschweig, Feb. 27-March. 3, 2023, pp. 1-6.
 - Mashdour, S., de Lamare, R. C., Schmeink, A., Lima, P. S. H., **Sequential Multiuser Scheduling and Power Allocation for Clustered Cell-Free Massive MIMO Networks**, Proceedings of Eusipco 2023, Helsinki, Finland.
 - Mashdour, S., Flores., A. R., Salehi, S., de Lamare, R. C., Schmeink, A., Lima, P. S. H., da Silva, P. B. **Robust User Scheduling and**

Power Allocation in Cell-Free Massive MIMO Networks,
Proceedings of ISWCS 2024, Rio de Janeiro, Brazil.

- Submitted Papers:

- Mashdour, S., Flores., A, R., Salehi, S., de Lamare, R. C., Schmeink, A., da Silva, P. B. **Robust Resource Allocation in Cell-Free Massive MIMO Systems**, submitted to IEEE Transactions on Communications.

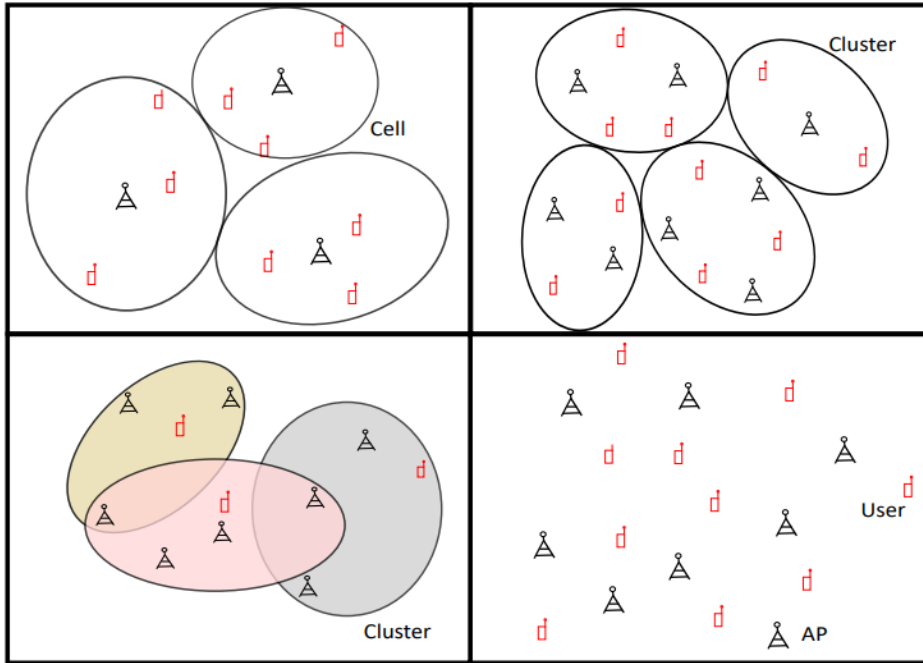


Figure 2.1: Presentation of different networks.

In this chapter, we first aim to exploration of network topologies and system models that form the basis of modern wireless communication. We will explore the characteristics of four key types of networks: traditional cellular networks, cell-free (CF) networks, user-centric cell-free (UCCF) networks, and Network-Centric Cell-Free or clustered cell-free (CLCF) networks, as depicted in Fig. 2.1. Each of these network structures offers unique benefits and presents distinct challenges, particularly in terms of performance, scalability, and user experience.

Following this overview, we examine the system models and downlink communication techniques applicable to cellular and cell-free networks. We will describe linear precoding techniques and multiuser scheduling algorithms, which are critical for optimizing network performance. These algorithms are especially pertinent in the context of multicell and CF-massive MIMO (CF-mMIMO) systems, where multiuser scheduling is essential for handling high user densities and ensuring efficient use of resources.

Furthermore, we evaluate the sum-rate performance of multicell and CF-mMIMO systems using a greedy user scheduling approach based on the zero-forcing beamforming with selection (ZFS) algorithm for downlink [12]. Multicell multiuser-MIMO systems have become an integral part of modern wireless networks due to their support for higher transmission rates, spectral and energy efficiencies, providing concurrent service to UE terminals within each cell [13–15]. One major motivation behind multiuser scheduling stems from the need to optimize system performance, especially in situations where the UE density surpasses the number of transmit antennas [12]. Furthermore, challenges such as pilot contamination, which hampers transmit power for each UE in massive MIMO, emphasize the importance of sophisticated multiuser scheduling techniques [16, 17]. Cell-free massive MIMO systems, on the other hand, comprise randomly dispersed single-antenna APs that serve all UEs simultaneously, which in turn results in increased throughput [1, 18, 19]. To tackle these challenges, we first employ a network-centric clustering approach to mitigate the computational cost in CF systems, alongside a novel greedy algorithm for multiuser scheduling. This algorithm is designed to approach the performance of the optimal exhaustive search. The efficacy of our proposed method is validated in both multicell and cell-free networks, using numerical results that reveal the sum-rate performance of the scheduling algorithm under a spectrum of channel knowledge conditions.

The remainder of this chapter is organized as follows: Section 2.1 provides an overview of the cellular network architecture, detailing its structural characteristics. Section 2.2 examines the CF network structure, outlining its unique properties. In Section 2.3, we explore the user-centric cell-free (UCCF) network configuration, while Section 2.4 discusses the clustered cell-free (CLCF) network design. Moving forward, Section 2.5 presents the channel and signal models applicable to multicell, CF, and network-centric CF networks. Section 2.6 introduces the zero-forcing beamforming with selection (ZFS) algorithm and an enhanced multiuser scheduling approach. Section 2.7 presents numerical results to assess performance, and finally, Section 2.8 summarizes the key insights derived from this chapter.

2.1 Cellular Networks

In the upper-left segment of Fig. 2.1, we depict a conventional cellular network. Each geographical cell in this network is served by a dedicated base station designed to support the UEs within its coverage area. This network model, characterized by its simplicity and clearly defined structure, has

been the cornerstone of most contemporary wireless communication systems. However, this simplicity comes at the cost of inter-cell interference. As each base station operates independently, UEs positioned near the cell edges often experience cross-interference from neighboring base stations. Despite this drawback, the defined structure and manageability of cellular networks make them a simple and cost-effective solution for areas with low UE density.

2.2 CF Networks

We now shift our focus to the lower-right part of the figure, which illustrates a CF network. Unlike its cellular counterpart, CF networks envision a large-scale cooperative area where all UEs are served by all APs within their transmission range. This wide-ranging, cooperative support reduces inter-cell interference to a large extent and improves the overall network performance. However, this comes with the trade-off of increased complexity in network management, mainly due to the intricate coordination required among the numerous APs. This cooperative paradigm, although providing a superior signal quality, necessitates complex signal processing and control algorithms, which can pose significant challenges to the network's operational efficiency.

2.3 UCCF Networks

The lower-left quadrant of the illustrative figure introduces the concept of the UCCF network. In this approach, the APs are strategically grouped, or "clustered," based on the UEs they serve. The primary criterion for this clustering revolves around the UEs that exhibit the highest large-scale fading. This selective cooperation among APs significantly streamlines the network's complexity. However, the pivot towards UCCF networks also carries with it certain trade-offs. While the network complexity diminishes, the network performance also degrades as compared to CF networks. This decline is mainly due to the reduction in cooperation among APs, as the full potential of cooperation inherent in CF is not realized in UCCF networks. Their operational efficiency, combined with their ability to adapt to the evolving demands of modern communication networks, renders UCCF networks as an appealing alternative in certain application scenarios.

2.4

CLCF Networks

The upper-right quadrant of Fig. 2.1 presents the CLCF network, a promising approach in network architectures. Unlike UCCF, the CLCF network organizes the network area into distinct, non-overlapping regions. Indeed, in this approach, the CF network is divided into smaller networks each of which is a much smaller CF network with much less dimension. All the UEs within a specific region are served by the APs within the same geographic area, which results in much lower complexity than that of the original CF network.

This particular configuration, however, comes with its challenges, specifically in the form of inter-cluster interference. This interference is a direct result of the clustered network, where each region operates somewhat independently of the others. Nevertheless, the main advantage of this plan compared to the UCCF network is a reduction in network complexity.

2.5

Multicell and CF-mMIMO System Models

In order to discuss the cellular and CF networks, we evaluate both configurations within a shared geographical area to ensure a fair and consistent basis for comparison. We consider K single-antenna UEs distributed in the whole area. The multicell network consists of L_t cells each including $K_c = \frac{K}{L_t}$ UEs and a BS equipped with N_t antennas. We also consider the cell-free system with $M = L_t \times N_t$ randomly located single antenna APs. For network-centric clustering of the CF network, we also consider L clusters where the cluster c includes K_c single antenna UEs and $M_c = \frac{M}{L_t}$ single antenna APs.

2.5.1

Multicell Channel and Signal Model

We consider $\mathcal{L} = \{1, 2, \dots, L_t\}$ as the set of all existing cells in the area. We also model h_{smk} as the Rayleigh fading coefficient between the m th transmit antenna and k th receive antenna in the cell s and denote the row vector $\mathbf{h}_{sm} = [h_{sm1} \quad h_{sm2} \quad \dots \quad h_{smK_c}]$. Then, $\mathbf{H}_s \in \mathbb{C}^{K_c \times N_t}$ channel matrix including channel coefficient from the BS s to all UEs located in the related cell is

$$\mathbf{H}_s = [\mathbf{h}_{s1}^T \quad \mathbf{h}_{s2}^T \quad \dots \quad \mathbf{h}_{sN_t}^T] \quad (2-1)$$

With $\mathbf{x}_s = [x_{s1} \quad \dots \quad x_{sK_c}]^T$ as the vector of information symbols from BS s intended for all its UEs where $\mathbf{x}_s \sim \mathcal{CN}(\mathbf{0}, \mathbf{I}_{K_c})$, and $\mathbf{P}_s \in \mathbb{C}^{N_t \times K_c}$ as the precoding matrix, the total downlink signal received by all UEs in the cell s is given by

$$\mathbf{y}_s = \mathbf{H}_s \mathbf{P}_s \mathbf{x}_s + \sum_{l=1, l \neq s}^{L_t} \mathbf{H}_l \mathbf{P}_l \mathbf{x}_l + \mathbf{w}_s \quad (2-2)$$

where $\mathbf{w}_s = [w_{s_1} \ \cdots \ w_{s_{K_c}}]^T$ is the additive white Gaussian noise vector of the UEs located in cell s with $w_{s_k} \sim \mathcal{CN}(0, \sigma_w^2)$ and covariance matrix $\mathbf{C}_{\mathbf{w}_s} = \sigma_w^2 \mathbf{I}_{K_c}$. The term $\sum_{l=1, l \neq s}^{L_t} \mathbf{H}_l \mathbf{P}_l \mathbf{x}_l$ is considered as the interference caused by other cells called inter-cell interference (ICI). Considering \mathbf{y}_a as (2-2), we write the terms for interference and noise as $\mathbf{y}_{s_{e,w}} = \sum_{l=1, l \neq s}^{L_t} \mathbf{H}_l \mathbf{P}_l \mathbf{x}_l + \mathbf{w}_s$. Then, an upper bound on the achievable sum-rate under imperfect channel knowledge is given by:

$$C_{ch} = \log_2 (\det (\pi e \mathbf{R}_{\mathbf{y}_s})) - \log_2 (\det (\pi e \mathbf{R}_{\mathbf{y}_{s_{e,w}}})) , \quad (2-3)$$

where

$$\mathbf{R}_{\mathbf{y}_s} = \mathbb{E} [\mathbf{y}_s \mathbf{y}_s^H] , \quad (2-4)$$

and

$$\mathbf{R}_{\mathbf{y}_{s_{e,w}}} = \mathbb{E} [\mathbf{y}_{s_{e,w}} \mathbf{y}_{s_{e,w}}^H] . \quad (2-5)$$

We expand the inner argument of the expectation in $\mathbf{R}_{\mathbf{y}_s}$, which lead to the multiplication of statistically independent terms described by

$$\begin{aligned} \mathbf{y}_s \mathbf{y}_s^H &= \left(\sum_{l=1, l \neq s}^{L_t} \mathbf{H}_l \mathbf{P}_l \mathbf{x}_l + \mathbf{w}_s \right) \left(\sum_{l=1, l \neq s}^{L_t} \mathbf{H}_l \mathbf{P}_l \mathbf{x}_l + \mathbf{w}_s \right)^H + \\ &\quad \mathbf{H}_s \mathbf{P}_s \mathbf{x}_s (\mathbf{H}_s \mathbf{P}_s \mathbf{x}_s)^H + \\ &\quad \mathbf{H}_s \mathbf{P}_s \mathbf{x}_s \left(\sum_{l=1, l \neq s}^{L_t} \mathbf{H}_l \mathbf{P}_l \mathbf{x}_l + \mathbf{w}_s \right)^H + \\ &\quad \left(\sum_{l=1, l \neq s}^{L_t} \mathbf{H}_l \mathbf{P}_l \mathbf{x}_l + \mathbf{w}_s \right) (\mathbf{H}_s \mathbf{P}_s \mathbf{x}_s)^H \end{aligned} \quad (2-6)$$

Expanding each term in (2-6) and taking expectations to compute $\mathbb{E}[\mathbf{y}_s \mathbf{y}_s^H]$, we proceed as follows:

The expectation from the first term in the right hand side of Equation (2-6) expands as:

$$\mathbb{E} \left[\left(\sum_{l=1, l \neq s}^{L_t} \mathbf{H}_l \mathbf{P}_l \mathbf{x}_l + \mathbf{w}_s \right) \left(\sum_{l=1, l \neq s}^{L_t} \mathbf{H}_l \mathbf{P}_l \mathbf{x}_l + \mathbf{w}_s \right)^H \right] . \quad (2-7)$$

In (2-7), there are two contributions as $\mathbb{E} [\sum_{l=1, l \neq s}^{L_t} \mathbf{H}_l \mathbf{P}_l \mathbf{x}_l \mathbf{w}_s^H]$ and $\mathbb{E} [\sum_{l=1, l \neq s}^{L_t} \mathbf{w}_s \mathbf{x}_l^H \mathbf{P}_l^H \mathbf{H}_l^H]$, which evaluate to zero because \mathbf{x}_l and \mathbf{w}_s are uncorrelated and zero-mean. Thus, (2-7) results in two non-zero contributions as follows:

$$\mathbb{E} \left[\sum_{l=1, l \neq s}^{L_t} \mathbf{H}_l \mathbf{P}_l \mathbf{x}_l \mathbf{x}_l^H \mathbf{P}_l^H \mathbf{H}_l^H \right] + \mathbb{E} [\mathbf{w}_s \mathbf{w}_s^H] . \quad (2-8)$$

Here, $\mathbb{E}[\mathbf{x}_l \mathbf{x}_l^H] = \mathbf{I}_{K_c}$ and $\mathbb{E}[\mathbf{w}_s \mathbf{w}_s^H] = \sigma_w^2 \mathbf{I}_{K_c}$, which yields:

$$\sum_{l=1, l \neq s}^{L_t} \mathbf{H}_l \mathbf{P}_l \mathbf{P}_l^H \mathbf{H}_l^H + \sigma_w^2 \mathbf{I}_{K_c}. \quad (2-9)$$

Taking expectation from the second term in right hand side of (2-6) expands as:

$$\mathbb{E} \left[\mathbf{H}_s \mathbf{P}_s \mathbf{x}_s (\mathbf{H}_s \mathbf{P}_s \mathbf{x}_s)^H \right]. \quad (2-10)$$

Since $\mathbb{E}[\mathbf{x}_l \mathbf{x}_l^H] = \mathbf{I}_{K_c}$, this term becomes $\mathbf{H}_s \mathbf{P}_s \mathbf{P}_s^H \mathbf{H}_s^H$. The next two terms in (2-6) go to zero since \mathbf{x}_s and \mathbf{w}_s are uncorrelated and $\mathbb{E}[\mathbf{x}_l \mathbf{x}_s^H] = 0, l \neq s$. Thus, we have the following simplifications:

$$\mathbf{R}_{\mathbf{y}_s} = \mathbf{H}_s \mathbf{P}_s \mathbf{P}_s^H \mathbf{H}_s^H + \sum_{l=1, l \neq s}^{L_t} \mathbf{H}_l \mathbf{P}_l \mathbf{P}_l^H \mathbf{H}_l^H + \sigma_w^2 \mathbf{I}_{K_c} \quad (2-11)$$

$$\mathbf{R}_{\mathbf{y}_{s_e, w}} = \sum_{l=1, l \neq s}^{L_t} \mathbf{H}_l \mathbf{P}_l \mathbf{P}_l^H \mathbf{H}_l^H + \sigma_w^2 \mathbf{I}_{K_c} \quad (2-12)$$

Now, we substitute (2-11) and (2-12), which yields

$$\begin{aligned} & \log(\det(\pi e \mathbf{R}_{\mathbf{y}_s})) - \log(\det(\pi e \mathbf{R}_{\mathbf{y}_{s_e, w}})) = \\ & \log\left(\frac{\det(\pi e \mathbf{R}_{\mathbf{y}_s})}{\det(\pi e \mathbf{R}_{\mathbf{y}_{s_e, w}})}\right) = \log(\det(\mathbf{R}_{\mathbf{y}_s} \mathbf{R}_{\mathbf{y}_{s_e, w}}^{-1})) \end{aligned} \quad (2-13)$$

Thus, the sum-rate of the received signals in the network is achieved by the summation over the sum-rates of all the cells, which results in

$$R_t = \sum_{s=1}^{L_t} R_s = \sum_{s=1}^{L_t} \log_2(\det[\mathbf{R}_s + \mathbf{I}_{K_c}]), \quad (2-14)$$

where the covariance matrix \mathbf{R}_s is given by

$$\mathbf{R}_s = \mathbf{H}_s \mathbf{P}_s \mathbf{P}_s^H \mathbf{H}_s^H \left(\sum_{l=1, l \neq s}^{L_t} \mathbf{H}_l \mathbf{P}_l \mathbf{P}_l^H \mathbf{H}_l^H + \sigma_w^2 \mathbf{I}_{K_c} \right)^{-1} \quad (2-15)$$

2.5.2

Cell-Free Channel and Signal Model

According to [1, 19], we use $g_{mk} = \sqrt{\beta_{mk}} h_{mk}$ to denote the cell-free channel coefficient between m th AP and k th user where β_{mk} is the large-scale fading coefficient (path loss and shadowing effects) and $h_{mk} \sim \mathcal{CN}(0, 1)$ is the small-scale fading coefficient, defined as independent and identically distributed (i.i.d) random variables (RVs) that remain constant during a coherence interval and are independent over different coherence intervals.

Large scale coefficients are modeled as $\beta_{mk} = \text{PL}_{mk} \cdot 10^{\frac{\sigma_{sh} z_{mk}}{10}}$ where PL_{mk} is the path loss and $10^{\frac{\sigma_{sh} z_{mk}}{10}}$ refers to the shadow fading with $\sigma_{sh} = 8\text{dB}$ and

$z_{mk} \sim \mathcal{N}(0, 1)$. Following [20], the path loss is modeled as

$$\text{PL}_{mk} = \begin{cases} -D - 35 \log_{10}(d_{mk}), & \text{if } d_{mk} > d_1 \\ -D - 10 \log_{10}(d_1^{1.5} d_{mk}^2), & \text{if } d_0 < d_{mk} \leq d_1 \\ -D - 10 \log_{10}(d_1^{1.5} d_0^2), & \text{if } d_{mk} \leq d_0 \end{cases}, \quad (2-16)$$

where d_{mk} is the distance between the m th AP and k th UE,

$$\begin{aligned} D &= 46.3 + 33.9 \log_{10}(f) - 13.82 \log_{10}(h_{AP}) \\ &- [1.11 \log_{10}(f) - 0.7] h_u + 1.56 \log_{10}(f) - 0.8 \end{aligned} \quad (2-17)$$

where $f = 1900\text{MHz}$ is the carrier frequency, $h_{AP} = 15\text{m}$ and $h_r = 1.5\text{m}$ are the AP and UE antenna heights, respectively, $d_0 = 10\text{m}$ and $d_1 = 50\text{m}$. When $d_{mk} \leq d_1$ there is no shadowing. In downlink transmissions, the received signal at the k th UE is described by

$$y_k = \sqrt{\rho_f} \mathbf{g}_k \mathbf{P} \mathbf{x} + w_k, \quad (2-18)$$

where ρ_f is maximum transmitted power of each antenna, $\mathbf{g}_k = [g_{1k}, \dots, g_{Mk}]$ are the channel coefficients for UE k , $\mathbf{P} \in \mathbb{C}^{M \times K}$ is the precoder matrix such as MMSE or ZF, $\mathbf{x} = [x_1, \dots, x_K]^T$ is the zero mean symbol vector with x_k the data symbol for UE k and $\mathbf{x} \sim \mathcal{CN}(\mathbf{0}, \mathbf{I}_K)$, and $w_k \sim \mathcal{CN}(0, \sigma_w^2)$ is the additive noise for UE k . We consider that the elements of \mathbf{x} are mutually independent, and independent of all noise and channel coefficients. Combining all the UEs, we have

$$\mathbf{y} = \sqrt{\rho_f} \mathbf{G}^T \mathbf{P} \mathbf{x} + \mathbf{w}, \quad (2-19)$$

where $\mathbf{G} \in \mathbb{C}^{M \times K}$ is the channel matrix with elements $[\mathbf{G}]_{m,k} = g_{mk}$ and $\mathbf{w} = [w_1, \dots, w_K]^T$ is the noise vector. In the presence of imperfect CSI, (2-19) is rewritten as

$$\begin{aligned} \mathbf{y} &= \sqrt{\rho_f} (\hat{\mathbf{G}} + \tilde{\mathbf{G}})^T \mathbf{P} \mathbf{x} + \mathbf{w} \\ &= \sqrt{\rho_f} \hat{\mathbf{G}}^T \mathbf{P} \mathbf{x} + \sqrt{\rho_f} \tilde{\mathbf{G}}^T \mathbf{P} \mathbf{x} + \mathbf{w}, \end{aligned} \quad (2-20)$$

where $\hat{\mathbf{G}} \in \mathbb{C}^{M \times K}$ is the channel matrix estimate and $\tilde{\mathbf{G}} \in \mathbb{C}^{M \times K}$ is the estimation error matrix. Considering noise covariance matrix as $\mathbf{C}_w = \sigma_w^2 \mathbf{I}_K$, the sum-rate of the cell-free system can be computed by

$$R_{CF} = \log_2(\det[\mathbf{R} + \mathbf{I}_K]), \quad (2-21)$$

where the covariance matrix \mathbf{R} is expressed by

$$\mathbf{R} = \rho_f \hat{\mathbf{G}}^T \mathbf{P} \mathbf{P}^H \hat{\mathbf{G}}^* (\rho_f \tilde{\mathbf{G}}^T \mathbf{P} \mathbf{P}^H \tilde{\mathbf{G}}^* + \sigma_w^2 \mathbf{I}_K)^{-1}, \quad (2-22)$$

where \mathbf{x} and \mathbf{w} are statistically independent.

2.5.3

Network-Centric Cell-Free

We divide a CF network into L clusters, each operating like a smaller CF network as illustrated in Fig. 2.2. The signal received by the UEs of the c th cluster is given by

$$\begin{aligned} \mathbf{y}_c &= \sqrt{\rho_f} (\hat{\mathbf{G}}_{cc} + \tilde{\mathbf{G}}_{cc})^T \mathbf{P}_c \mathbf{x}_c + \sum_{i=1, i \neq c}^L \sqrt{\rho_f} (\hat{\mathbf{G}}_{ic} + \tilde{\mathbf{G}}_{ic})^T \mathbf{P}_i \mathbf{x}_i + \mathbf{w}_c = \\ & \sqrt{\rho_f} \hat{\mathbf{G}}_{cc}^T \mathbf{P}_c \mathbf{x}_c + \sqrt{\rho_f} \tilde{\mathbf{G}}_{cc}^T \mathbf{P}_c \mathbf{x}_c + \sum_{i=1, i \neq c}^L \sqrt{\rho_f} \hat{\mathbf{G}}_{ic}^T \mathbf{P}_i \mathbf{x}_i + \sum_{i=1, i \neq c}^L \sqrt{\rho_f} \tilde{\mathbf{G}}_{ic}^T \mathbf{P}_i \mathbf{x}_i + \mathbf{w}_c, \end{aligned} \quad (2-23)$$

where $\hat{\mathbf{G}}_{ic}, \tilde{\mathbf{G}}_{ic} \in \mathbb{C}^{M_i \times K_c}$ are respectively channel estimation and estimation error matrices from APs of the cluster i , $i \in \{1, 2, \dots, C\}$, to UEs of the cluster c , $\mathbf{P}_i \in \mathbb{C}^{M_i \times K_i}$ is the linear precoding matrix of the cluster i , and $\mathbf{x}_i = [x_{i1}, \dots, x_{iK_i}]^T$, $\mathbf{x}_i \sim \mathcal{CN}(\mathbf{0}, \mathbf{I}_{K_i})$ is the symbol vector of the cluster i . Accordingly, the achievable sum-rate of the clustered network is

$$R_{cl} = \sum_{c=1}^L R_c \quad (2-24)$$

where the sum-rate expression in cluster c is

$$R_c = \log_2 \left(\det \left[\left(\rho_f \hat{\mathbf{G}}_{cc}^T \mathbf{P}_c \mathbf{P}_c^H \hat{\mathbf{G}}_{cc}^* \right) \mathbf{R}_c^{-1} + \mathbf{I}_{K_c} \right] \right) \quad (2-25)$$

and the covariance matrix \mathbf{R}_c is described by

$$\begin{aligned} \mathbf{R}_c &= E \left[\left(\mathbf{y}_c - \sqrt{\rho_f} \hat{\mathbf{G}}_{cc}^T \mathbf{P}_c \mathbf{x}_c \right) \left(\mathbf{y}_c - \sqrt{\rho_f} \hat{\mathbf{G}}_{cc}^T \mathbf{P}_c \mathbf{x}_c \right)^H \right] \\ &= \rho_f \tilde{\mathbf{G}}_{cc}^T \mathbf{P}_c \mathbf{P}_c^H \tilde{\mathbf{G}}_{cc}^* + \sum_{i=1, i \neq c}^L \rho_f \hat{\mathbf{G}}_{ic}^T \mathbf{P}_i \mathbf{P}_i^H \hat{\mathbf{G}}_{ic}^* + \\ & \quad \sum_{i=1, i \neq c}^L \rho_f \tilde{\mathbf{G}}_{ic}^T \mathbf{P}_i \mathbf{P}_i^H \tilde{\mathbf{G}}_{ic}^* + \sigma_w^2 \mathbf{I}_{K_c}, \end{aligned} \quad (2-26)$$

where \mathbf{x}_c and \mathbf{w}_c are statistically independent.

2.6

ZFS User Scheduling and the Proposed Enhanced Scheduling Algorithm

Using an exhaustive search, we can schedule the UE set with best performance among all possible UE sets. However, it implies a high computational complexity which makes it impractical. Thus, alternative methods such as greedy algorithms are suggested in literature to reduce the selection complexity [21–23]. Greedy methods are important mathematical techniques that compute a locally optimal solution to complex problems in a step-by-step man-

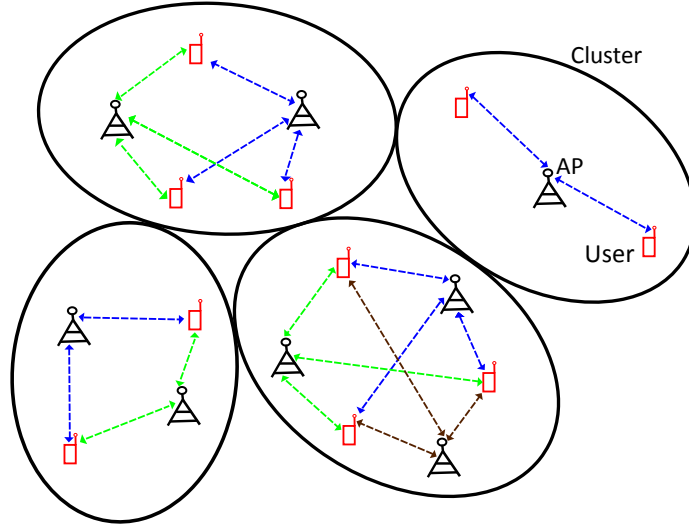


Figure 2.2: Network-centric CF Model.

ner. Since these algorithms are effective to find the global optimal solution and usually present lower cost compared to similar approaches, we were motivated to devise the solution to our problem based on them.

In this section, we extend the greedy ZFS scheduling algorithm developed in [12] and to the scenarios of interest. Then, exploiting ZFS and introducing a strategy based on multiple candidates for choosing the subset of UEs, we develop an enhanced greedy algorithm which leads to a UE subset closer to the optimal subset obtained by exhaustive search.

2.6.1 ZFS Algorithm

ZF precoder creates orthogonal channels between transmitter and receivers by inverting the channel matrix at the transmitter using precoding matrix $\mathbf{P} = \mathbf{H}^H (\mathbf{H}\mathbf{H}^H)^{-1}$ where $\mathbf{H} \in \mathbb{C}^{K \times M}$ is the channel matrix. However, if $K > M$, $\mathbf{H}\mathbf{H}^H$ becomes singular and it is not possible to use ZF precoder. Therefore, it is required to schedule $n \leq M$ out of K UEs as a set of UEs S_n resulting in a row-reduced channel matrix $\mathbf{H}(S_n)$ which gives the highest achievable sum-rate

$$\begin{aligned} & \max_{1 \leq n \leq M} \max_{S_n} R_{zf}(S_n) \\ & \text{subject to } \sum_{i \in S_n} \left[\mu - \frac{1}{c_i(S_n)} \right]_+ = P. \end{aligned} \quad (2-27)$$

where P is the upper limit of the signal covariance matrix $\text{Trace}[\mathbf{C}_x] \leq P$, $R_{zf}(S_n)$ is the throughput of the ZF algorithm given by

$$R_{zf}(S_n) = \sum_{i \in S_n} [\log_2(\mu c_i(S_n))]_+ \quad (2-28)$$

where $c_i(S_n) = \left\{ \left[\left(\mathbf{H}(S_n) \mathbf{H}(S_n)^H \right)^{-1} \right]_{ii} \right\}^{-1}$. Then, the reduced-complexity sub-optimal ZFS algorithm is outlined in the Algorithm 1 considering $\mathcal{K} = \{1, 2, \dots, K\}$ as the set of indices of all K UEs, K_s as number of UEs to be scheduled, and \mathbf{h}_k as the channel vector of UE k . Note that we have used equal power loading to obtain μ .

Algorithm 1: Reduced-complexity sub-optimal ZFS

```

1 Initialization ;
2 set  $n = 1$  ;
3 find a UE  $s_1$  such that  $s_1 = \underset{k \in \mathcal{K}}{\operatorname{argmax}} \mathbf{h}_k \mathbf{h}_k^H$  ;
4 set  $S_1 = \{s_1\}$  and denote the achieved rate  $R_{ZF}(S_1)_{max}$  ;
5 while  $n < K_s$  do
6   | increase  $n$  by 1 ;
7   | find a UE  $s_n$  such that  $s_n = \underset{k \in (\mathcal{K} \setminus S_{n-1})}{\operatorname{argmax}} R_{ZF}(S_{n-1} \cup \{k\})$  ;
8   | set  $S_n = S_{n-1} \cup \{s_n\}$  and denote the achieved rate  $R_{ZF}(S_n)_{max}$  ;
9   | if  $R_{ZF}(S_n)_{max} \leq R_{ZF}(S_{n-1})_{max}$  then
10  | | break and decrease  $n$  by 1 ;
11  | end
12 end
13 Precoding  $\mathbf{P} = \mathbf{H}(S_n)^H \left( \mathbf{H}(S_n) \mathbf{H}(S_n)^H \right)^{-1}$ 

```

2.6.2

Enhanced Greedy Algorithm

Here, we devise a scheduling strategy that assesses more sets of UEs so that we can achieve a system performance closer to the performance achieved by an exhaustive search while saving significant computational complexity. In this regard, we consider the set achieved by ZFS as the first UE set $S_{n(1)}$. Then, we choose $k_{ex(1)}$ as the least channel power UE among the UEs of the first set which is called the first excluded UE and is obtained by

$$k_{ex(1)} = \underset{k \in S_{n(1)}}{\operatorname{argmin}} \mathbf{h}_k \mathbf{h}_k^H \quad (2-29)$$

We also select the UE with the highest channel power from the remaining UEs other than the first selected set called first new UE $k_{new(1)}$ defined as

$$k_{new(1)} = \underset{k \in \mathcal{K}_r(1)}{\operatorname{argmax}} \mathbf{h}_k \mathbf{h}_k^H \quad (2-30)$$

where $\mathcal{K}_r(1) = \mathcal{K} \setminus S_{n(1)}$ is set of the remaining or unselected UEs. Substituting the excluded UE by the new UE in the first set, we achieve a new UE set as the second set. Then, excluding the new UE from the remaining UEs we achieve the second remaining UE set. Repeating the described procedure for the second

set and so on, we achieve $\frac{K-K_s}{2}$ sets together with the first set. Therefore, the UE set $S_{n(j)}$ and the remaining UE set $\mathcal{K}_{r(j)}$, $j \in \{2, \dots, \frac{K-K_s}{2} + 1\}$, are respectively derived as

$$S_{n(j)} = \left(S_{n(j-1)} \setminus k_{ex(j-1)} \right) \cup k_{new(j-1)} \quad (2-31)$$

$$\mathcal{K}_{r(j)} = \mathcal{K}_{r(j-1)} \setminus k_{new(j-1)} \quad (2-32)$$

Thereafter, we assess all the considered sets to determine the best set S_{n_f} using two different criteria each of which implying a different complexity to the system. The first criterion would be the sum-rates according to Equations (2-14) and (2-24) for multicell and cell-free networks, respectively. The second one, would be $C_s(S_{n(i)})$ the sum channel correlation among the UEs of i th set, $i \in \{1, 2, \dots, \frac{K-K_s}{2} + 1\}$ defined as

$$C_s(S_{n(i)}) = \sum_{u \in S_{n(i)}} \sum_{v \in S_{n(i)}, v \neq u} C_{u,v} \quad (2-33)$$

where $C_{u,v}$ is channel correlation of the UEs u and v in the set $S_{n(i)}$. Thus, depending on the sum-rate or sum correlation criteria, the desired set is respectively derived as

$$S_{n_f} = \operatorname{argmax}_{S_n \in S_{n(i)}} \{R_{CF}(S_n)\} \quad (2-34)$$

or alternatively as

$$S_{n_f} = \operatorname{argmin}_{S_n \in S_{n(i)}} \{C_s(S_n)\} \quad (2-35)$$

Accordingly, the enhanced greedy algorithm for cell-free networks is outlined as Algorithm 2. Note that for the multicell network, number of the UEs in a cell and the UEs to be selected in that cell will change to K_c and K_{c_s} respectively, R_{CF} is changed to R_t , and the overall sum channel correlation is obtained by summation over all the cells.

2.7

Numerical Results

In this section, we assess in terms of sum-rates the proposed and existing scheduling algorithms in multicell and CF scenarios considering perfect and imperfect CSI using Matlab. Note that as we mentioned at the beginning of this chapter, we use a network-centric version of the CF network. In the considered model for imperfect CSI, the signal is transmitted through the channel $\mathbf{H} = \hat{\mathbf{H}} + \tilde{\mathbf{H}}$, where $\hat{\mathbf{H}}$ is the channel estimate and $\tilde{\mathbf{H}}$ is the estimation error which models the CSI quality [24]. In particular, we consider a squared area of size 400m as the whole area of the cell-free system with $M = 64$

Algorithm 2: Enhanced Greedy User Scheduling

```

1 Input  $\mathcal{K}$ ,  $\mathbf{H}$ ,  $K_s$  ;
2 stage=1 ;
3 Find initial UE set  $S_{n(\text{stage})}$  using ZFS ;
4 Compute  $R_{CF}(S_{n(\text{stage})})$  or  $C_s(S_{n(\text{stage})})$  depending on the used
   criterion ;
5  $\mathcal{K}_{r(\text{stage})} = \mathcal{K} \setminus S_{n(\text{stage})}$  % set of  $K - K_s$  unselected UEs ;
6  $k_{ex(\text{stage})} = \underset{k \in S_{n(\text{stage})}}{\operatorname{argmin}} \mathbf{h}_k \mathbf{h}_k^H$  ;
7  $k_{new(\text{stage})} = \underset{k \in \mathcal{K}_{r(\text{stage})}}{\operatorname{argmax}} \mathbf{h}_k \mathbf{h}_k^H$  ;
8 for stage = 2 to  $\frac{K-K_s}{2} + 1$  do
9    $S_{n(\text{stage})} = (S_{n(\text{stage}-1)} \setminus k_{ex(\text{stage}-1)}) \cup k_{new(\text{stage}-1)}$  ;
10   $\mathcal{K}_{r(\text{stage})} = \mathcal{K}_{r(\text{stage}-1)} \setminus k_{new(\text{stage}-1)}$  ;
11   $k_{ex(\text{stage})} = \underset{k \in S_{n(\text{stage})}}{\operatorname{argmin}} \mathbf{h}_k \mathbf{h}_k^H$  ;
12   $k_{new(\text{stage})} = \underset{k \in \mathcal{K}_{r(\text{stage})}}{\operatorname{argmax}} \mathbf{h}_k \mathbf{h}_k^H$  ;
13  Compute  $R_{CF}(S_{n(\text{stage})})$  or  $C_s(S_{n(\text{stage})})$ 
14 end
15  $S_{n_f} = \underset{S_n \in S_{n(i)}}{\operatorname{argmax}} \{R_{CF}(S_n)\}$  or  $\underset{S_n \in S_{n(i)}}{\operatorname{argmin}} \{C_s(S_n)\}$  ;
16 Precoding ;

```

single-antenna randomly located APs and $K = 16$ uniformly distributed single antenna UEs. For the multicell system, we consider the same area divided in $L_t = 4$ non-overlapping cells each including $K_c = \frac{K}{L_t} = 4$ UEs with the same location as the cell-free system and a BS located at the center of the cell with $N_t = \frac{M}{L_t} = 16$ antennas. We adopt the cell-free channel model in [18, 19] and the cellular channel model in 2.5, and consider a static channel over each transmission packet in both networks. In Table 2.1, we provide more details on the parameters used for simulation.

Table 2.1: Characteristics of the simulated systems

	Multicell	Cell-free
Carrier frequency	1900MHz	1900MHz
Symbol energy	$P_s=1$	$P_s=1$
Transmit power	$N_t \times P_s$	$M \times P_s$

With perfect and imperfect CSI, we have used ZF and MMSE precoders

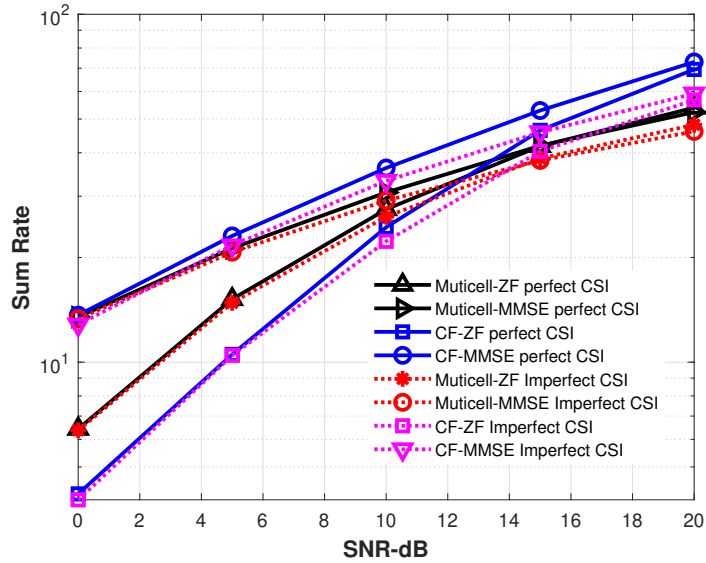


Figure 2.3: Performance comparison of cell-free and multicell networks considering all UEs.

for performance comparison of the multicell and cell-free networks and the corresponding sum-rates are shown in Fig. 2.3 against the SNR when user scheduling is not considered. For all plots, the sum-rates increase with the SNR, however, the MMSE precoder has resulted in higher sum-rates as compared with the ZF precoder in both networks. As the SNR increases, the performance of the cell-free system has shown a significant improvement over the multicell system. Since cellular networks suffer from ICI in addition to multiuser interference, there exist bad channel conditions for the near border UEs in each cell which results in performance degradation. However, since cell-free systems use distributed APs throughout the network, they can offer a better coverage for all UEs and the use of coherent transmission could result in high received power at each UE. When CSI is imperfect, there is a degradation in performance as compared to the perfect CSI case for all techniques.

Fig. 2.4 and 2.5 show how different scheduling methods work in cell-free and multicell networks, respectively, when the sum-rate criterion is used. In Fig. 2.4, implementing an exhaustive search, the proposed enhanced greedy and ZFS user scheduling algorithms in cell-free networks, we have scheduled half of the UEs when ZF and MMSE precoders are used and both perfect and imperfect CSI cases are considered. The results show that the proposed enhanced greedy method outperforms ZFS and its performance is very close to the optimal exhaustive search method in cell-free networks for both CSI scenarios. For multicell network as shown in Fig. 2.5, where perfect CSI is considered, we also have a significant improvement in performance using the proposed method.

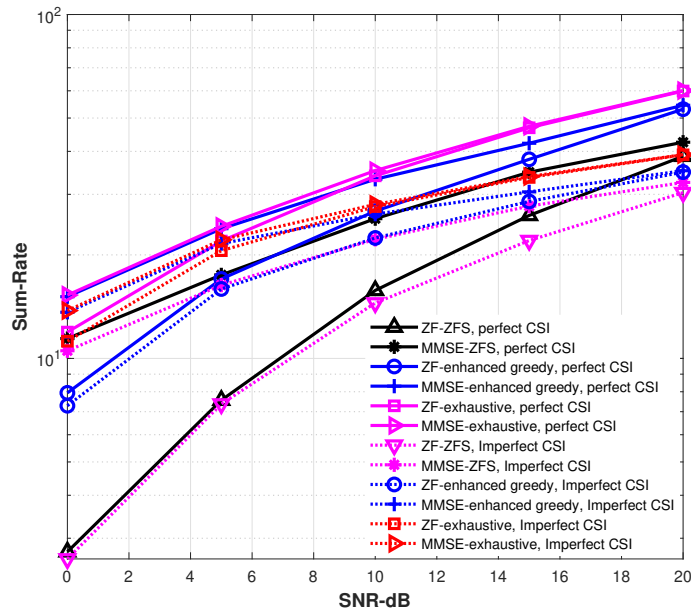


Figure 2.4: Performance of cell-free network with different scheduling methods

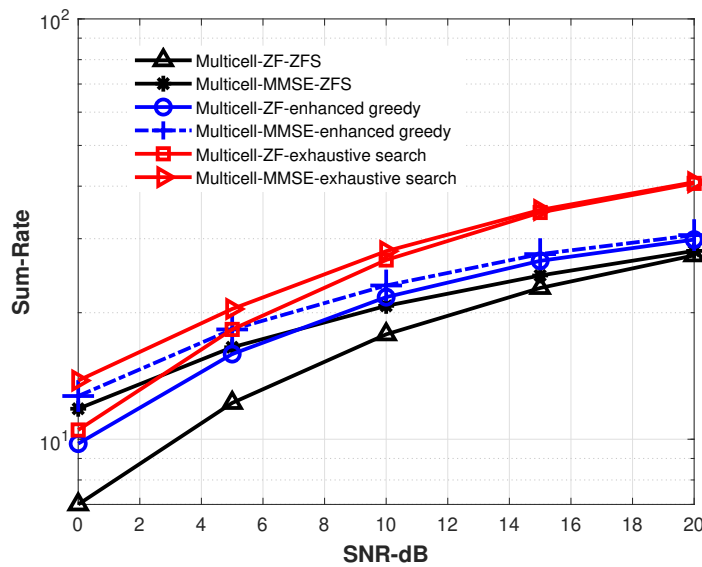


Figure 2.5: Performance of multicell network with different scheduling methods

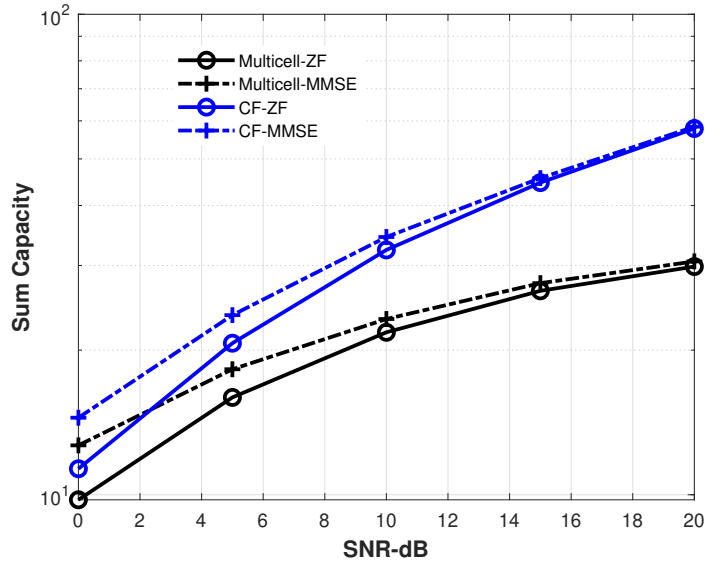


Figure 2.6: Performance comparison using enhanced greedy algorithm, cell-free and multicell networks

In Fig. 2.6, performance comparison of the cell-free and multicell networks with perfect CSI for the proposed enhanced greedy algorithm is shown where the cell-free system has outperformed the multicell system as expected. In Fig. 2.7, the performance of the enhanced greedy algorithm in a cell-free network is shown when the sum-rate and channel-correlation criteria are used and perfect CSI is considered. We can see that using the sum-rate criterion provides an improvement in system performance while the results for the channel-correlation criterion are slightly worse. The choice of the sum-rate and the channel-correlation criteria depends on the available computational power and application.

In Table 2.2, the computational complexity of the ZFS and the proposed enhanced greedy methods for the sum-rate and channel-correlation criteria are shown in cellular and cell-free networks with network-centric clustering. We notice that the complexity of the proposed method is higher than that of the benchmark. However, as shown in the results, the proposed method provides a significant improvement in system performance. Since the additional cost is not much higher, it is expected that this could be accommodated in the hardware required for the proposed algorithm. The results also show that the improvement in the method using the sum-rate criterion comes at the cost of more required flops.

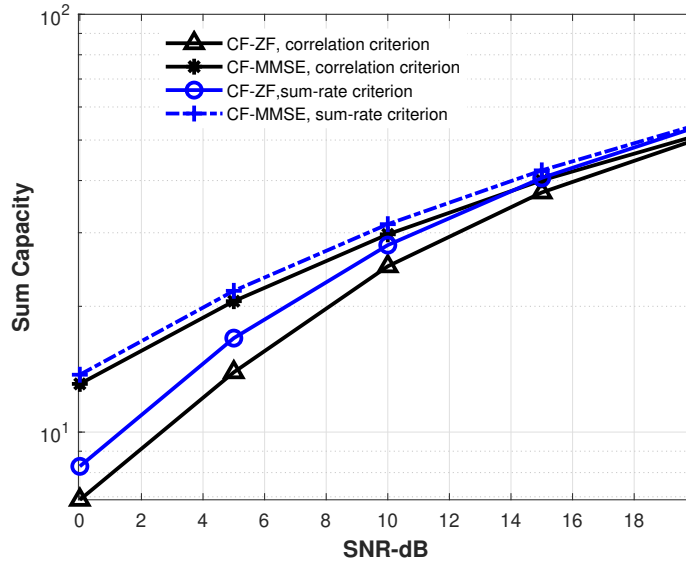


Figure 2.7: Performance comparison using enhanced greedy algorithm, cell-free network using sum-rate and channel-correlation criteria

Table 2.2: Computational complexity in flops

	Multicell	Cell-free
ZFS	3580	3580
Enhanced greedy (channel-correlation)	9484	9484
Enhanced greedy (sum-rate)	12148	12148

2.8 Summary

This chapter introduced various network structures, including cellular, CF, and CLCF architectures, with a brief overview of the UCCF configuration. Following this, the chapter provided an in-depth sum-rate analysis for both multicell and CF networks and described the development of an enhanced greedy user scheduling technique based on ZFS approach. Numerical results have shown that this multiuser scheduling approach significantly improves system performance across various scenarios. These findings have established a foundation for the subsequent exploration of network optimization strategies in this thesis.

3

Sequential Multiuser Scheduling and Power Allocation in CF-mMIMO Networks

In this chapter, we present a Sequential Multiuser Scheduling and Power Allocation (SMSPA) resource allocation approach designed to enhance the performance of cell-free (CF) and clustered cell-free (CLCF) massive MIMO networks. This technique combines user scheduling with advanced power allocation, which are sequentially performed to optimize network efficiency and user experience.

For the SMSPA approach, we first propose a multiuser scheduling technique known as Clustered Enhanced Subset Greedy (C-ESG). To this end, we begin with an equal power loading strategy and introduce the C-ESG method, which selects multiple user equipment (UE) sets based on predetermined criteria, allowing for an efficient selection that closely approximates the optimal exhaustive search. This approach is particularly useful for assessing down-link performance in CF and CLCF networks, where it reduces computational complexity and improves network performance. We carry out an analysis of C-ESG, including deriving closed-form expressions for the sum-rate, and perform simulations to evaluate its effectiveness compared to existing scheduling techniques.

Following the multiuser scheduling phase, we employ gradient-based optimization techniques for power allocation within the SMSPA framework. Specifically, we employ gradient descent (GD) and gradient ascent (GA) methods to achieve efficient power distribution. In the power allocation phase, the GD technique minimizes the Mean Square Error (MSE) by iteratively adjusting the power levels in the direction of the steepest descent, while the GA method maximizes a simplified sum-rate expression. By integrating these gradient-based methods, the SMSPA scheme provides a comprehensive framework for resource management in CF and CLCF networks, which will be examined in detail throughout the chapter.

The remainder of this chapter is organized as follows: Section 3.1 provides an overview of the SMSPA resource allocation technique, including a schematic representation of the approach. Section 3.2 introduces the C-ESG multiuser scheduling technique. In Section 3.3, we conduct a detailed mathe-

mathematical analysis of the proposed scheduling method. Section 3.4 examines the signaling load and computational complexity associated with C-ESG in both CF and CLCF networks. Section 3.5 presents some simulation to assess the performance of the C-ESG multiuser scheduling approach. Moving forward, Section 3.6 describes the gradient descent-based power allocation technique within the SMSPA framework, focused on minimizing the MSE, followed by relevant simulation outcomes. Section 3.7 introduces a gradient ascent power allocation method designed to maximize a simplified sum-rate expression, with a discussion of corresponding simulation results. Finally, the chapter concludes with a summary in Section 3.8.

3.1 SMSPA Overview

In our study, we consider CLCF-mMIMO networks, specifically looking into the downlink aspect. Our focus is on the scheduling of multiple UEs and the allocation of power among them. To this end, we developed an approach denoted as the SMSPA scheme. This scheme is specially designed to maximize the sum-rate in the network.

The SMSPA scheme first considers the C-ESG technique, which is an approach to scheduling multiple UEs. When this technique is employed, we start with the assumption that power is distributed equally among all selected UEs. Using the C-ESG technique, we carefully examine different groups of UEs, evaluating them based on the sum-rate criterion which is going to give us the best performance. After this careful selection, the allocation of power is put into motion, targeting the chosen group of UEs using a GD or GA method also with the aim of maximizing the sum-rate. What we found from simulation results is that our SMSPA scheme for resource allocation consistently outperformed other existing methods. For a visual representation of how the SMSPA method works, we have created a block diagram shown in Fig. 3.1. This provides an illustration of our proposed method, allowing for a better understanding of its mechanism.

3.2 Proposed Clustered Enhanced Subset Greedy Algorithm

We consider the downlink of a CF-mMIMO network with M single-antenna APs and K uniformly distributed single-antenna UEs so that the total number of UEs in the network is much larger than the number of APs $K \gg M$. We employ a clustering approach which divides the whole area into C non-overlapping equal size areas each including the APs and the UEs of that

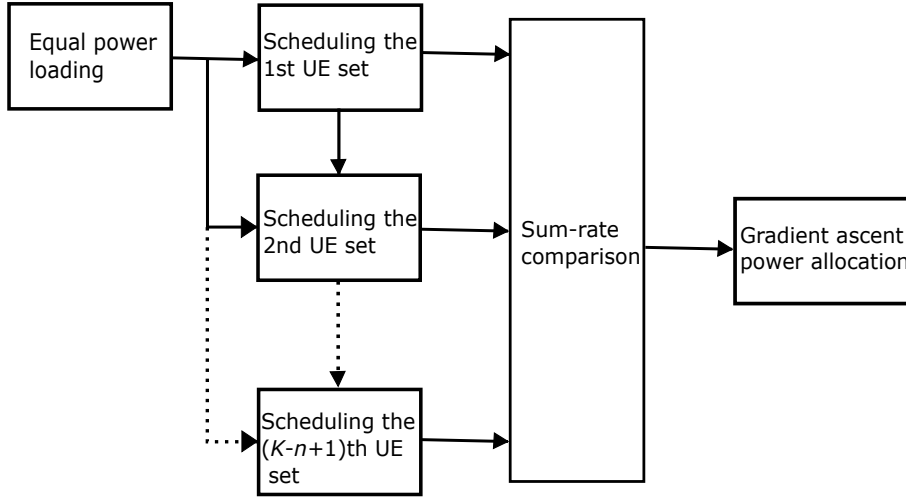


Figure 3.1: Block diagram of the proposed SMSPA resource allocation.

area that form a cluster. Thus the system model and the sum-rate expressions are the same as described in Section 2.5.2 and Section 2.5.3, and the only difference is that here we have shown the number of clusters by C instead of L .

Since M single-antenna APs cannot serve K single-antenna UEs, we have to find a smaller set of UEs which satisfies a system performance criterion. We can use an exhaustive search that compares performance of the all possible sets of UEs and selects the best set in each cluster. However, an exhaustive search has a huge computational cost and is thus impractical. Greedy algorithms are important mathematical techniques which have low cost and are simple and effective at approaching the global optimal solutions of complex problems, which motivates us to develop C-ESG. Therefore, based on the enhanced greedy algorithm in [25], we propose C-ESG which has much lower computational cost while approaching the performance of the optimal exhaustive search. C-ESG introduces a refined search with multiple sets of UEs and an evaluation step of the sets that departs from existing greedy techniques and allows a specific number of UEs to be scheduled.

In the proposed C-ESG algorithm, we first find a primary set of UEs in each cluster by adapting a similar approach to that of [12]. We apply the MMSE precoder considering the channel matrix of the UEs as $\mathbf{G}_{cc} \in \mathbb{C}^{M_c \times K_c}$, where K_c and M_c are the number of UEs and APs in the intended cluster, respectively. When the number of receive antennas is larger than the number of transmit antennas $K_c > M_c$, we aim to schedule n UEs out of K_c UEs so that $n \leq M_c$ and we can achieve a desirable sum-rate in those UEs. The selected set of UEs is shown by S_n and results in a row-reduced channel matrix $\mathbf{G}_{cc}(S_n)$. The goal is to obtain the highest achievable sum-rate as a solution

to the problem

$$\begin{aligned} & \max_{S_n} R_{MMSE}(S_n) \\ & \text{subject to } \|\mathbf{P}_c(S_n)\|^2 \leq P. \end{aligned} \quad (3-1)$$

where $R_{MMSE}(S_n)$ is defined as the sum-rate with the MMSE precoder when S_n is the set of intended UEs, P is the upper limit of the signal covariance matrix $\text{Trace}[\mathbf{C}_x] \leq P$, $\mathbf{P}_c(S_n) = \mathbf{W}_n \mathbf{D}_n$ is the precoding matrix including the normalized MMSE weight matrix $\mathbf{W}_n \in \mathbb{C}^{M_c \times n}$ and the power allocation matrix \mathbf{D}_n defined as

$$\mathbf{D}_n = \begin{bmatrix} \sqrt{p_1} & 0 & \cdots & 0 \\ 0 & \sqrt{p_2} & \cdots & 0 \\ \vdots & \vdots & \cdots & \vdots \\ 0 & 0 & \cdots & \sqrt{p_n} \end{bmatrix} \quad (3-2)$$

With equal power loading for simplicity and to focus on scheduling, a suboptimal greedy algorithm to solve the problem is used in the 1st stage of Algorithm 3, and the primary UE set $S_{n(1)}$ in each cluster is obtained. Then, to assess more sets, and in order to identify the minimum sum-rate, we select the UE with the lowest channel power from the first selected set $S_{n(1)}$, which we call the first excluded UE as

$$k_{ex(1)} = \arg \min_{k \in S_{n(1)}} \mathbf{g}_k^H \mathbf{g}_k \quad (3-3)$$

where $\mathbf{g}_k \in \mathbb{C}^{M_c \times 1}$ is channel vector to k th UE. Considering $\mathcal{K}_{cl} = \{1, 2, \dots, K_c\}$ as set of all UEs of the cluster, we define the first set of remaining or unselected UEs of the cluster as $\mathcal{K}_{clr(1)} = \mathcal{K}_{cl} \setminus S_{n(1)}$, which include the UEs other than $S_{n(1)}$. From the first set of remaining UEs, we select the UE with the highest channel power as the first new UE as

$$k_{new(1)} = \arg \max_{k \in \mathcal{K}_{clr(1)}} \mathbf{g}_k^H \mathbf{g}_k \quad (3-4)$$

Substituting the first excluded UE by the first new UE in $S_{n(1)}$, we achieve the second set of UEs as $S_{n(2)}$. We continue this procedure for the second set and so on, until we get $K_c - n$ UE sets in addition to the first set. Then, the i th UE set and the i th remaining UE set are shown as follows:

$$S_{n(i)} = \left(S_{n(i-1)} \setminus k_{ex(i-1)} \right) \cup k_{new(i-1)} \quad (3-5)$$

$$\mathcal{K}_{clr(i)} = \mathcal{K}_{clr(i-1)} \setminus k_{new(i-1)} \quad (3-6)$$

where $i \in \{2, \dots, K_c - n + 1\}$. In order to select the best set among the acquired sets, we can use the sum-rate expression in (2-24) for clustered CF network. Thus, the best set is chosen:

$$S_{n_b} = \arg \max_{S_n \in S_{n(j)}} \{R_c(S_n)\} \quad (3-7)$$

where $j \in \{1, \dots, K_c - n + 1\}$. The details of C-ESG are shown in Algorithm 3. We note that for applying the C-ESG algorithm to the CF system, we would change the K_c to K as the number of UEs in the CF network, \mathcal{K}_{cl} to $\mathcal{K} = \{1, 2, \dots, K\}$, $\mathcal{K}_{clr(i)}$ to $\mathcal{K}_{r(i)}$ as the i th remaining UE set, and accordingly, other functions and parameters would change to the network-wide level such as R_{CF} instead of R_c .

3.3

Analysis of the Proposed C-ESG Algorithm

In the proposed C-ESG algorithm, we use the channel power of the UEs so that there are different sets of UEs and we can assess more possible sets, approaching the optimal set while the complexity is significantly less than that of the exhaustive search. In each step of the C-ESG algorithm, we drop the UE with the lowest channel power and add the UE with the highest channel power so that a new set is achieved. If we schedule the maximum possible number of UEs $n = M_c$, we can show the sets of the selected UEs in stages $\{1, 2, \dots, j, \dots, K_c - M_c + 1\}$ as

$$\mathcal{S}_{EG} = \left\{ S_{EG_1}, S_{EG_2}, \dots, S_{EG_j}, \dots, S_{EG_{K_c - M_c + 1}} \right\} \quad (3-8)$$

where S_{EG_j} is the j th set of the proposed C-ESG method. Then, for C-ESG, there would be $K_c - M_c + 1$ sets in each cluster of the clustered CF system and $K - M + 1$ sets in the CF network. For the exhaustive search, we have the following sets as all the possible UE sets for all possible stages

$$\mathcal{S}_{Ex} = \left\{ 1, 2, \dots, j, \dots, \frac{K_c!}{M_c!(K_c - M_c)!}, S_{Ex_1}, S_{Ex_2}, \dots, S_{Ex_i}, \dots, S_{Ex_{\frac{K_c!}{M_c!(K_c - M_c)!}}} \right\} \quad (3-9)$$

where S_{Ex_i} is the i th set of the exhaustive search method. Therefore, there are $\frac{K_c!}{M_c!(K_c - M_c)!}$ sets in each cluster of the clustered CF network, and $\frac{K!}{M!(K - M)!}$ sets in the CF network. Thus, the cost of the C-ESG algorithm is much lower than that of the exhaustive search especially for large K_c or K .

Proposition. The sum-rate of C-ESG is bounded as

$$R_c(S_G) \leq R_c(S_C) \leq R_c(S_X) \quad (3-10)$$

where S_G is the set selected by the standard greedy method [12] as shown by S_n in the first stage of the Algorithm 3, S_C is the set selected by C-ESG algorithm, and S_X is the selected set by the exhaustive search

$$S_C = \operatorname{argmax}_{S_{EG_j}, j=1:K_c - M_c + 1} \left\{ R_c(S_{EG_j}) \right\}$$

$$S_X = \operatorname{argmax}_{S_{Ex_i}, i=1:\frac{K_c!}{M_c!(K_c - M_c)!}} \left\{ R_c(S_{Ex_i}) \right\}$$

Proof. Considering $S_G = \{n_{g_1}, n_{g_2}, \dots, n_{g_{M_c-1}}, n_{g_{M_c}}\}$ as the first set in C-

Algorithm 3: Proposed C-ESG Scheduling Algorithm.

```

1 stage=1
2   set  $l = 1$ ;
3   find a UE such that
4    $u_1 = \operatorname{argmax}_{k \in \mathcal{K}_{cl}} \mathbf{g}_k^H \mathbf{g}_k$ ;
5   set  $U_1 = u_1$  and denote the achieved rate
6    $R_{MMSE}(U_1)$ ;
7   while  $l < n$  do
8      $l = l + 1$ ;
9     find a UE  $u_l$  such that
10     $u_l = \operatorname{argmax}_{k \in (\mathcal{K}_{cl} \setminus U_{l-1})} R_{MMSE}(U_{l-1} \cup \{k\})$ ;
11    set  $U_l = U_{l-1} \cup \{u_l\}$  and denote the rate
12     $R_{MMSE}(U_l)$ ;
13    If  $R_{MMSE}(U_l) \leq R_{MMSE}(U_{l-1})$ , break
14     $l = l - 1$ ;
15  end
16   $S_{n(\text{stage})} = U_l$ ;
17  compute:  $R_c(S_{n(\text{stage})})$ ;
18   $\mathcal{K}_{clr(\text{stage})} = \mathcal{K}_{cl} \setminus S_{n(\text{stage})}$ ;
19   $k_{ex(\text{stage})} = \operatorname{argmin}_{k \in S_{n(\text{stage})}} \mathbf{g}_k^H \mathbf{g}_k$ ;
20   $k_{new(\text{stage})} = \operatorname{argmax}_{k \in \mathcal{K}_{clr(\text{stage})}} \mathbf{g}_k^H \mathbf{g}_k$ ;
21  for stage = 2 to  $K_c - n + 1$  do
22     $S_{n(\text{stage})} = (S_{n(\text{stage}-1)} \setminus k_{ex(\text{stage}-1)}) \cup k_{new(\text{stage}-1)}$ ;
23     $\mathcal{K}_{clr(\text{stage})} = \mathcal{K}_{clr(\text{stage}-1)} \setminus k_{new(\text{stage}-1)}$ ;
24     $k_{ex(\text{stage})} = \operatorname{argmin}_{k \in S_{n(\text{stage})}} \mathbf{g}_k^H \mathbf{g}_k$ ;
25     $k_{new(\text{stage})} = \operatorname{argmax}_{k \in \mathcal{K}_{clr(\text{stage})}} \mathbf{g}_k^H \mathbf{g}_k$ ;
26    compute:  $R_c(S_{n(\text{stage})})$ ;
27  end
28   $S_{n_b} = \operatorname{argmax}_{S_n \in S_{n(j)}} \{R_c(S_n)\}$ ;
29  Linear MMSE precoding of  $n$  scheduled UEs

```

ESG, suppose that we are at the second stage and the corresponding set is considered as $S_{En_2} = \{n_{g_1}, n_{g_2}, \dots, n_{g_{M_c-1}}, m_1\}$ which is different from S_G in one element, if m_1 and $n_{g_{M_c}}$ provide equal sum-rates, then, we would have $R_c(S_G) = R_c(S_C)$. In the case that we are in the j th stage (including $j = 2$), if we can have a better choice of subsets and if there is a subset in S_{En_j} that differs from S_G , then this would result in $R_c(S_C) = R_c(S_G) + \epsilon$, where $\epsilon > 0$. Thus, we can conclude that $R_c(S_C) \geq R_c(S_G)$. On the other hand, according to the combinations for the exhaustive search which includes all the possible cases, S_C is a special set of the exhaustive search combinations. Therefore, considering $S_X = \{n_1, n_2, \dots, n_{M_c}\}$, if C-ESG results in the same set $S_C = \{n_1, n_2, \dots, n_{M_c}\}$, then, $R_c(S_C) = R_c(S_X)$. However, if the set selected by the exhaustive search is a different set from the selected set by C-ESG, S_X would clearly be with a higher sum-rate than S_C . Thus, we would obtain $R_c(S_C) \leq R_c(S_X)$. Note that the same proposition holds for the analysis of the ESG algorithm in the CF network.

3.4

Impact of Clustering on Signaling Load and Scheduling Cost

The network-centric clustering technique divides the APs into non-overlapping cooperation clusters where the APs of each cluster collaborate in serving the UEs located in their joint coverage area [26, 27]. Note that extensions to overlapping clusters are also possible. Although the inter-cluster interference degrades the performance compared to the network-wide CF system, there is a substantial saving because the dimension reduction in each cluster results in significant signaling load and computational cost reduction. In addition, since the number of all UEs and the scheduled UEs in each cluster are substantially reduced compared to the network-wide CF, the scheduling costs are significantly reduced as well.

In order to assess the cost of the scheduling methods in terms of floating point operations (FLOPs), we notice that if the maximum possible number of UEs ($n = M_c$) are scheduled, according to the first stage of C-ESG, to obtain s_1 , $2M_cK_c$ FLOPs are required in each cluster and $2MK$ FLOPs for the CF. We also need $\frac{M_c(M_c+1)}{2} - 1$ FLOPs for all $R_{MMSE}(U_{l-1} \cup \{k\})$ during the while loop in each cluster, and $\frac{M(M+1)}{2} - 1$ FLOPs for CF. For the sum-rate in a cluster, we need $4M_cK_c^2 + 2K_c^3 + K_c$ FLOPs for calculating (2-25), $28M_cK_c^2 + 14K_c^3 + K_c + 4$ FLOPs for (2-26), thus, we need $32M_cK_c^2 + 16K_c^3 + 2K_c + 4$ FLOPs. For calculating the sum-rate in the CF network, we need K flops to compute (2-21) and $8MK^2 + 6K^3 + K$ FLOPs to calculate (4-5) and therefore, $8MK^2 + 6K^3 + 2K$ FLOPs for R_{CF} . Then, for k_{ex} the calculations are done when calculating s_1 , and for k_{new} , we need

$2M_c(K_c - M_c)$ or $2M(K - M)$ FLOPs for the cluster or CF, respectively. In the other stages (stage ≥ 2), assuming that in each stage we have only one new UE, for k_{ex} we need only $2M_c$ or $2M$ FLOPs in cluster or CF, respectively, and for k_{new} , the calculations are done in the first stage and we only select the new UE. We also require $32M_cK_c^2 + 16K_c^3 + 2K_c + 4$ FLOPs for R_c or $8MK^2 + 6K^3 + 2K$ FLOPs for R_{CF} . Accordingly, the number of required FLOPs for a cluster and for the CF network are as follows, respectively

$$N_{cl} = 16K_c^4 + 16(M_c + 1)K_c^3 + 2(-16M_c^2 + 16M_c + 1)K_c^2 + (4M_c + 6)K_c - \frac{7}{2}M_c^2 - \frac{7}{2}M_c + 3 \quad (3-11)$$

$$N_{CF} = 6K^4 + (2M + 6)K^3 + 2(-4M^2 + 4M + 1)K^2 + (4M + 2)K - \frac{7}{2}M^2 + \frac{1}{2}M - 1 \quad (3-12)$$

Note that Equation (3-11) should be summed over all clusters.

For a simple comparison of the number of channel parameters, we consider the CF channel coefficient $g_{m,k}$ as shown in section 2.5.2, which includes 1 parameter for small scale fading coefficient $h_{m,k}$, and 2 parameters for large scale fading coefficient $\beta_{m,k}$ including shadow fading and path loss as described in section 2.5.2. Then, the number of parameters for channels of a cluster and for CF channels are, respectively,

$$L_{cl} = 3M_cK_c \quad (3-13)$$

$$L_{CF} = 3MK \quad (3-14)$$

For clustered networks, Equation (3-13) must be summed over all clusters.

3.5

C-ESG Assessment

In this section, the performance of C-ESG, ESG (C-ESG for CF networks) and other existing scheduling approaches are assessed in terms of sum-rates. To this end, we have compared the exhaustive search, the greedy and C-ESG algorithms and the WSR method proposed in [9]. Since the WSR based user scheduling was designed for user-centric clustering, we have adapted it to our scenario so that we can maximize the WSR for the UEs in a cluster supported by the corresponding APs. We consider \mathbf{G} as the perfect CSI channel matrix, the channel estimate model as $\hat{\mathbf{G}} = \gamma\mathbf{G}$ and the channel estimation error represented by $\tilde{\mathbf{G}} = \alpha\mathbf{G}_e$, where \mathbf{G}_e is the estimation error of \mathbf{G} . Consequently, the channel matrix with imperfect CSI is given by $\mathbf{G}_I = \hat{\mathbf{G}} + \tilde{\mathbf{G}}$, such that $\alpha^2 + \gamma^2 = 1$ and $\gamma > \alpha$; here, we set $\gamma = \sqrt{0.95}$ and $\alpha = \sqrt{0.05}$. The channel coefficient between the m th AP and the k th

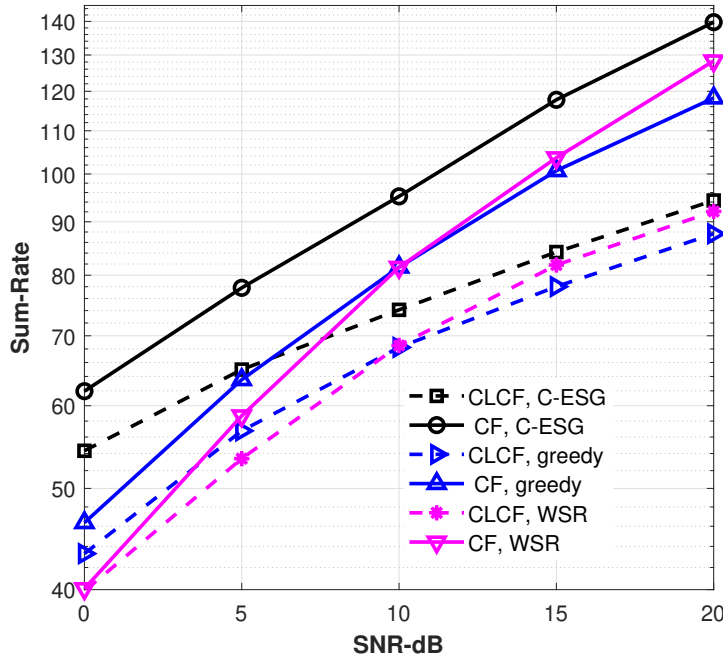


Figure 3.2: Performance of scheduling schemes for CLCF and CF, $M = 64$, $K = 256$ and $n = 64$

UE is $g_{mk} = [\mathbf{G}]_{m,k} = \sqrt{\beta_{mk}}h_{mk}$, where β_{mk} represents the large-scale fading coefficient accounting for path loss and shadowing effects, and $h_{mk} \sim \mathcal{CN}(0, 1)$ is the small-scale fading coefficient. These terms, h_{mk} , are independent and identically distributed (i.i.d.) random variables that are constant over a coherence interval and vary independently across different intervals. Similarly, $[\mathbf{G}_e]_{m,k} = \sqrt{\beta_{mk}}\tilde{h}_{mk}$, where \tilde{h}_{mk} represents the estimation error of h_{mk} . The matrices \mathbf{G} and \mathbf{G}_e each follow a complex Gaussian distribution with zero mean and unit variance [28], with \mathbf{G}_e independent of \mathbf{G} , as established in [19, 29]. A squared area with the side length of 400m is considered for the CF network equipped with M randomly located APs. The area includes K UEs, which are uniformly distributed for simplicity. We have used network-centric clustering with $C = 4$ non-overlapping clusters, where cluster c includes M_c randomly located APs and K_c uniformly distributed UEs with uniform power allocation.

Fig. 3.2 shows the sum-rate performance versus SNR of the CLCF and CF for different scheduling schemes when the MMSE precoder and imperfect CSI are considered. For all cases, the sum-rate increases with the SNR, however, that C-ESG outperforms other approaches. We also notice that for each scheduling algorithm, the advantage in information rates of CF over CLCF increases with the SNR because of the additional interference terms in Equation (2-26) for CLCF.

In Fig. 3.3, we have considered a network with a small number of UEs

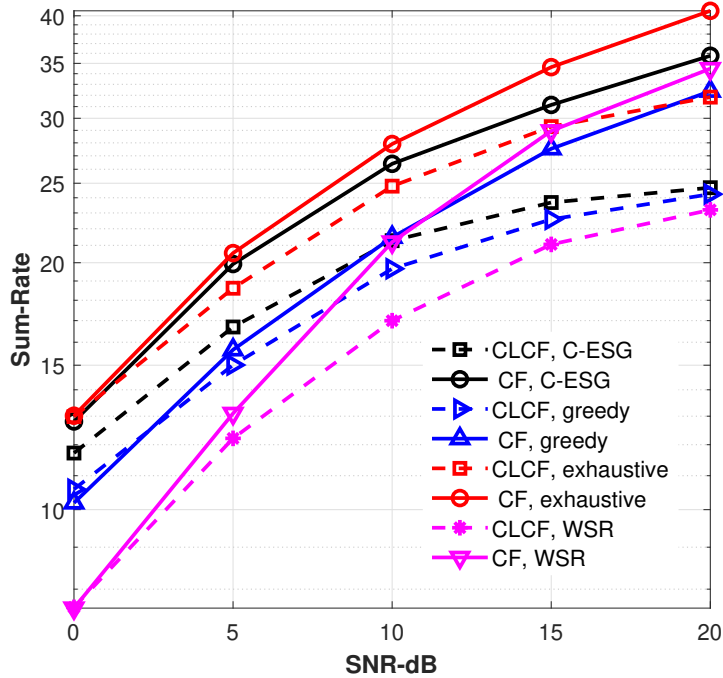


Figure 3.3: Performance of scheduling schemes for CLCF and CF, $M = 64$, $K = 16$ and $n = 8$ and exhaustive search scheduling included.

and scheduled up to half of the UEs, so that we can compare C-ESG with the optimal exhaustive search. We notice that the performance of C-ESG is closer to that of the exhaustive search especially in the CF case.

With the same ratio between UEs and APs as considered in Fig. 3.3, the number of FLOPs required for user scheduling in networks with different number of APs are shown in Fig. 3.4a. We can notice that when the size of the network increases, the number of FLOPs also increases. However, the use of clustering resulted in a remarkable decrease in the FLOPs so that for CLCF, it is negligible compared with the CF network. For a large number of APs, C-ESG has better performance than WSR, which requires less FLOPs. Fig. 3.4b shows that the signaling load in the CLCF is much lower than that of the CF network. Table 3.1 shows the complexity of the analyzed techniques for CLCF networks. C-ESG requires much less FLOPs than the exhaustive search. Although the complexity of C-ESG is slightly higher, its performance is significantly improved as compared to the greedy and WSR algorithms.

3.6

GD Power Allocation in the SMSPA Scheme

Upon the successful application of the C-ESG technique for multiuser scheduling, we proceed to present a power allocation algorithm that leverages the gradient descent method to minimize the MSE. The rationale behind this

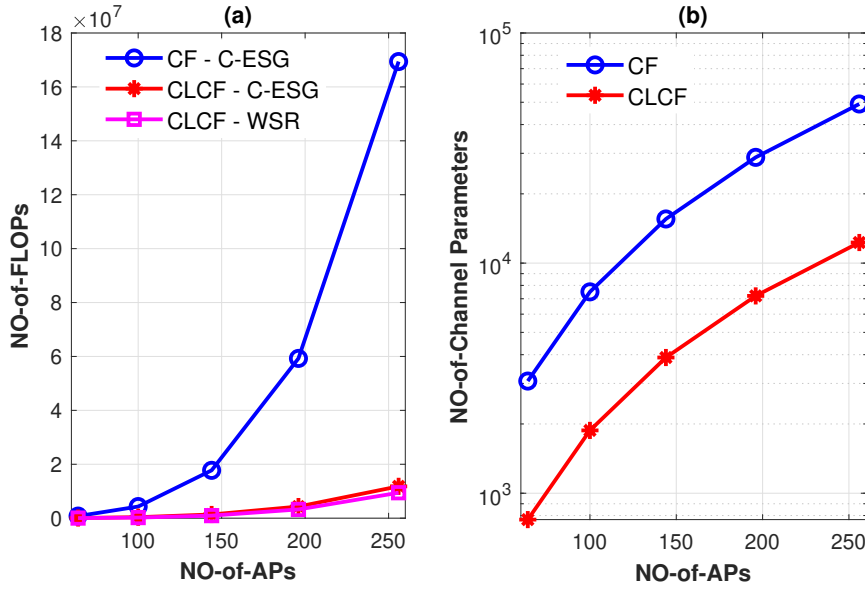


Figure 3.4: Computational complexity for the CF and the CLCF networks, (a): Number of required FLOPs for scheduling the UEs by C-ESG and WSR methods, (b): Signaling load.

Table 3.1: Computational complexity of different methods, $M = 64$, $K = 16$, and $n = 8$.

Network	Scheduling method	NO of FLOPs
CLCF	C-ESG	70728
CLCF	Greedy	37432
CLCF	WSR	52864
CLCF	Exhaustive search	221472

is that minimizing MSE maximizes the signal to interference-plus-noise ratio (SINR), which corresponds to maximizing the sum-rate [30] under Gaussian signaling. This equivalence arises because reducing the MSE between the transmitted and estimated symbols at the receiver increases the SINR. In a system employing Gaussian signaling, the maximization of SINR translates directly into the maximization of the information rates, thereby achieving the objective of sum-rate maximization. By focusing on more tractable MSE minimization power allocation strategy, we develop simpler algorithms. Our proposed power allocation approach notably enhances the sum-rate performance.

Here, for a mathematical proof that shows MSE minimization leads to sum-rate maximization, we proceed as follows:

In a communication system, consider the received signal \mathbf{y}_k for user k modeled as:

$$\mathbf{y}_k = \mathbf{h}_k \mathbf{x}_k + \mathbf{n}_k, \quad (3-15)$$

where \mathbf{x}_k is the transmitted signal, \mathbf{h}_k is the channel vector, and \mathbf{n}_k is the

noise vector with variance N_0 .

The linear estimate $\hat{\mathbf{x}}_k$ that minimizes the Mean Squared Error (MSE) for user k is given by [31]:

$$\hat{\mathbf{x}}_k = \frac{\mathbb{E}[|\mathbf{x}_k|^2]}{\mathbb{E}[|\mathbf{x}_k|^2]\|\mathbf{h}_k\|^2 + N_0} \mathbf{h}_k^H \mathbf{y}_k. \quad (3-16)$$

The corresponding Minimum Mean Squared Error (MMSE) for user k is then [31]:

$$\text{MMSE}_k = \frac{\mathbb{E}[|\mathbf{x}_k|^2]N_0}{\mathbb{E}[|\mathbf{x}_k|^2]\|\mathbf{h}_k\|^2 + N_0}. \quad (3-17)$$

We can express the MMSE in terms of the Signal-to-Noise Ratio (SNR) as follows. By defining the SNR for user k as:

$$\text{SNR}_k = \frac{\mathbb{E}[|\mathbf{x}_k|^2]\|\mathbf{h}_k\|^2}{N_0}, \quad (3-18)$$

we can rewrite the MMSE equation as:

$$\text{MMSE}_k = \frac{\mathbb{E}[|\mathbf{x}_k|^2]}{\text{SNR}_k + 1}. \quad (3-19)$$

In the case when $\mathbf{x}_k \sim \mathcal{CN}(0, \sigma_x^2)$, this estimator yields the minimum mean squared error among all estimators, linear or non-linear. Given this, we can replace $\mathbb{E}[|\mathbf{x}_k|^2]$ with σ_x^2 :

$$\text{MMSE}_k = \frac{\sigma_x^2}{\text{SNR}_k + 1}. \quad (3-20)$$

The achievable rate for user k can be expressed using the Shannon capacity formula:

$$R_k = \log_2(1 + \text{SNR}_k). \quad (3-21)$$

The total sum-rate for K users is then:

$$\text{SR} = \sum_{k=1}^K R_k = \sum_{k=1}^K \log_2(1 + \text{SNR}_k). \quad (3-22)$$

From the MMSE expression, we observe that:

$$\text{SNR}_k = \frac{\sigma_x^2}{\text{MMSE}_k} - 1. \quad (3-23)$$

Substituting this back into the rate expression, we obtain:

$$R_k = \log_2 \left(1 + \left(\frac{\sigma_x^2}{\text{MMSE}_k} - 1 \right) \right) = \log_2 \left(\frac{\sigma_x^2}{\text{MMSE}_k} \right), \quad (3-24)$$

which simplifies to

$$R_k = \log_2 \left(\frac{\sigma_x^2}{\text{MMSE}_k} \right) = \log_2(\sigma_x^2) - \log_2(\text{MMSE}_k). \quad (3-25)$$

Thus, the total sum-rate can be written as:

$$\text{SR} = \sum_{k=1}^K R_k = \sum_{k=1}^K \log_2(\sigma_x^2) - \sum_{k=1}^K \log_2(\text{MMSE}_k). \quad (3-26)$$

Since $f(x) = \log_2(x)$ is a concave function [32], we use Jensen's inequality for concave functions, which states that for any set of positive real numbers $\{x_k\}$ and weights $\{a_k\}$ such that $a_k \geq 0$ and $\sum_{k=1}^K a_k = 1$:

$$f\left(\sum_{k=1}^K a_k x_k\right) \geq \sum_{k=1}^K a_k f(x_k) \quad (3-27)$$

We set $a_k = \frac{1}{K}$ and thus we have:

$$K \log_2\left(\frac{1}{K} \sum_{k=1}^K \text{MMSE}_k\right) \geq \sum_{k=1}^K \log_2(\text{MMSE}_k). \quad (3-28)$$

Since we are minimizing $\sum_{k=1}^K \log_2(\text{MMSE}_k)$, we can consider the minimum of its upperbound which is as follows as well

$$K \log_2\left(\frac{1}{K} \sum_{k=1}^K \text{MMSE}_k\right) \quad (3-29)$$

Given that monotonic transformations of functions preserve the locations of their extrema and that the logarithm function $\log_2(x)$ is monotonically increasing for $x > 0$, minimizing $\log_2\left(\frac{1}{K} \sum_{k=1}^K \text{MMSE}_k\right)$ is equivalent to minimizing $\frac{1}{K} \sum_{k=1}^K \text{MMSE}_k$, which in turn minimizes $\sum_{k=1}^K \text{MMSE}_k$.

3.6.1 GD Power Allocation Formulation

Since the estimated received signal of the cluster c of Equation (2-23) consists of a desired term and the terms associated with imperfect CSI, inter-cluster interference and noise, applying power allocation, we rewrite the estimated signal as follows

$$\begin{aligned} \mathbf{y}_c = & \sqrt{\rho_f} \hat{\mathbf{G}}_{cc}^T \mathbf{W}_c \mathbf{D}_c \mathbf{x}_c + \sqrt{\rho_f} \tilde{\mathbf{G}}_{cc}^T \mathbf{P}_c \mathbf{x}_c + \\ & \sum_{i=1, i \neq c}^C \sqrt{\rho_f} \mathbf{G}_{ic}^T \mathbf{P}_i \mathbf{x}_i + \mathbf{w}_c \end{aligned} \quad (3-30)$$

We use the MSE between the transmitted signal and the estimated signal at the receiver as the objective function because MSE minimization is equivalent to sum-rate maximization as described before. Therefore, the following power allocation problem is defined:

$$\begin{aligned} \min_{\mathbf{d}_c} & \mathbb{E}[\varepsilon] \\ \text{subject to} & \|\mathbf{W}_c \text{diag}(\mathbf{d}_c)\|^2 \leq P \end{aligned} \quad (3-31)$$

where the error is

$$\varepsilon = \|\mathbf{x}_c - \mathbf{y}_c\|^2 \quad (3-32)$$

and

$$\begin{aligned} \mathbf{x}_c - \mathbf{y}_c &= \mathbf{x}_c - \sqrt{\rho_f} \hat{\mathbf{G}}_{cc}^T \mathbf{W}_c \text{diag}(\mathbf{d}_c) \mathbf{x}_c \\ &\quad - \sqrt{\rho_f} \tilde{\mathbf{G}}_{cc}^T \mathbf{P}_c \mathbf{x}_c - \sum_{i=1, i \neq c}^C \sqrt{\rho_f} \mathbf{G}_{ic}^T \mathbf{P}_i \mathbf{x}_i - \mathbf{w}_c \end{aligned} \quad (3-33)$$

Using Equations (3-32) and (3-33), the error equation is derived as follows,

$$\begin{aligned} \varepsilon &= \mathbf{x}_c^H \mathbf{x}_c + \mathbf{w}_c^H \mathbf{w}_c + \rho_f \mathbf{x}_c^H \text{diag}(\mathbf{d}_c) \mathbf{W}_c^H \hat{\mathbf{G}}_{cc}^* \hat{\mathbf{G}}_{cc}^T \mathbf{W}_c \text{diag}(\mathbf{d}_c) \mathbf{x}_c + \\ &\quad \rho_f \mathbf{x}_c^H \mathbf{P}_c^H \tilde{\mathbf{G}}_{cc}^* \tilde{\mathbf{G}}_{cc}^T \mathbf{P}_c \mathbf{x}_c + \sum_{i=1, i \neq c}^C \rho_f \mathbf{x}_i^H \mathbf{P}_i^H \mathbf{G}_{ic}^* \mathbf{G}_{ic}^T \mathbf{P}_i \mathbf{x}_i - \sqrt{\rho_f} \mathbf{x}_c^H \hat{\mathbf{G}}_{cc}^T \mathbf{W}_c \text{diag}(\mathbf{d}_c) \mathbf{x}_c - \\ &\quad \sqrt{\rho_f} \mathbf{x}_c^H \text{diag}(\mathbf{d}_c) \mathbf{W}_c^H \hat{\mathbf{G}}_{cc}^* \mathbf{x}_c - \sqrt{\rho_f} \mathbf{x}_c^H \tilde{\mathbf{G}}_{cc}^T \mathbf{P}_c \mathbf{x}_c - \sqrt{\rho_f} \mathbf{x}_c^H \mathbf{P}_c^H \tilde{\mathbf{G}}_{cc}^* \mathbf{x}_c - \\ &\quad \sum_{i=1, i \neq c}^C \sqrt{\rho_f} \mathbf{x}_c^H \mathbf{G}_{ic}^T \mathbf{P}_i \mathbf{x}_i - \sum_{i=1, i \neq c}^C \sqrt{\rho_f} \mathbf{x}_i^H \mathbf{P}_i^H \mathbf{G}_{ic}^* \mathbf{x}_c - \mathbf{x}_c^H \mathbf{w}_c - \mathbf{w}_c^H \mathbf{x}_c + \\ &\quad \rho_f \mathbf{x}_c^H \text{diag}(\mathbf{d}_c) \mathbf{W}_c^H \hat{\mathbf{G}}_{cc}^* \tilde{\mathbf{G}}_{cc}^T \mathbf{P}_c \mathbf{x}_c + \rho_f \mathbf{x}_c^H \mathbf{P}_c^H \tilde{\mathbf{G}}_{cc}^* \hat{\mathbf{G}}_{cc}^T \mathbf{W}_c \text{diag}(\mathbf{d}_c) \mathbf{x}_c + \\ &\quad \sum_{i=1, i \neq c}^C \rho_f \mathbf{x}_c^H \text{diag}(\mathbf{d}_c) \mathbf{W}_c^H \hat{\mathbf{G}}_{cc}^* \mathbf{G}_{ic}^T \mathbf{P}_i \mathbf{x}_i + \sum_{i=1, i \neq c}^C \rho_f \mathbf{x}_i^H \mathbf{P}_i^H \mathbf{G}_{ic}^* \hat{\mathbf{G}}_{cc}^T \mathbf{W}_c \text{diag}(\mathbf{d}_c) \mathbf{x}_c + \\ &\quad \sqrt{\rho_f} \mathbf{x}_c^H \text{diag}(\mathbf{d}_c) \mathbf{W}_c^H \hat{\mathbf{G}}_{cc}^* \mathbf{w}_c + \sqrt{\rho_f} \mathbf{w}_c^H \hat{\mathbf{G}}_{cc}^T \mathbf{W}_c \text{diag}(\mathbf{d}_c) \mathbf{x}_c + \\ &\quad \sum_{i=1, i \neq c}^C \sqrt{\rho_f} \mathbf{x}_c^H \mathbf{P}_c^H \tilde{\mathbf{G}}_{cc}^* \mathbf{G}_{ic}^T \mathbf{P}_i \mathbf{x}_i + \sum_{i=1, i \neq c}^C \sqrt{\rho_f} \mathbf{x}_i^H \mathbf{P}_i^H \mathbf{G}_{ic}^* \tilde{\mathbf{G}}_{cc}^T \mathbf{P}_c \mathbf{x}_c + \sqrt{\rho_f} \mathbf{w}_c^H \tilde{\mathbf{G}}_{cc}^T \mathbf{P}_c \mathbf{x}_c + \\ &\quad \sqrt{\rho_f} \mathbf{x}_c^H \mathbf{P}_c^H \tilde{\mathbf{G}}_{cc}^* \mathbf{w}_c + \sum_{i=1, i \neq c}^C \sqrt{\rho_f} \mathbf{x}_i^H \mathbf{P}_i^H \mathbf{G}_{ic}^* \mathbf{w}_c + \sum_{i=1, i \neq c}^C \sqrt{\rho_f} \mathbf{w}_c^H \mathbf{G}_{ic}^T \mathbf{P}_i \mathbf{x}_i \end{aligned} \quad (3-34)$$

Since (3-34) is scalar, it remains the same when the trace operator is applied over the right hand side. Then, using the property $Tr(\mathbf{A} + \mathbf{B}) = Tr(\mathbf{A}) + Tr(\mathbf{B})$, where \mathbf{A} and \mathbf{B} are two equal dimension matrices, the error is rewritten as follows

$$\begin{aligned}
\varepsilon = & Tr(\mathbf{x}_c^H \mathbf{x}_c) - Tr(\mathbf{x}_c^H \mathbf{w}_c) - Tr(\mathbf{w}_c^H \mathbf{x}_c) + Tr(\mathbf{w}_c^H \mathbf{w}_c) + \\
& Tr\left(\rho_f \mathbf{x}_c^H \text{diag}(\mathbf{d}_c) \mathbf{W}_c^H \hat{\mathbf{G}}_{cc}^* \hat{\mathbf{G}}_{cc}^T \mathbf{W}_c \text{diag}(\mathbf{d}_c) \mathbf{x}_c\right) + \\
& Tr\left(\rho_f \mathbf{x}_c^H \mathbf{P}_c^H \tilde{\mathbf{G}}_{cc}^* \tilde{\mathbf{G}}_{cc}^T \mathbf{P}_c \mathbf{x}_c\right) + Tr\left(\sum_{i=1, i \neq c}^C \rho_f \mathbf{x}_i^H \mathbf{P}_i^H \mathbf{G}_{ic}^* \mathbf{G}_{ic}^T \mathbf{P}_i \mathbf{x}_i\right) - \\
& Tr\left(\sqrt{\rho_f} \mathbf{x}_c^H \hat{\mathbf{G}}_{cc}^T \mathbf{W}_c \text{diag}(\mathbf{d}_c) \mathbf{x}_c\right) - Tr\left(\sqrt{\rho_f} \mathbf{x}_c^H \text{diag}(\mathbf{d}_c) \mathbf{W}_c^H \hat{\mathbf{G}}_{cc}^* \mathbf{x}_c\right) - \\
& Tr\left(\sqrt{\rho_f} \mathbf{x}_c^H \tilde{\mathbf{G}}_{cc}^T \mathbf{P}_c \mathbf{x}_c\right) - Tr\left(\sqrt{\rho_f} \mathbf{x}_c^H \mathbf{P}_c^H \tilde{\mathbf{G}}_{cc}^* \mathbf{x}_c\right) - \\
& Tr\left(\sum_{i=1, i \neq c}^C \sqrt{\rho_f} \mathbf{x}_c^H \mathbf{G}_{ic}^T \mathbf{P}_i \mathbf{x}_i\right) - Tr\left(\sum_{i=1, i \neq c}^C \sqrt{\rho_f} \mathbf{x}_i^H \mathbf{P}_i^H \mathbf{G}_{ic}^* \mathbf{x}_c\right) + \\
& Tr\left(\rho_f \mathbf{x}_c^H \text{diag}(\mathbf{d}_c) \mathbf{W}_c^H \hat{\mathbf{G}}_{cc}^* \hat{\mathbf{G}}_{cc}^T \mathbf{P}_c \mathbf{x}_c\right) + Tr\left(\rho_f \mathbf{x}_c^H \mathbf{P}_c^H \tilde{\mathbf{G}}_{cc}^* \hat{\mathbf{G}}_{cc}^T \mathbf{W}_c \text{diag}(\mathbf{d}_c) \mathbf{x}_c\right) + \\
& Tr\left(\sum_{i=1, i \neq c}^C \rho_f \mathbf{x}_c^H \text{diag}(\mathbf{d}_c) \mathbf{W}_c^H \hat{\mathbf{G}}_{cc}^* \mathbf{G}_{ic}^T \mathbf{P}_i \mathbf{x}_i\right) + Tr\left(\sum_{i=1, i \neq c}^C \rho_f \mathbf{x}_i^H \mathbf{P}_i^H \mathbf{G}_{ic}^* \hat{\mathbf{G}}_{cc}^T \mathbf{W}_c \text{diag}(\mathbf{d}_c) \mathbf{x}_c\right) + \\
& Tr\left(\sqrt{\rho_f} \mathbf{x}_c^H \text{diag}(\mathbf{d}_c) \mathbf{W}_c^H \hat{\mathbf{G}}_{cc}^* \mathbf{w}_c\right) + Tr\left(\sqrt{\rho_f} \mathbf{w}_c^H \hat{\mathbf{G}}_{cc}^T \mathbf{W}_c \text{diag}(\mathbf{d}_c) \mathbf{x}_c\right) + \\
& Tr\left(\sum_{i=1, i \neq c}^C \sqrt{\rho_f} \mathbf{x}_c^H \mathbf{P}_c^H \tilde{\mathbf{G}}_{cc}^* \mathbf{G}_{ic}^T \mathbf{P}_i \mathbf{x}_i\right) + Tr\left(\sum_{i=1, i \neq c}^C \sqrt{\rho_f} \mathbf{x}_i^H \mathbf{P}_i^H \mathbf{G}_{ic}^* \tilde{\mathbf{G}}_{cc}^T \mathbf{P}_c \mathbf{x}_c\right) + \\
& Tr\left(\sqrt{\rho_f} \mathbf{w}_c^H \tilde{\mathbf{G}}_{cc}^T \mathbf{P}_c \mathbf{x}_c\right) + Tr\left(\sqrt{\rho_f} \mathbf{x}_c^H \mathbf{P}_c^H \tilde{\mathbf{G}}_{cc}^* \mathbf{w}_c\right) + \\
& Tr\left(\sum_{i=1, i \neq c}^C \sqrt{\rho_f} \mathbf{x}_i^H \mathbf{P}_i^H \mathbf{G}_{ic}^* \mathbf{w}_c\right) + Tr\left(\sum_{i=1, i \neq c}^C \sqrt{\rho_f} \mathbf{w}_c^H \mathbf{G}_{ic}^T \mathbf{P}_i \mathbf{x}_i\right)
\end{aligned} \tag{3-35}$$

Considering the transmitted signal of each cluster uncorrelated with the transmitted signal from other clusters, the expected value of Equation (3-35) changes as follows

$$\begin{aligned}
 \mathbb{E}[\varepsilon] = & Tr(\mathbf{C}_{\mathbf{x}_c}) + Tr(\mathbf{C}_{\mathbf{w}_c}) + \\
 & Tr\left(\rho_f \text{diag}(\mathbf{d}_c) \mathbf{W}_c^H \hat{\mathbf{G}}_{cc}^* \hat{\mathbf{G}}_{cc}^T \mathbf{W}_c \text{diag}(\mathbf{d}_c) \mathbf{C}_{\mathbf{x}_c}\right) + \\
 & Tr\left(\rho_f \mathbf{P}_c^H \tilde{\mathbf{G}}_{cc}^* \tilde{\mathbf{G}}_{cc}^T \mathbf{P}_c \mathbf{C}_{\mathbf{x}_c}\right) + \sum_{i=1, i \neq c}^C Tr\left(\rho_f \mathbf{P}_i^H \mathbf{G}_{ic}^* \mathbf{G}_{ic}^T \mathbf{P}_i \mathbf{C}_{\mathbf{x}_i}\right) - \\
 & Tr\left(\sqrt{\rho_f} \hat{\mathbf{G}}_{cc}^T \mathbf{W}_c \text{diag}(\mathbf{d}_c) \mathbf{C}_{\mathbf{x}_c}\right) - Tr\left(\sqrt{\rho_f} \text{diag}(\mathbf{d}_c) \mathbf{W}_c^H \hat{\mathbf{G}}_{cc}^* \mathbf{C}_{\mathbf{x}_c}\right) - \\
 & Tr\left(\sqrt{\rho_f} \tilde{\mathbf{G}}_{cc}^T \mathbf{P}_c \mathbf{C}_{\mathbf{x}_c}\right) - Tr\left(\sqrt{\rho_f} \mathbf{P}_c^H \tilde{\mathbf{G}}_{cc}^* \mathbf{C}_{\mathbf{x}_c}\right) + \\
 & Tr\left(\rho_f \text{diag}(\mathbf{d}_c) \mathbf{W}_c^H \hat{\mathbf{G}}_{cc}^* \tilde{\mathbf{G}}_{cc}^T \mathbf{P}_c \mathbf{C}_{\mathbf{x}_c}\right) + Tr\left(\rho_f \mathbf{P}_c^H \tilde{\mathbf{G}}_{cc}^* \hat{\mathbf{G}}_{cc}^T \mathbf{W}_c \text{diag}(\mathbf{d}_c) \mathbf{C}_{\mathbf{x}_c}\right) \\
 = & n + n\sigma_w^2 + Tr\left(\rho_f \text{diag}(\mathbf{d}_c) \mathbf{W}_c^H \hat{\mathbf{G}}_{cc}^* \hat{\mathbf{G}}_{cc}^T \mathbf{W}_c \text{diag}(\mathbf{d}_c)\right) + \\
 & Tr\left(\rho_f \mathbf{P}_c^H \tilde{\mathbf{G}}_{cc}^* \tilde{\mathbf{G}}_{cc}^T \mathbf{P}_c\right) + \sum_{i=1, i \neq c}^C Tr\left(\rho_f \mathbf{P}_i^H \mathbf{G}_{ic}^* \mathbf{G}_{ic}^T \mathbf{P}_i\right) - \\
 & Tr\left(\sqrt{\rho_f} \hat{\mathbf{G}}_{cc}^T \mathbf{W}_c \text{diag}(\mathbf{d}_c)\right) - Tr\left(\sqrt{\rho_f} \text{diag}(\mathbf{d}_c) \mathbf{W}_c^H \hat{\mathbf{G}}_{cc}^*\right) - \\
 & Tr\left(\sqrt{\rho_f} \tilde{\mathbf{G}}_{cc}^T \mathbf{P}_c\right) - Tr\left(\sqrt{\rho_f} \mathbf{P}_c^H \tilde{\mathbf{G}}_{cc}^*\right) + \\
 & Tr\left(\rho_f \text{diag}(\mathbf{d}_c) \mathbf{W}_c^H \hat{\mathbf{G}}_{cc}^* \tilde{\mathbf{G}}_{cc}^T \mathbf{P}_c\right) + Tr\left(\rho_f \mathbf{P}_c^H \tilde{\mathbf{G}}_{cc}^* \hat{\mathbf{G}}_{cc}^T \mathbf{W}_c \text{diag}(\mathbf{d}_c)\right)
 \end{aligned} \tag{3-36}$$

In Equation (3-36), we take the derivation with respect to the power loading matrix \mathbf{D}_c and the equality $\frac{\partial Tr(\mathbf{AB})}{\partial \mathbf{A}} = \mathbf{B} \odot \mathbf{I}$ is used where \mathbf{A} is a diagonal matrix and \odot shows the Hadamard product. Thus, we obtain

$$\begin{aligned}
 \frac{\partial \mathbb{E}(\varepsilon)}{\partial \mathbf{D}_c} = & 2\rho_f \left(\mathbf{W}_c^H \hat{\mathbf{G}}_{cc}^* \hat{\mathbf{G}}_{cc}^T \mathbf{W}_c \text{diag}(\mathbf{d}_c) \right) \odot \mathbf{I} - \\
 & \sqrt{\rho_f} \hat{\mathbf{G}}_{cc}^T \mathbf{W}_c \odot \mathbf{I} - \sqrt{\rho_f} \mathbf{W}_c^H \hat{\mathbf{G}}_{cc}^* \odot \mathbf{I} + \\
 & \rho_f \mathbf{W}_c^H \tilde{\mathbf{G}}_{cc}^* \tilde{\mathbf{G}}_{cc}^T \mathbf{P}_c \odot \mathbf{I} + \rho_f \mathbf{P}_c^H \tilde{\mathbf{G}}_{cc}^* \hat{\mathbf{G}}_{cc}^T \mathbf{W}_c \odot \mathbf{I} = \\
 & 2\rho_f \left(\mathbf{W}_c^H \hat{\mathbf{G}}_{cc}^* \hat{\mathbf{G}}_{cc}^T \mathbf{W}_c \text{diag}(\mathbf{d}_c) \right) \odot \mathbf{I} - \\
 & 2\sqrt{\rho_f} Re \left\{ \mathbf{W}_c^H \hat{\mathbf{G}}_{cc}^* \odot \mathbf{I} \right\} + 2\rho_f Re \left\{ \mathbf{W}_c^H \hat{\mathbf{G}}_{cc}^* \tilde{\mathbf{G}}_{cc}^T \mathbf{P}_c \odot \mathbf{I} \right\}
 \end{aligned} \tag{3-37}$$

where $Re \{ \mathbf{A} \}$ shows the real part of matrix \mathbf{A} . We can use a stochastic gradient descent approach to update the power allocation coefficient as follows:

$$\begin{aligned}
 \mathbf{d}_c(i) = & \mathbf{d}_c(i-1) - \lambda \frac{\partial \mathbb{E}(\varepsilon)}{\partial \mathbf{D}_c} = \\
 & \mathbf{d}_c(i-1) - 2\rho_f \lambda \left(\mathbf{W}_c^H \hat{\mathbf{G}}_{cc}^* \hat{\mathbf{G}}_{cc}^T \mathbf{W}_c \text{diag}(\mathbf{d}_c(i-1)) \right) \odot \mathbf{I} + \\
 & 2\sqrt{\rho_f} \lambda Re \left\{ \mathbf{W}_c^H \hat{\mathbf{G}}_{cc}^* \odot \mathbf{I} \right\} - 2\rho_f \lambda Re \left\{ \mathbf{W}_c^H \hat{\mathbf{G}}_{cc}^* \tilde{\mathbf{G}}_{cc}^T \mathbf{P}_c \odot \mathbf{I} \right\}
 \end{aligned} \tag{3-38}$$

where i is the iteration index, and λ is the positive step size. Before running the adaptive algorithm, the transmit power constraint should be satisfied so

that $\|\mathbf{W}_c \text{diag}(\mathbf{d}_c)\|^2 = \|\mathbf{P}_c\|^2 \leq P$ where \mathbf{P}_c is the precoding matrix, \mathbf{W}_c is the normalized precoding matrix and $\text{diag}(\mathbf{d}_c)$ is the power allocation matrix. Therefore, the power scaling factor $\eta = \sqrt{\frac{\text{Tr}(\mathbf{P}_c \mathbf{P}_c^H)}{\text{Tr}(\mathbf{W}_c \text{diag}(\mathbf{d}_c) \mathbf{W}_c^H)}}$ is employed in each iteration to scale the coefficients properly. The adaptive power allocation is summarized in Algorithm 4 where I_t iterations are considered.

Algorithm 4: Gradient Descent Power Allocation Algorithm for MSE Minimization.

```

1 Input  $\mathbf{G}_{cc}$ ,  $\mathbf{P}_c$ ,  $\mathbf{W}_c$ ,  $\lambda$  ;
2  $\mathbf{d}_c(1) = \mathbf{0}$  ;
3 for  $i = 2$  to  $I_t$  do
4    $\frac{\partial \mathbb{E}(\varepsilon)}{\partial \mathbf{D}_c} = 2\rho_f \left( \mathbf{W}_c^H \hat{\mathbf{G}}_{cc}^* \hat{\mathbf{G}}_{cc}^T \mathbf{W}_c \text{diag}(\mathbf{d}_c(i-1)) \right) \odot \mathbf{I}$ 
5    $-2\sqrt{\rho_f} \text{Re} \left\{ \mathbf{W}_c^H \hat{\mathbf{G}}_{cc}^* \odot \mathbf{I} \right\} + 2\rho_f \text{Re} \left\{ \mathbf{W}_c^H \hat{\mathbf{G}}_{cc}^* \tilde{\mathbf{G}}_{cc}^T \mathbf{P}_c \odot \mathbf{I} \right\}$ ;
6    $\mathbf{d}_c(i) = \mathbf{d}_c(i-1) - \lambda \frac{\partial \mathbb{E}(\varepsilon)}{\partial \mathbf{D}_c}$  ;
7   if  $\text{Tr}(\mathbf{W}_c \text{diag}(\mathbf{d}_c(i) \cdot \mathbf{d}_c(i)) \mathbf{W}_c^H) \neq \text{Tr}(\mathbf{P}_c \mathbf{P}_c^H)$  then
8      $\eta = \sqrt{\frac{\text{Tr}(\mathbf{P}_c \mathbf{P}_c^H)}{\text{Tr}(\mathbf{W}_c \text{diag}(\mathbf{d}_c(i) \cdot \mathbf{d}_c(i)) \mathbf{W}_c^H)}}$ ;
9      $\mathbf{d}_c(i) = \eta \mathbf{d}_c(i)$ ;
10  end
11 end

```

3.6.2 Simulation Results for SMSPA with GD

In this section, we assess the sum-rate performances of the CF and CLCF scenarios for the proposed SMSPA scheme and algorithms and the existing techniques including exhaustive search (ExS), greedy (Gr) and the WSR method proposed in [9] which is adapted to the proposed clustering by maximizing WSR for the UEs of the clusters supported by the corresponding APs. The CF network is particularly considered as a squared area with the side length of 400m including M single-antennas randomly located APs and K uniformly distributed single antenna UEs. For a CLCF network, we consider the same area divided into $C = 4$ non-overlapping clusters so that cluster c includes M_c single-antennas randomly located APs and K_c uniformly distributed single antenna UEs. To summarize, the main simulation parameters are described in Table 3.2.

To highlight the power allocation effect, the performance of the proposed resource allocation technique is compared with the system which has employed the proposed user scheduling and equal power loading (EPL) for CF and CLCF networks in Fig. 3.5 while ZF and MMSE precoders are used. As it

Table 3.2: Simulation parameters

Parameter	Value
Carrier frequency	1900 MHz
AP antenna height	15 m
UE antenna height	1.5 m
Shadowing factor	8 dB
Area size	400 m ²
NO of clusters	4
Symbol energy	$P_s=1$
Transmit power	$M \times P_s$

is visible, sum-rates improve by increasing the SNR and MMSE precoder has outperformed ZF. We can also note that implementing the proposed SMSPA method has significantly improved the performance against the case of EPL in both CF and CLCF networks. In addition, the CF network shows a better performance compared to CLCF which is in result of the additional interference caused by other clusters as shown in Equation (2-26). This is while the CLCF network substantially reduces the computational complexity and the signaling load compared to CF network as shown in Table 3.3.

In Fig. 3.6, using MMSE precoder, we have compared the proposed SMSPA resource allocation technique in CF and CLCF networks with different techniques where the proposed GD algorithm is implemented for power allocation. However, in order to consider the comparison with the optimal ExS method, we have examined a small number of UEs in the network and half of the UEs are scheduled. We can note that the proposed SMSPA algorithm has outperformed other techniques and the results approach the optimal ExS method.

3.7

GA Power Allocation in the SMSPA Scheme

In this section, we detail the proposed GA power allocation algorithms used in the SMSPA scheme.

3.7.1

GA Power Allocation Formulation

Using equation (3-30), we combine the received signal of the UEs using a linear receiver $\mathbf{a} = \frac{1}{\sqrt{K_c}} \mathbf{1}_{K_c}^T$, where $\mathbf{1}_{K_c}$ is a $1 \times K_c$ vector of all 1 entities so that $\mathbf{a}^H \mathbf{a} = 1$ and we obtain a simpler expression for sum-rate [33]. After finding the power loading factors using the simplified sum-rate expression, we apply

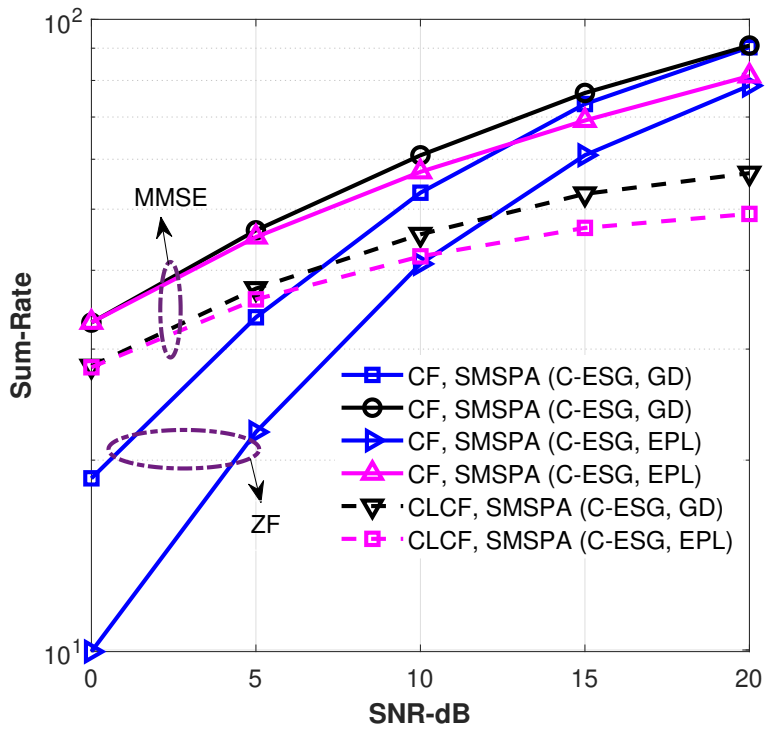


Figure 3.5: Comparison of the proposed SMSPA technique in CF and CLCF networks with the system that uses the proposed C-ESG scheme and EPL for ZF and MMSE precoders, ($M = 64$, $K = 128$, $n = 24$)

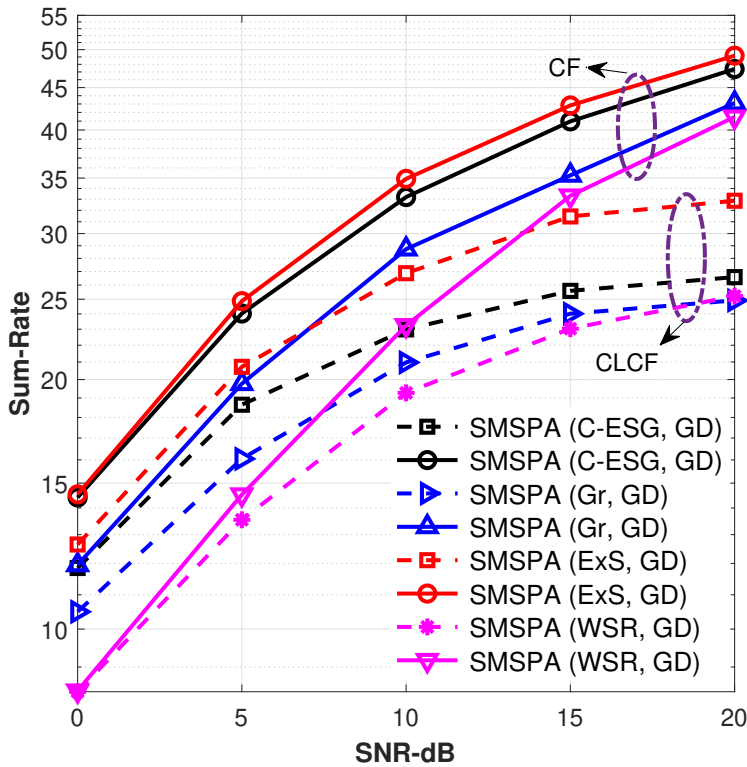


Figure 3.6: Comparison of different resource allocation techniques considering a GD power allocation algorithm in CF and CLCF networks when an MMSE precoder is used, ($M = 64$, $K = 16$, $n = 8$)

Table 3.3: Computational complexity of the proposed resource allocation algorithm and the signaling load for CF and CLCF networks

Network	NO of APs, UEs and scheduled UEs	Signaling load	NO of FLOPs
CF	$M = 64, K = 16$ and $n = 8$	3072	0.78×10^6
CLCF	$M = 64, K = 16$ and $n = 8$	768	0.75×10^5
CF	$M = 128, K = 256$ and $n = 128$	98304	2.1643×10^{10}
CLCF	$M = 128, K = 256$ and $n = 128$	24576	1.1073×10^9

the obtained power allocation matrix in the sum-rate expressions defined in equations (2-21) and (2-25) to determine the sum-rates.

Thus, the combined received signal at cluster c and the power ratio of the desired part of the SINR are given as follows, respectively,

$$\begin{aligned} \mathbf{a}^T \mathbf{y}_c &= \sqrt{\rho_f} \mathbf{a}^T \hat{\mathbf{G}}_{cc}^T \mathbf{W}_c \mathbf{D}_c \mathbf{x}_c + \sqrt{\rho_f} \mathbf{a}^T \tilde{\mathbf{G}}_{cc}^T \mathbf{P}_c \mathbf{x}_c \\ &+ \sum_{i=1, i \neq c}^C \sqrt{\rho_f} \mathbf{a}^T \mathbf{G}_{ic}^T \mathbf{P}_i \mathbf{x}_i + \mathbf{a}^T \mathbf{w}_c \end{aligned} \quad (3-39)$$

$$\text{SINR} = \frac{\rho_f \mathbf{a}^T \hat{\mathbf{G}}_{cc}^T \mathbf{W}_c \mathbf{D}_c \mathbf{D}_c^H \mathbf{W}_c^H \hat{\mathbf{G}}_{cc}^* \mathbf{a}}{\sigma_w^2 \mathbf{a}^T \mathbf{Z} \mathbf{a}} \quad (3-40)$$

where

$$\mathbf{Z} = \tilde{\mathbf{G}}_{cc}^T \mathbf{P}_c \mathbf{P}_c^H \tilde{\mathbf{G}}_{cc}^* + \sum_{i=1, i \neq c}^C \rho_f \mathbf{G}_{ic}^T \mathbf{P}_i \mathbf{P}_i^H \mathbf{G}_{ic}^T + \mathbf{I} \quad (3-41)$$

Assuming Gaussian signaling, the rate expression is obtained by $\frac{1}{2} \log_2(1 + \text{SINR})$. Accordingly, the simplified sum-rate expression is given by

$$SR = \frac{1}{2} \log_2 \left[1 + \frac{\rho_f \mathbf{a}^T \hat{\mathbf{G}}_{cc}^T \mathbf{W}_c \mathbf{D}_c \mathbf{D}_c^H \mathbf{W}_c^H \hat{\mathbf{G}}_{cc}^* \mathbf{a}}{\sigma_w^2 \mathbf{a}^T \mathbf{Z} \mathbf{a}} \right]. \quad (3-42)$$

Equation (3-42) is similar to $\frac{1}{2} \log_2(1 + bx)$ where $b = \frac{\rho_f}{\sigma_w^2 \mathbf{a}^T \mathbf{Z} \mathbf{a}}$ and $x = \mathbf{a}^T \hat{\mathbf{G}}_{cc}^T \mathbf{W}_c \mathbf{D}_c \mathbf{D}_c^H \mathbf{W}_c^H \hat{\mathbf{G}}_{cc}^* \mathbf{a}$ which is a monotonically increasing function of x , $b > 0$. Thus, we can maximize x which is equivalent to the sum-rate using the following problem

$$\begin{aligned} \max_{\mathbf{d}_c} & \left(\mathbf{a}^T \hat{\mathbf{G}}_{cc}^T \mathbf{W}_c \text{diag}(\mathbf{d}_c) \text{diag}(\mathbf{d}_c)^H \mathbf{W}_c^H \hat{\mathbf{G}}_{cc}^* \mathbf{a} \right) \\ \text{subject to} & \|\mathbf{W}_c \text{diag}(\mathbf{d}_c)\|^2 \leq P. \end{aligned} \quad (3-43)$$

Since the objective function x is scalar, $\text{trace}(x) = x$. Therefore, by taking the derivative of the objective function with respect to the power loading matrix \mathbf{D}_c and using the equality $\frac{\partial \text{trace}(\mathbf{A}\mathbf{B})}{\partial \mathbf{A}} = \mathbf{B} \odot \mathbf{I}$ where \mathbf{A} is a diagonal matrix and \odot shows the Hadamard product, we obtain

$$\frac{\partial x}{\partial \mathbf{D}_c} = 2 \left(\mathbf{W}_c^H \hat{\mathbf{G}}_{cc}^* \mathbf{a} \mathbf{a}^T \hat{\mathbf{G}}_{cc}^T \mathbf{W}_c \text{diag}(\mathbf{d}_c) \right) \odot \mathbf{I} \quad (3-44)$$

We can use a stochastic GA approach to update the power allocation coefficients as follows

$$\begin{aligned} \mathbf{d}_c(i) &= \mathbf{d}_c(i-1) + \lambda \frac{\partial x}{\partial \mathbf{D}_c} = \mathbf{d}_c(i-1) \\ &+ 2\lambda \left(\mathbf{W}_c^H \hat{\mathbf{G}}_{cc}^* \mathbf{a} \mathbf{a}^T \hat{\mathbf{G}}_{cc}^T \mathbf{W}_c \text{diag}(\mathbf{d}_c(i-1)) \right) \odot \mathbf{I} \end{aligned} \quad (3-45)$$

where i and λ represent the iteration index and the positive step size, respectively. Before running the GA adaptive algorithm, the transmit power constraint should be satisfied so that $\|\mathbf{W}_c \text{diag}(\mathbf{d}_c)\|_F^2 = \|\mathbf{P}_c\|_F^2 \leq P$. Therefore, the power scaling factor $\eta = \sqrt{\frac{\text{trace}(\mathbf{P}_c \mathbf{P}_c^H)}{\text{trace}(\mathbf{W}_c \text{diag}(\mathbf{d}_c) \mathbf{d}_c \mathbf{W}_c^H)}}$ is employed in each iteration to scale the coefficients properly. The adaptive power allocation is summarized in Algorithm 5 where I_t iterations are used.

Algorithm 5: GA Power Allocation Algorithm for Sum-Rate Maximization.

```

1 Input  $\mathbf{G}_{cc}, \mathbf{P}_c, \mathbf{W}_c, \mathbf{a}$  and  $\lambda$ 
2  $\mathbf{d}_c(1) = \mathbf{0}$ 
3 for  $i = 2$  to  $I_t$  do
4    $\frac{\partial x}{\partial \mathbf{D}_c} = 2 \left( \mathbf{W}_c^H \hat{\mathbf{G}}_{cc}^* \mathbf{a} \mathbf{a}^T \hat{\mathbf{G}}_{cc}^T \mathbf{W}_c \text{diag}(\mathbf{d}_c(i-1)) \right) \odot \mathbf{I};$ 
5    $\mathbf{d}_c(i) = \mathbf{d}_c(i-1) + \lambda \frac{\partial x(\varepsilon)}{\partial \mathbf{D}_c};$ 
6   if  $\text{trace}(\mathbf{W}_c \text{diag}(\mathbf{d}_c(i)) \mathbf{d}_c(i) \mathbf{W}_c^H) \neq \text{trace}(\mathbf{P}_c \mathbf{P}_c^H)$  then
7      $\eta = \sqrt{\frac{\text{trace}(\mathbf{P}_c \mathbf{P}_c^H)}{\text{trace}(\mathbf{W}_c \text{diag}(\mathbf{d}_c(i)) \mathbf{d}_c(i) \mathbf{W}_c^H)}};$ 
8      $\mathbf{d}_c(i) = \eta \mathbf{d}_c(i);$ 
9   end
10 end

```

3.7.2

Simulation Results for SMSPA with GA

In order to assess the proposed SMSPA resource allocation scheme, we compare the sum-rate of the networks that use the proposed C-ESG, standard greedy (SG), exhaustive search (ES) or WSR user scheduling techniques and the proposed GA power allocation or EPL. We consider the CF and CLCF networks as considered for the last section.

In Fig. 3.7, the sum-rate performances of the proposed SMSPA scheme is assessed with the ESG scheduling algorithm using EPL or the GA power allocation when ZF or MMSE precoders are applied. While the sum-rates are increasing with the increase in the SNR, the MMSE precoder outperforms the ZF precoder. In addition, the GA power allocation yields significant performance improvement at low-to-medium SNR values.

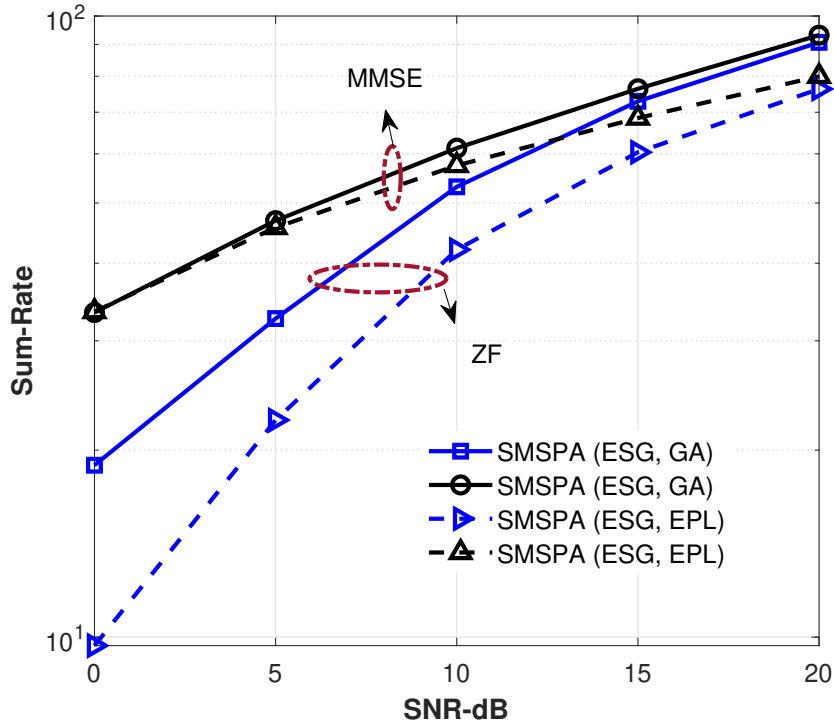


Figure 3.7: Comparison of the proposed SMSPA resource allocation technique in CF networks for ZF and MMSE precoders with the system which has implemented the proposed C-ESG algorithm and EPL ($M = 64$, $K = 128$, $n = 24$)

Fig. 3.8 shows a comparison of different resource allocation techniques when the MMSE precoder is used. We employ a network with a small number of UEs while half of the UEs are scheduled so that we can show the results for the ES method as well as other methods. We notice that the proposed SMSPA resource allocation which has used the C-ESG and GA algorithms has outperformed other approaches and in the CF network the performance is close to that of the optimal ES method. As expected and according to Equation (2-23), CF shows better performance than that of the CLCF network because of the extra interference terms caused by other clusters.

We clarify that Fig. 3.7 and Fig. 3.8 are plotted according to the sum-rate expressions of Equations (2-21) and (2-25) and simplified sum-rate expression of (3-42) is used only to derive the power loading factors. However, as shown

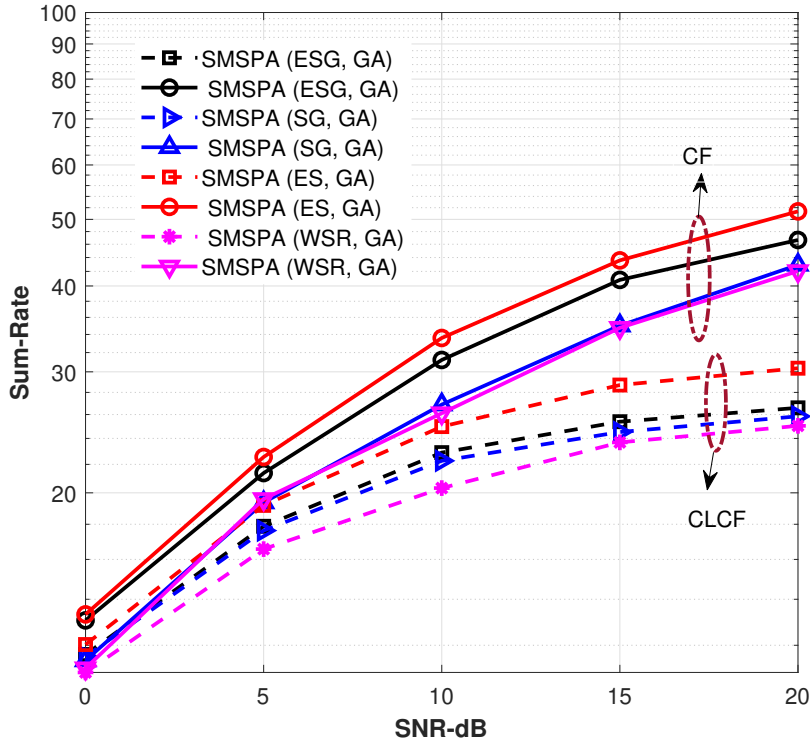


Figure 3.8: Comparison of the different resource allocation techniques in CF and CLCF networks adapting GA power allocation when MMSE precoder is used ($M = 64$, $K = 16$, $n = 8$).

in Table 3.4, the computational cost of the proposed SMSPA scheme and the signaling load as the number of channel parameters for CLCF network are substantially lower than CF.

Table 3.4: Computational complexity of the proposed SMSPA scheme in floating point operations and the signaling load in parameters for CF and CLCF networks when $M = 64$, $K = 128$ and $n = 64$.

Network	CF	CLCF
Signaling load	24576	6144
Computational cost	1.3632×10^9	69.354×10^6

3.8 Summary

In this chapter, we have presented a comprehensive outline of the SMSPA resource allocation technique, which includes the development of the C-ESG multiuser scheduling method and two novel power allocation strategies based on GD and GA algorithms. The C-ESG technique effectively addresses multiuser scheduling, while the GD and GA power allocation strategies focus on

minimizing MSE and maximizing a simplified sum-rate expression, respectively. Simulation results demonstrate significant performance improvements achieved by the SMSPA framework when compared to EPL and other existing user scheduling methods. These findings establish a strong foundation for further exploration of advanced resource allocation strategies in CF and CLCF massive MIMO networks.

4

Clustering Strategies based on Information Rates and Fair Resource Distribution in CF-mMIMO Networks

In this chapter, we develop and evaluate advanced strategies for clustering and resource allocation in CF-mMIMO networks, focusing on user-centric approaches to enhance network performance and fairness. To harness the full potential of CF-mMIMO while maintaining system simplicity and reducing signaling overhead, several clustering strategies have been proposed [25, 28, 34, 35]. Among these, the user-centric CF (UCCF) clustering approach has been highlighted as particularly effective [2, 36–39]. This approach tailors clusters of APs to individual UEs based on various criteria, such as large scale fading and signal-to-noise ratios, enhancing the direct support to each user [9, 40, 41]. Furthermore, efficient resource allocation within these networks is critical for ensuring fair resource distribution among UEs and maximizing spectral efficiency. Studies like [42] and [43] have developed resource allocation strategies focusing on minimizing power consumption while maximizing infrastructure operator revenue and maintaining service quality. Other research has aimed at optimizing network performance through approaches such as weighted sum rate maximization and user association algorithms [9, 34, 44].

In this chapter, unlike last chapters, we consider CF-mMIMO networks with multi-antenna APs, which are likely to become more relevant in future wireless networks. We introduce a novel user-centric clustering approach for downlink scenarios. Our technique involves selecting APs for each UE based on a threshold of information rates, ensuring tailored service quality and optimal network resource utilization. We impose a unique constraint that increases the minimum number of APs dedicated to serving each UE, thus enhancing the quality of service by guaranteeing substantial AP coverage for each user. Additionally, we propose a new resource allocation strategy that integrates our clustering approach with a fair user scheduling mechanism. Numerical simulations are provided to demonstrate that our methods significantly outperform existing techniques in terms of service quality and network efficiency.

The rest of this chapter is organized as follows: Section 4.1 provides an overview of the system model, detailing the network structures and relevant sum-rate expressions. Section 4.2 introduces our proposed AP selection tech-

nique for user-centric clustering. Section 4.3 discusses the resource allocation challenges and presents our solution for scheduling multiple users fairly. In Section 4.4, we analyze the performance of our proposed methods through numerical results. Finally, Section 4.5 concludes the chapter.

4.1 Network Model

In this section, we examine the network model for multiple-antenna CF and UCCF systems.

4.1.1 Multi-Antenna CF-mMIMO Network Model

We detail the downlink setup of a CF-mMIMO network comprising L APs, each equipped with N uniformly spaced antennas, serving K randomly distributed single-antenna UEs. The network is characterized by a significantly greater number of UEs compared to the total number of AP antennas, i.e., $K \gg M = LN$, necessitating the scheduling of $n \leq M$ out of the K UEs. Thus, the downlink received signal model is expressed the same as Equation (2-19). The channel matrix $\mathbf{G} = \hat{\mathbf{G}} + \tilde{\mathbf{G}} \in \mathbb{C}^{LN \times n}$ consists of the estimated channel $\hat{\mathbf{G}}$ and the estimation error $\tilde{\mathbf{G}}$, accounting for CSI imperfections. Both $\hat{\mathbf{G}}$ and $\tilde{\mathbf{G}}$ are composed of independent zero-mean variables, and the estimation error is assumed to be sufficiently small to enable effective communication. However, the dimensions of the linear precoder matrix should be $\mathbf{P} \in \mathbb{C}^{LN \times n}$, while the transmitted symbol vector \mathbf{x} and the additive noise vector \mathbf{w} should both have dimensions $\mathbb{C}^{n \times 1}$. Assuming Gaussian signaling with statistical independence among the elements of \mathbf{x} and independence from all noise and channel coefficients, and treating $\hat{\mathbf{G}}_a$ as remaining constant within a coherence interval and independent across different coherence intervals while Conversely, $\tilde{\mathbf{G}}_a$ being considered as a stochastic variable reflecting the channel error, the upper bound on the achievable sum-rate under imperfect channel knowledge for the CF system is expressed by the following equation, similar to Equation (2-21), with the difference being in the dimension of the signal vector and considering the stochastic nature of the channel estimation error for more correct assessment

$$SR_{cf} = \log_2 (\det [\mathbf{R}_{cf} + \mathbf{I}_n]), \quad (4-1)$$

where the covariance matrix \mathbf{R}_{cf} is defined as:

$$\mathbf{R}_{cf} = \rho_f \hat{\mathbf{G}}^T \mathbf{P} \mathbf{P}^H \hat{\mathbf{G}}^* \left(\mathbb{E}_{\tilde{\mathbf{G}}_a} [\rho_f \tilde{\mathbf{G}}^T \mathbf{P} \mathbf{P}^H \tilde{\mathbf{G}}^*] + \sigma_w^2 \mathbf{I}_n \right)^{-1}. \quad (4-2)$$

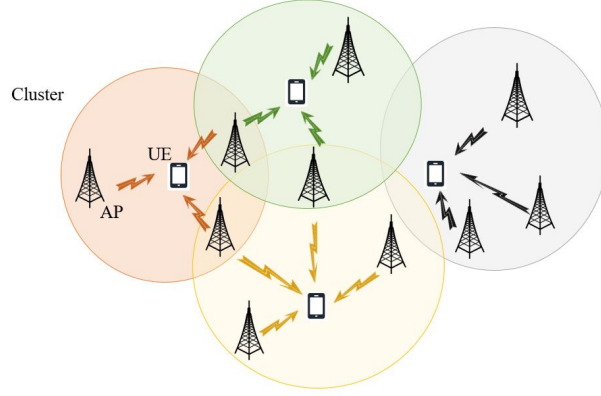


Figure 4.1: User-centric cell-free network.

4.1.2 UCCF-mMIMO Network Model

We employ a UCCF massive MIMO network, depicted in Fig. 4.1. In this network, each UE is served by a selected subset of APs. The downlink received signal model in this context is described by:

$$\mathbf{y} = \sqrt{\rho_f} \mathbf{G}_a^T \mathbf{P}_a \mathbf{x} + \mathbf{w}. \quad (4-3)$$

In a manner analogous to the CF network, the upper bound on the achievable sum-rate under imperfect channel knowledge for the UCCF system is defined as:

$$R_{UC} = \log_2 (\det [\mathbf{R}_{UC} + \mathbf{I}_K]), \quad (4-4)$$

where the matrix \mathbf{R}_{UC} is given by:

$$\mathbf{R}_{UC} = \rho_f \hat{\mathbf{G}}_a^T \mathbf{P}_a \mathbf{P}_a^H \hat{\mathbf{G}}_a^* \left(\mathbb{E}_{\tilde{\mathbf{G}}_a} [\rho_f \tilde{\mathbf{G}}_a^T \mathbf{P}_a \mathbf{P}_a^H \tilde{\mathbf{G}}_a^*] + \sigma_w^2 \mathbf{I}_K \right)^{-1}, \quad (4-5)$$

and the vectors \mathbf{x} and \mathbf{w} are statistically independent.

The channel and precoding matrices in a UCCF network are represented as $\mathbf{G}_a = [\mathbf{g}_{a1}, \dots, \mathbf{g}_{an}]$ and \mathbf{P}_a as a function of \mathbf{G}_a , respectively. Each channel vector $\mathbf{g}_{ak} \in \mathbb{C}^{LN \times 1}$, for $k \in \{1, \dots, n\}$, is formulated as $\mathbf{g}_{ak} = \mathbf{A}_k \mathbf{g}_k$, where $\mathbf{A}_k = \text{diag}(a_{k1}, \dots, a_{kLN})$ are diagonal matrices with elements defined by:

$$a_{kl} = \begin{cases} 1 & \text{if } l \in U_k, \\ 0 & \text{if } l \notin U_k \end{cases}, \quad l \in \{1, \dots, LN\}, \quad (4-6)$$

where U_k denotes the subset of APs serving the k th UE, and $\mathbf{g}_k \in \mathbb{C}^{LN \times 1}$, $k \in \{1, \dots, n\}$ is the k th column of the $LN \times n$ CF channel matrix $\mathbf{G} = [\mathbf{g}_1, \dots, \mathbf{g}_n]$.

4.2 AP Clustering Strategies

In wireless networks, the process of selecting APs to serve UEs, commonly referred to as clustering, can follow different criteria. This section begins

with an overview of standard clustering based on the Large Scale Fading (LSF) criterion. Subsequently, we introduce a novel approach that utilizes the sum-rate (SR) criterion, termed Boosted SR (BSR), to achieve improved AP clustering.

4.2.1 LSF-Based Clustering

AP Clustering using the LSF method depends on extensive propagation features such as path loss and shadowing to identify suitable APs for UEs. This approach concentrates on the typical signal attenuation observed over significant distances and overlooks various aspects of the wireless environment.

In this clustering method, an AP m , is selected for a user k if its average channel gain exceeds a predetermined threshold α_{lsf} , such that $\beta_{mk} \geq \alpha_{lsf}$, where β_{mk} represents the large-scale fading coefficient. If no AP meets this criterion for a user, the AP with the highest average channel gain is chosen as the fallback, ensuring that each UE is served by at least one AP. The set of selected APs for UE k is thus given by:

$$U_{k,lsf} = \{m : \beta_{mk} \geq \alpha_{lsf}\} \cup \left\{ \underset{m}{\operatorname{argmax}} \beta_{mk} \right\}, \quad (4-7)$$

where the threshold α_{lsf} is defined as:

$$\alpha_{lsf} = \frac{1}{LNK} \sum_{m=1}^{LN} \sum_{k=1}^K \beta_{mk} \quad (4-8)$$

In this user-centric clustering approach, the set of APs $U_{k,lsf}$ serving UE k is determined based on the LSF criterion. Specifically, the set $U_{k,lsf}$ includes all APs where the LSF coefficient β_{mk} exceeds a predefined threshold α_{lsf} , ensuring that only APs with sufficiently strong signals are selected. Therefore, the AP with the maximum LSF coefficient for each UE is always included in the set $U_{k,lsf}$ [28]. However, this approach does not account for instantaneous channel conditions or the specific requirements of UEs. While beneficial for providing a general overview of the wireless environment, it may not always yield the optimal AP selection in every scenario due to its macroscopic view. The lack of customization to dynamic channel conditions or a focus on maximizing information rates may lead to reduced spectral efficiency.

4.2.2 Proposed Information Rate-Based Clustering

In this section, we discuss AP clustering based on the sum-rate (SR) criterion. We present an analysis of our proposed method, which centers on optimizing the sum-rate achievable between an AP and UEs to ensure

reliable communication. This method considers multiple factors impacting communication quality and information rates, including actual channel gains, channel estimation errors, and noise levels. By utilizing the SR criterion, this approach ensures that UEs are served by APs that can deliver the possible rates. The downlink signal model from AP m to UE k is given by:

$$y_{km} = \sqrt{\rho_f} \hat{g}_{km}^T \mathbf{p}_k \mathbf{x} + \sqrt{\rho_f} \tilde{g}_{km}^T \mathbf{p}_k \mathbf{x} + w_k, \quad (4-9)$$

where \hat{g}_{km} represents the estimated channel gain from AP m to UE k , \tilde{g}_{km} denotes the channel gain estimation error, and $\mathbf{p}_k \in \mathbb{C}^{LN \times 1}$ is the precoder for UE k . Assuming Gaussian signaling, the rate from AP m to UE k is calculated as:

$$SR_{km} = \log_2 \left(1 + \frac{\sqrt{\rho_f} |\hat{g}_{km}|^2 \mathbf{p}_k^H \mathbf{p}_k}{\sqrt{\rho_f} |\tilde{g}_{km}|^2 \mathbf{p}_k^H \mathbf{p}_k + \sigma_w^2} \right). \quad (4-10)$$

For effective AP selection, we compute the average rate across all UEs and APs. To ensure efficient coverage and quality of service, every UE should ideally be served by an AP or a cluster of APs offering a rate higher than or equal to the average rate α_{src} defined as:

$$\alpha_{src} = \frac{1}{KM} \sum_{k=1}^K \sum_{m=1}^M SR_{km} \quad (4-11)$$

For each UE, APs with rates surpassing α_{src} are designated as the AP cluster serving that UE. In scenarios where no AP meets this criterion for a UE, the AP delivering the highest rate is selected, even if below the desired threshold. Consequently, the cluster of APs designated to serve UE k is defined as:

$$U_{k,asr} = \{m : SR_{km} \geq \alpha_{src}\} \cup \left\{ \underset{m}{\operatorname{argmax}} SR_{km} \right\}. \quad (4-12)$$

This methodology prioritizes information rates over traditionally used metrics, ensuring that UEs are served by the APs providing the best rates in any scenario. To confirm the effectiveness of the approach in (4-12), we also enforce a constraint that increases the minimum number of APs dedicated to serving each UE. The BSR algorithm adopts a dynamic approach to AP clustering, focusing on maximizing sum rates to enhance communication quality and network efficiency. The BSR algorithm is outlined in Algorithm 6, where \mathcal{K} and \mathcal{A} represent the sets of all UEs and all APs, respectively.

Algorithm 6: Boosted SR (BSR) Algorithm

- 1 Input rate matrix \mathbf{SR} , threshold α_{src}
- 2 For every UE k , assign an empty cluster AP_k^{BSR}
- 3 **Step 1: SR calculation and initial AP selection**
- 4 **for** each UE k and AP m **do**
- 5 **if** $\mathbf{SR}_{k,m} \geq \alpha_{src}$ **then**
- 6 Add m to AP_k^{BSR}
- 7 **end**
- 8 **end**
- 9 **Step 2: Evaluation of AP coverage**
- 10 Calculate $N_{AP_{Av}}$:

$$N_{AP_{Av}} = \frac{1}{|\mathcal{K}|} \sum_{k \in \mathcal{K}} |AP_k^{\text{BSR}}|$$

- 11 **Step 3: Identification of under-supported UEs**
- 12 Determine set \mathcal{S}_{Low} :

$$\mathcal{S}_{Low} = \{k \in \mathcal{K} : |AP_k^{\text{BSR}}| < N_{AP_{Av}}\}$$

- 13 **Step 4: Augmenting AP coverage**
 - 14 **for** each k in \mathcal{S}_{Low} **do**
 - 15 **while** $|AP_k^{\text{BSR}}| < N_{AP_{Av}}$ **do**
 - 16 Add $m \notin AP_k^{\text{BSR}}$ $\mathbf{SR}_{k,m}$ to AP_k^{BSR}
 - 17 **end**
 - 18 **end**
-

4.2.3

Analysis of the Proposed BSR Technique

In AP clustering via the BSR method, the selection of APs that offer the highest rates inherently optimizes the network's overall sum-rate. This strategy adapts to the real-time conditions of the network, enabling BSR-based clustering to target optimal performance given the current network state. Additionally, BSR potentially enhances spectral efficiency as it takes information rates into consideration.

To evaluate the BSR method, we reference Equation (4-10) which is similar to $SR_{km} = \log_2 \left(1 + \frac{\|S_{km}\|^2}{\|IN_{km}\|^2} \right)$. For two distinct links $\{j, i\}$ to UE k , the rates are defined as follows:

$$SR_{kj} = \log_2 \left(1 + \frac{\|S_{kj}\|^2}{\|IN_{kj}\|^2} \right) \quad (4-13)$$

$$SR_{ki} = \log_2 \left(1 + \frac{\|S_{ki}\|^2}{\|IN_{ki}\|^2} \right) \quad (4-14)$$

Assuming:

- $\|S_{kj}\|^2$ is slightly larger than $\|S_{ki}\|^2$, indicating a marginally better channel for link j .
- $\|IN_{kj}\|^2$ is significantly larger than $\|IN_{ki}\|^2$, implying substantially more noise on link j .

Consequently, it could result in $SR_{ki} > SR_{kj}$, leading to:

- LSF would select link j due to a larger $\|S_{kj}\|^2$.
- BSR would opt for link i because $SR_{ki} > SR_{kj}$.

In situations with high noise variance, choosing an AP solely based on high channel gain may not maximize the sum-rate performance effectively. By considering both channel conditions and noise levels, and leveraging the SR metric, the approach is more inclined to select the AP that offers a superior link for the UE, thereby enhancing the overall sum-rate performance of the system.

We consider identical LSF values from all antennas of an AP to a UE are, which implies that the subset $\{a_{k(j-1)N+1}, \dots, a_{jN}\}$ in \mathbf{A}_k consists entirely of ones when AP j is serving UE k , and zeros otherwise. Conversely, BSR incorporates small-scale fading in its evaluation, which varies across different antennas of APs, providing a more adaptive assessment of each AP's performance. The BSR algorithm not only ensures reliability through adaptive coverage but also accounts for the unique fading characteristics of each antenna. Unlike the static LSF-based criterion, BSR leads to a network with higher sum rates and enhanced reliability, optimizing AP selection for UEs to ensure balanced and efficient network load with high-quality connections. By dynamically assigning UEs to APs according to their information rates and improving coverage for UEs with inadequate support, BSR not only guarantees reliability by adaptive coverage but also considers the distinct fading properties of each antenna. Compared to the LSF-based criterion, BSR is more dynamic and results in a network with increased sum rates and enhanced reliability.

4.3 Resource Allocation with Fairness

In CF-mMIMO networks where $K \gg LN$, it is important to consider clustering and multiuser scheduling together. Given that a primary objective of CF-mMIMO networks is to deliver uniform performance among UEs, we have developed a multiuser scheduling algorithm to ensure fairness among UEs. However, the sequence in which clustering and multiuser scheduling are executed leads to varying costs. To minimize these costs, we implement clustering first, followed by multiuser scheduling.

4.3.1 Proposed Resource Allocation Problem

In every time slot i , our objective is to schedule a subset of n UEs from a total of K UEs, where $n \leq LN$, to achieve a desirable sum-rate. This subset is denoted as S_n^i , leading to a column-reduced channel matrix $\mathbf{G}_{cc}(S_n^i)$. Our goal is to maximize the sum-rate for the chosen UEs in a UCCF network, while also maintaining fairness, as outlined by

$$\underset{S_n^i, \mathbf{d}}{\text{maximize}} \quad SR_{UC}(S_n^i) \quad (4-15a)$$

$$\text{subject to} \quad \left\| \mathbf{P}_a(S_n^i) \right\|_F^2 \leq P, \forall i = 1, \dots, T \quad (4-15b)$$

$$S_n^i \cap S_n^j = \emptyset, i \neq j, \forall i, j = 1, \dots, T \quad (4-15c)$$

$$\cup_{i=1}^T S_n^i = \mathcal{K} \quad (4-15d)$$

$$\frac{1}{|\mathcal{S}_c|} \sum_{k \in \mathcal{S}_c} t_{wk} = \frac{1}{|\mathcal{S}_p|} \sum_{k \in \mathcal{S}_p} t_{wk} \quad (4-15e)$$

In the i -th time slot, SR_{UC} represents the sum-rate for UEs with the signal covariance matrix's upper boundary defined by $\text{Trace}[\mathbf{C}_x] \leq P$. We denote T as the number of time slots and $\mathcal{K} = \{1, 2, \dots, K\}$ to indicate all UEs. The sets \mathcal{S}_c and \mathcal{S}_p correspond to UEs contributing to the maximum sum-rate and those with poor channels, respectively. The waiting time for UE k is denoted by $t_{w,k}$. Constraints (4-15c) and (4-15d) ensure that every UE is selected at least once, while (4-15e) aims to ensure similar average waiting times for both sets. The problem's complexity arises from the dynamics of rates and user scheduling challenges.

4.3.2

Proposed F-Gr Algorithm

To address the optimization problem described in (4-15), we develop a fair greedy (F-Gr) multiuser scheduling method, based on the greedy (Gr) user scheduling approach outlined in [45]. This method aims to maximize the sum-rate while adhering to the constraint specified in (4-15b). Unlike the strategy in [45], our F-Gr technique emphasizes ensuring fairness among UEs.

This approach is implemented to maintain an average equal waiting time for both groups of UEs (\mathcal{S}_c and \mathcal{S}_p). After excluding UEs that have been previously scheduled, we then select those with the lowest channel gain in the next time slot. This process is repeated alternately until all UEs have been scheduled.

In particular, we define $\mathbf{SR} \in \mathbb{C}^{K \times LN}$ as the rate matrix, where $\mathbf{SR}_{k,m} = SR_{km}$ as specified in (4-10), and \mathcal{K} represents the set of all UEs. We also calculate the threshold as in (4-11). Utilizing the proposed BSR algorithm, APs are clustered for each UE. For the scheduling phase, which spans T timeslots, the operation in the i th timeslot varies depending on whether i is even or odd. If i is odd, the system schedules the best n UEs in the set $S_c^{\frac{i+1}{2}}$ to maximize the sum-rate. Specifically, in an odd i , given \mathcal{K}_i as all UEs in the current timeslot, a UE s_1 is selected in the first iteration $l = 1$ as follows,

$$s_1 = \underset{k \in \mathcal{K}_i}{\operatorname{argmax}} \mathbf{g}_k^H \mathbf{g}_k. \quad (4-16)$$

Let $S_1 = \{s_1\}$. The maximum achieved rate $SR(S_1)_{\max}$ is calculated, and subsequently, we identify a UE in the next iteration that maximizes the rate, defined as

$$s_l = \underset{k \in (\mathcal{K}_i \setminus S_{l-1})}{\operatorname{argmax}} SR(S_{l-1} \cup \{k\}) \quad (4-17)$$

This process is repeated until n UEs have been scheduled as the best n UEs in an odd timeslot. Conversely, in every even timeslot, n UEs with the weakest channel powers are scheduled as $S_p^{\frac{i}{2}}$. After the scheduling process, we compute the weighted sum-rate for each set and the average sum-rate over all timeslots is given by

$$SR_{Av} = \frac{1}{T} \sum_{i=1}^T \frac{n_i}{n} \times SR^i \quad (4-18)$$

The outlined resource allocation framework, including clustering and multi-user scheduling, is summarized as Algorithm 7. The greedy selection in the F-Gr algorithm effectively balances computational complexity with high performance, making it scalable for large networks while ensuring convergence through a finite set of UEs and deterministic scheduling steps.

Algorithm 7: Proposed F-Gr Resource Allocation

```

1 Input: rate matrix  $\mathbf{SR}$ , set  $\mathcal{K}_1 = \mathcal{K}$ 
2 Calculate threshold using eq. (4-11)
3 Cluster APs per UE using BSR
4 Determine  $n$  (UEs scheduled per timeslot)
5 for  $i = 1$  to  $T$  do
6   if  $i \bmod 2 = 1$  then
7      $l = 1, s_1 = \underset{k \in \mathcal{K}_i}{\operatorname{argmax}} \mathbf{g}_k^H \mathbf{g}_k, S_1 = \{s_1\}$ 
8     while  $l < n$  do
9        $l = l + 1$ 
10       $s_l = \underset{k \in (\mathcal{K}_i \setminus S_{l-1})}{\operatorname{argmax}} SR(S_{l-1} \cup \{k\})$ 
11      Update  $S_l = S_{l-1} \cup \{s_l\}$ 
12      if  $SR(S_l) \leq SR(S_{l-1})$  then
13        Break,  $l = l - 1$ 
14      end
15    end
16     $S_c^{\frac{i+1}{2}} = S_l$ 
17    Update UEs:  $\mathcal{K}_i = \mathcal{K}_i \setminus S_c^{\frac{i+1}{2}}$ 
18  else
19    Schedule  $n$  UEs with poorest channels  $S_p^{\frac{i}{2}}$ 
20    Update UEs:  $\mathcal{K}_i = \mathcal{K}_i \setminus S_p^{\frac{i}{2}}$ 
21  end
22 end
23 Calculate sum-rate for scheduled UEs
24 Compute average sum-rate using eq. (4-18)

```

4.4

Simulation Results

In this section, we evaluate the sum-rate performance of clustering methods. We analyze a CF network including a square area with a side length of 400 m, featuring $L = 16$ APs, each equipped with $N = 4$ antennas, and $K = 128$ single-antenna UEs distributed randomly. These assessments also consider imperfect CSI. For both sum-rate and BER performance evaluations, we base our findings on the average results from 1000 channel realizations, ensuring statistical reliability and robustness.

Figure 4.2 presents a comparison between UCCF networks using LSF and BSR criteria and a CF network without user scheduling. The results show that

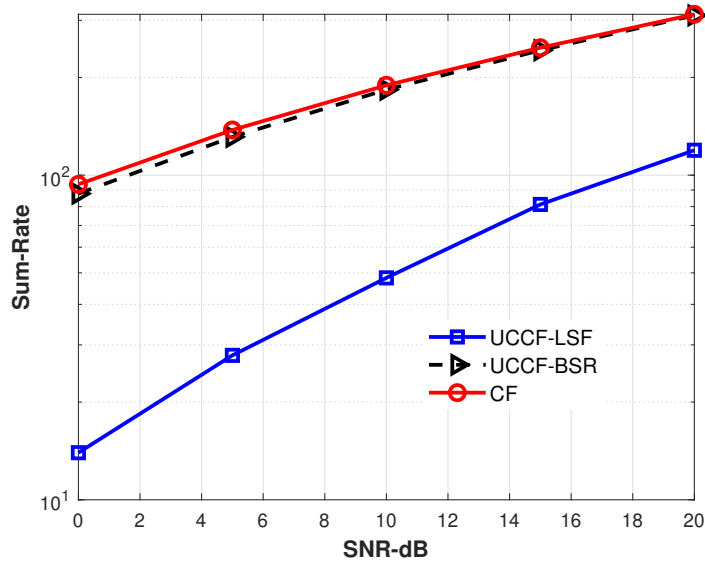


Figure 4.2: Sum-rate for UCCF with different clustering criteria and CF network with no user scheduling, $L = 16$, $N = 4$, $K = 128$

BSR significantly outperforms LSF, achieving performance close to that of the CF network, especially at higher SNR values. This highlights the effectiveness of the BSR criterion in improving network performance compared to the LSF approach.

Figure 4.3 further illustrates the improvements in BER achieved by the BSR criterion compared to the LSF criterion in the UCCF network setup without user scheduling. As SNR increases, the BER for the BSR approach significantly decreases, closely following the performance of the CF network, while the LSF-based network exhibits higher BER throughout the entire range. This highlights the clear advantage of using BSR in terms of error performance over LSF.

We assessed the performance of the F-Gr resource allocation algorithm within both CF and UCCF networks, the latter of which employed the BSR and LSF criteria for AP clustering. Figure 4.4 presents a performance comparison of the F-Gr algorithm in a CF network and UCCF networks utilizing BSR and LSF clustering, respectively, for setups with $M = 64$ and $K = 128$ UEs, scheduling $n = 20$ UEs per timeslot. The results indicate that the F-Gr algorithm substantially outperforms the LSF-based UCCF network and closely matches the performance of the CF network.

In order to offer a concise and informative visualization in terms of fairness, we have calculated the median rate for each user at a given SNR which represents the 50th percentile in the CDF. In other words, the median rate is the value at or below which 50 percent of the observed rates fall, thereby

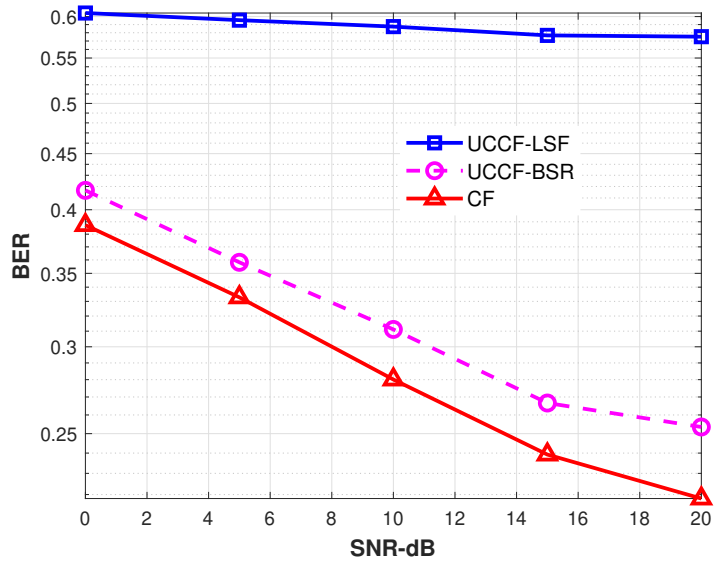


Figure 4.3: BER of UCCF networks with different clustering criteria and the CF network with no user scheduling, $L = 16$, $N = 4$, $K = 128$.

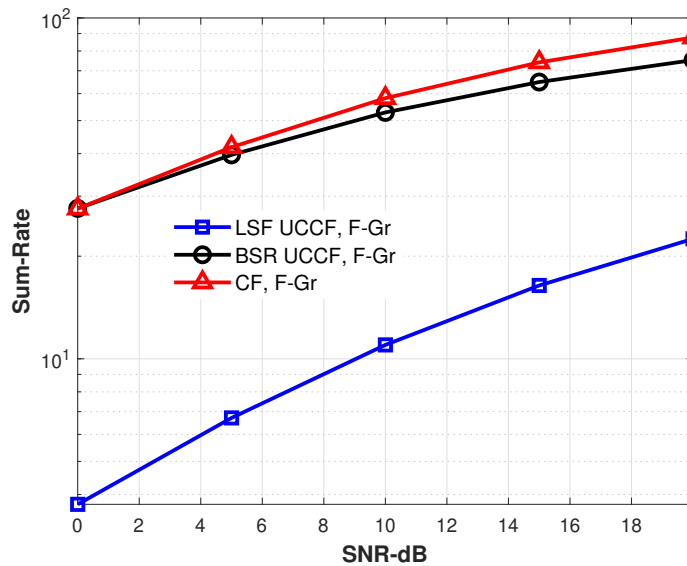


Figure 4.4: Performance of F-Gr resource allocation sum-rate in CF and UCCF networks, $L = 16$, $N = 4$, $K = 128$ and $n = 20$.

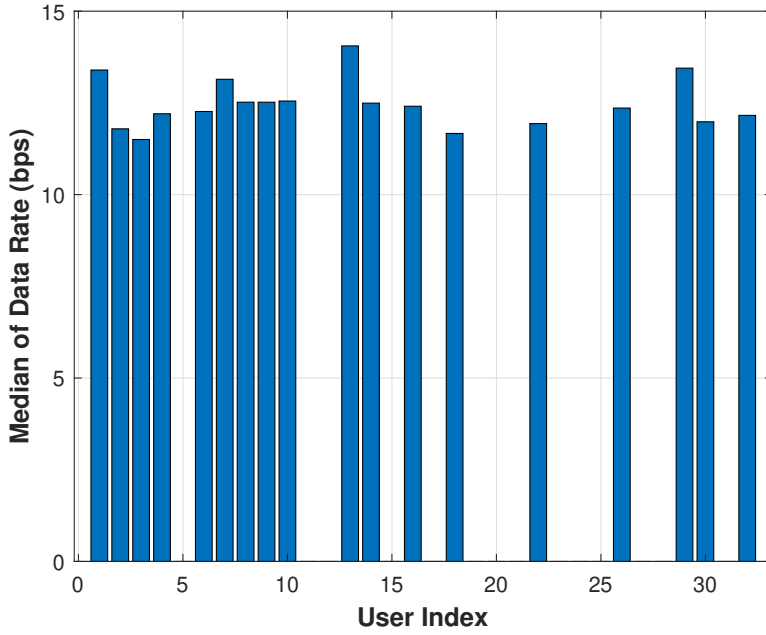


Figure 4.5: Median Rate Distribution for CF network using Gr scheduling for $K = 32$, $n = 16$ and 100 channel realizations.

serving as a robust indicator of the typical rate experience for each user. In this regard, Fig. 4.5 and Fig. 4.6 are given. As we can see, for the F-Gr technique, all the users have shown acceptable rates. In contrast, the Gr technique results in some UEs having zero rate across 100 channel realizations.

Figure 4.7 displays the computational cost in terms of floating-point operations (flops) for CF, BSR UCCF, and LSF UCCF networks, with scheduling of $n = LN$ UEs per network. It demonstrates that UCCF networks exhibit significantly lower complexity compared to CF networks. Additionally, the figure highlights the scalability and efficiency of BSR and the F-Gr algorithm, which maintain high performance even in densely populated networks with up to 100 APs. It also illustrates that LSF UCCF networks are less complex than those using BSR. This reduced complexity in LSF UCCF networks arises because, BSR UCCF networks that utilize both large-scale and small-scale fading information, resulting in a notable performance enhancement.

Accordingly, Table. 4.1 shows the calculated computational cost in terms of flops and the signaling load for these networks which shows that using LSF results in less signaling load compared to BSR.

About the proposed F-Gr method, the complexity is almost the same as when Gr technique with BSR AP selection is used in UCCF. Because in the first time slot, we calculate the power and rate of all the network links. In the next time slots, where we put aside a set of UEs, we do not need to recalculate power and rate of other links as are calculated in the first time slot,

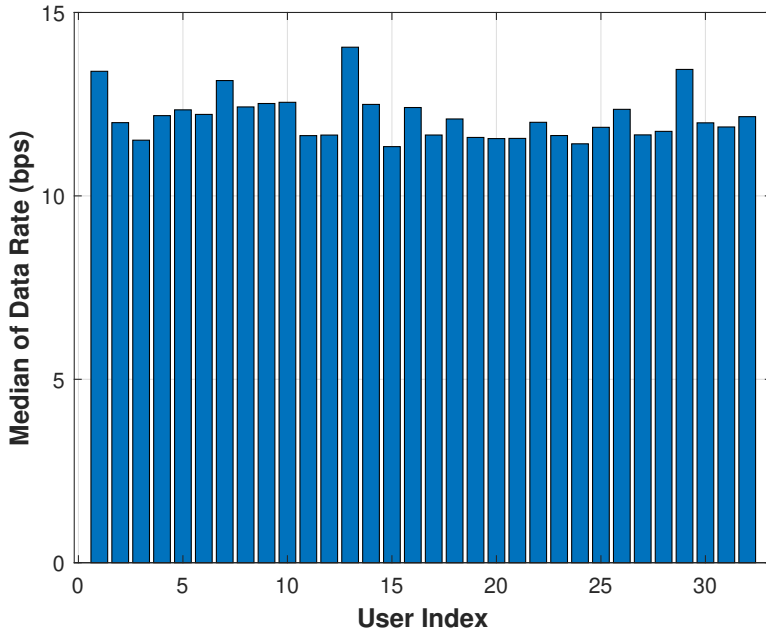


Figure 4.6: Median Rate Distribution for CF network using F-Gr scheduling for $K = 32$, $n = 16$ and 100 channel realizations.

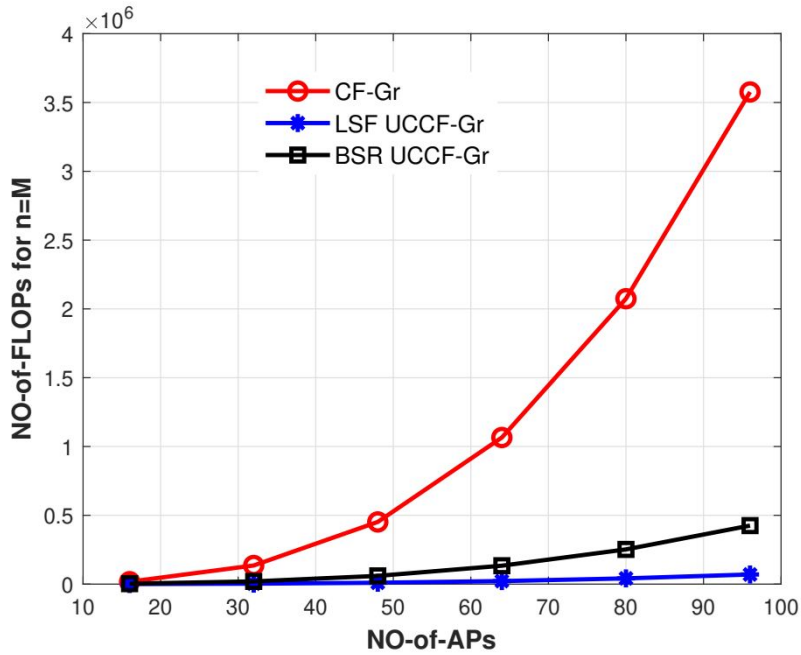


Figure 4.7: Complexity of F-Gr resource allocation for CF and UCCF networks when $n = LN$ UEs are scheduled.

Table 4.1: Computational complexity and signaling load of the proposed resource allocation algorithm

Network	NO of FLOPs	Signaling Load
CF, Gr	$4(LN)^3 + LN(2K + 6)$	
LSF UCCF, Gr	$\frac{9}{128}(LN)^3 + LN\left(\frac{3}{8}K + 7\right) + K + 1$	$2N^2L^2 + NL^2 + NL$
BSR UCCF, Gr	$\frac{27}{64}(LN)^3 + \frac{27}{32}(LN)^2 + \frac{1179}{256}LN + \frac{19}{8}LNK$	$4N^2L^2 + 2NL$

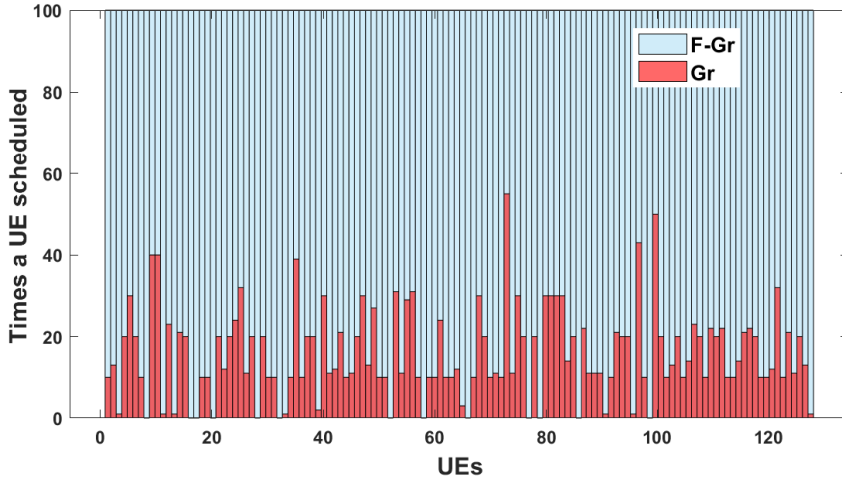


Figure 4.8: Scheduling times for each UE in CF network using Gr and F-Gr scheduling methods for $K = 128$, $n = 20$ and 100 channel realizations.

and we just calculate some new summations for sum-rate or some comparisons to decide which link to consider or not. Thus, the F-Gr technique will add a small calculations compared to the Gr method when UCCF is considered.

Fig. 4.8 considers 100 channel realizations and the number of scheduling times of each user in the CF network. In the standard Gr technique, there are some users which are not supported well in several channel realizations while in the F-Gr technique, all the users are supported in different time slots.

For a final evaluation of the proposed method and its optimal usage scenarios, our study extensively assesses the performance of the clustering and scheduling with fairness based on information rates. Through the analyses and the results, we demonstrated the robustness and network performance enhancement using the proposed technique across various user densities and operational conditions. This adaptive approach highlights significant improvements in fairness and network efficiency, ensures a desirable resource allocation and user coverage, and introduces a suitable method for scenarios with dense user distributions and demanding service quality requirements. In particular,

the proposed methods would excel in environments with a high density of UEs, or environments wherein temporary events, emergency situations or massive influx of UE within a limited area suddenly increase seeking for connection, as they focus on efficiently scheduling and managing resources among a large number of UEs. Applications or scenarios requiring high data rates would benefit from the enhanced performance provided by these methods. By incorporating fairness considerations into the optimization problem, the proposed methods strike a balance between maximizing system performance and ensuring service among UEs which is crucial in 6G networks, where diverse applications with varying quality of service requirements coexist, necessitating fair and efficient resource allocation mechanisms.

4.5

Summary

In this chapter, we assessed the F-Gr resource allocation algorithm across CF and UCCF networks using BSR and LSF criteria for access point clustering. The analysis demonstrated that the F-Gr algorithm notably improves performance in UCCF networks compared to those using LSF and performs comparably to traditional CF networks. This highlights its potential for enhancing network efficiencies in various settings. Moreover, UCCF networks, particularly those utilizing BSR, prove to be scalable and efficient, making them suitable for high-density network environments.

5

Robust Resource Allocation in CF-mMIMO Networks

User-centric CF-mMIMO networks represent a significant evolution from traditional cellular architectures, offering dramatic improvement data rates and reliability, crucial for the advancement toward next-generation wireless systems. However, optimizing resource allocation within these networks poses a major challenge. Effective strategies are required to balance the load and ensure equitable service across the numerous APs and UEs. This involves sophisticated techniques for power control, user scheduling, and bandwidth management, which are essential to maximize performance while minimizing interference and energy consumption [4, 46, 47].

An important feature in operation of CF-mMIMO networks is the management of channel state information (CSI). The precision of CSI impacts crucial network operations such as precoding, power control, and user scheduling. Accurate CSI allows for signals to be coherently combined at the UE, minimizing interference and optimizing overall network performance. However, achieving perfect CSI is challenging due to factors such as estimation errors and feedback delays, which can significantly impair network efficiency [48, 49].

Recognizing the limitations imposed by imperfect CSI, substantial research has been undertaken to develop robust resource allocation strategies. These strategies are designed to tolerate or compensate for CSI inaccuracies, with various studies focusing on worst-case performance optimization to enhance system resilience [50–52]. Notably, robust beamforming and power allocation strategies have been advanced to handle the variabilities in receiver CSI, enhancing joint space-time decoding and interference rejection [6, 53]. Specifically, the work of [50] investigates robust beamforming-type linear receiver techniques that enhance joint space-time decoding and interference rejection, using a worst-case performance optimization approach. [51] tackles the challenge of optimizing user scheduling in the uplink of massive MIMO systems, aiming to decrease the channel estimation overhead. [52] delves into the design of precoders for a multiuser MIMO system under conditions of imperfect CSI, introducing an energy-efficient precoder design. The study of [54] examines an energy-efficient resource allocation algorithm for a wireless power transfer (WPT) enabled multiuser massive MIMO system, incorporating imperfect CSI

to enhance the robustness of the proposed resource allocation algorithm. [6] focuses on the downlink of a CF-mMIMO system with single-antenna APs and UEs, introducing an iterative robust MMSE (RMMSE) precoder to mitigate interference caused by imperfect CSI.

This chapter introduces a robust resource allocation framework specifically tailored for the downlink of CF-mMIMO networks, addressing the challenges of imperfect CSI. The framework comprises a robust user scheduling algorithm and two novel power allocation strategies aimed at optimizing network sum-rate and minimizing MSE. In particular, we adopt linear and MMSE or Zero-Forcing precoders as the basic transmit processing filters for multiuser interference mitigation. Furthermore, a robust multiuser scheduling algorithm denoted robust clustered enhanced subset greedy (RC-ESG) algorithm that implements worst-case robust optimization techniques is developed, which accounts for imperfect CSI and ensures that user scheduling decisions are resilient to estimation errors. Moreover, we propose two robust power allocation algorithms to further enhance the network's information rates and robustness in the presence of imperfect CSI. The first strategy incorporates channel estimation errors into the optimization process, employing a robust gradient descent power allocation (RGDPA) algorithm, which enables a cost-effective power allocation. The second technique, rooted in worst-case robust optimization (WRGDPA), optimizes power allocation by preparing for the most unfavorable scenarios of channel uncertainty, ensuring consistent network performance.

The subsequent sections of this chapter will systematically outline the modeling of UCCF networks, the challenges pertaining to resource allocation, and detailed descriptions of our novel robust scheduling and power allocation strategies. We will also present a detailed analysis of the solutions to various optimization problems posed by these strategies, discuss the convexity of the objective functions, and compare the computational costs of the proposed algorithms. Finally, the chapter will culminate with a discussion of simulation results that showcase the effectiveness of our approaches, followed by a conclusion that summarizes the key insights and contributions of our research. Through this exploration, we aim to provide a comprehensive understanding of the advancements in CF-mMIMO networks and introduce innovative solutions to ensure high performance amidst the challenges posed by imperfect CSI.

5.1 Network Model

In this chapter, we continue to explore the UCCF network equipped with multi-antenna APs as described in the previous chapter, employing LSF for AP clustering. Consequently, the sum-rate expression remains consistent with that outlined in Equation (4-4). As outlined in previous chapters, the channel matrix \mathbf{G} , which represents the propagation effects between APs and UEs, is denoted as $\mathbf{G} = \hat{\mathbf{G}} + \tilde{\mathbf{G}} \in \mathbb{C}^{LN \times n}$. Here, $\hat{\mathbf{G}}$ represents the estimated channel matrix, and $\tilde{\mathbf{G}}$ denotes the channel estimation error. Accordingly, $g_{mk} = [\mathbf{G}]_{m,k}$ refers to the channel coefficient between the m th AP antenna (one of the $M = LN$ AP antennas) and the k th UE, representing the element of the channel matrix \mathbf{G} located at the m th row and the k th column, and is modeled as follows:

$$\begin{aligned} g_{mk} &= \hat{g}_{mk} + \tilde{g}_{mk} \\ &= \sqrt{1-\alpha} \sqrt{\beta_{mk}} h_{mk} + \sqrt{\alpha} \sqrt{\beta_{mk}} \tilde{h}_{mk}, \end{aligned} \quad (5-1)$$

where \hat{g}_{mk} is the channel coefficient estimate, \tilde{g}_{mk} is the channel coefficient estimation error, α is a CSI imperfection parameter that balances the contribution of the small scale channel estimation coefficient h_{mk} and its estimation error \tilde{h}_{mk} . Note that the large-scale fading (LSF) coefficient β_{mk} is assumed to be known, as it can be reliably estimated and tracked due to its slow variation, consistent with the findings in [19].

5.1.1 Resource Allocation in UCCF Networks

Given the constraint that the number of UEs K exceeds the total number of AP antennas M , user scheduling becomes necessary to ensure that a manageable and efficient subset of UEs is served at any given time. Defining the user scheduling task similar to the problem stated in Equation (3-1), the following optimization problem is considered:

$$\begin{aligned} \max_{\mathcal{S}_n} \quad & SR(\mathcal{S}_n) \\ \text{subject to} \quad & \|\mathbf{P}_a(\mathcal{S}_n)\|_F^2 \leq P, \end{aligned} \quad (5-2)$$

where SR denotes the sum-rate, and \mathcal{S}_n represents the set of n UEs to be scheduled, and P is the upper limit of the signal covariance matrix $\text{Tr}(\mathbf{C}_x) \leq P$. Additionally, $\mathbf{P}_a(\mathcal{S}_n) \in \mathbb{C}^{LN \times n}$ is the precoding matrix of the scheduled users.

The sum-rate equation, as defined in (4-4), is a complex expression that becomes even more intricate when the MMSE precoder is applied, due to its

reliance on matrix inversions and other advanced mathematical operations, making the optimization problem in (5-2) highly challenging. Therefore, to solve the optimization problem in (5-2) a greedy method is resorted.

Addressing the power allocation problem is essential for controlling interference and enhancing the overall sum-rate performance of the system. Initially, we rewrite the downlink UCCF received signal defined in (4-3) as follows:

$$\mathbf{y}_a = \sqrt{\rho_f} \hat{\mathbf{G}}_a^T \mathbf{P}_a \mathbf{x} + \sqrt{\rho_f} \tilde{\mathbf{G}}_a^T \mathbf{P}_a \mathbf{x} + \mathbf{w}, \quad (5-3)$$

where the precoding matrix in the desired term can be rewritten as $\mathbf{P}_a = \mathbf{W}\mathbf{D}$ such that $\mathbf{W} \in \mathbb{C}^{NL \times n}$ is the normalized linear precoder matrix and $\mathbf{D} \in \mathbb{C}^{n \times n}$ is the power allocation matrix as described in Equation (3-2), with the corresponding power allocation vector given by $\mathbf{d} = \text{diag}\{\mathbf{D}\} = [\sqrt{p_1} \ \sqrt{p_2} \ \cdots \ \sqrt{p_n}]^T$.

To perform power allocation, following the rationale described in Section 3.6, we use the Mean Squared Error (MSE) between the transmitted signal and the received signal as the objective function. The resulting optimization problem is similar to the one defined in Equation (3-31), as outlined below:

$$\begin{aligned} \min_{\mathbf{d}} \mathbb{E}[\varepsilon] \\ \text{subject to } \|\mathbf{W}\text{diag}(\mathbf{d})\|^2 \leq P, \end{aligned} \quad (5-4)$$

where the error is

$$\varepsilon = \|\mathbf{x} - \mathbf{y}_a\|^2. \quad (5-5)$$

As described in Section 3.6, adopting MSE is mathematically more tractable and can lead to a significant improvement in the sum-rate performance.

The network's scalability can be enhanced by first performing AP selection, ensuring each AP only serves a limited number of UEs, reducing computational load and fronthaul requirements. This approach, combined with linear MMSE precoder and user scheduling before power allocation, aligns with the findings in [2] and preserves scalability.

When examining the specified optimization problems, it becomes evident that imperfect CSI can lead to suboptimal decisions and performance degradation. This necessitates a robust optimization approach capable of mitigating the uncertainties introduced by CSI errors.

5.2

Robust Resource Allocation

In this section, we present the proposed robust resource allocation framework that is depicted in Fig. 5.1, which employs robust multiuser scheduling

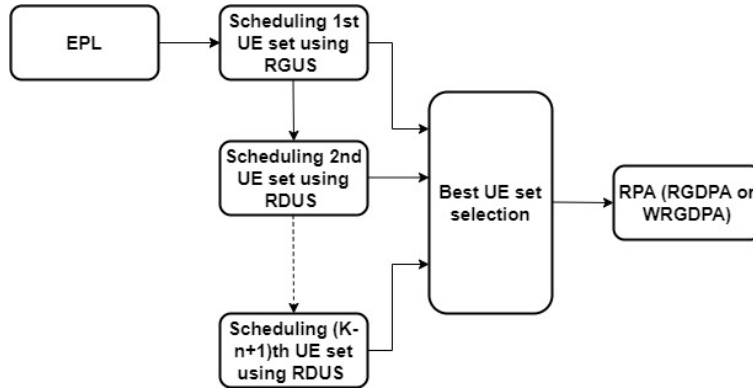


Figure 5.1: Block diagram of the proposed robust resource allocation.

and power allocation algorithms operating sequentially. The proposed framework employs a robust greedy user scheduling (RGUS) technique to initially select a set of UEs under the assumption of equal power loading (EPL). The adoption of a greedy technique is due to its low computational cost and reliable performance, which makes it an effective and practical solution for optimization. RGUS uses a robust dynamic UE substitution (RDUS) technique to consider potential UE sets and approach the optimal set identified. Following the selection of the best UE set based on the sum-rate criterion, our framework incorporates a robust power allocation (RPA) strategy, which is designed to allocate the power efficiently, further enhancing the performance ¹.

5.2.1 Robust multiuser scheduling

The proposed robust multiuser scheduling algorithm is presented based on worst-case optimization, which can be formulated as the following optimization problem:

$$\begin{aligned}
 & \max_{\mathcal{S}_n} \min_{\tilde{\mathbf{G}}_a} SR(\mathcal{S}_n) \\
 & \text{subject to} \\
 & \|\mathbf{P}_a(\mathcal{S}_n)\|_F^2 \leq P, \\
 & \beta \leq \|\tilde{\mathbf{g}}_k\|^2 \leq \beta_0, \forall k \in \mathcal{S}_n.
 \end{aligned} \tag{5-6}$$

where $\tilde{\mathbf{G}}_a$ is the channel estimation error, $\tilde{\mathbf{g}}_k$ is the channel estimation error for UE k , and β and β_0 bound the estimation error vector power for each UE in the selected set. The problem in (5-6) aims to optimize the sum-rate while targeting worst-case scenarios. It introduces a minimization operation over $\tilde{\mathbf{G}}_a$, which represents the uncertainty on CSI. In contrast to (5-2), this dual-layered optimization ensures that the sum-rate is maximized while the

¹This work focuses on robust resource allocation with standard MMSE and ZF precoders, which are not optimized for imperfect CSI at the transmitter. Exploring robust precoding techniques could further enhance performance and is a potential topic for future research.

robustness against the worst possible channel outcomes is enforced. As it will be shown later, using $\tilde{\mathbf{G}}_a$ leads us to the optimization of the parameter α that models the uncertainty on CSI.

In order to solve the problem in (5-6), inspired by the C-ESG multiuser scheduling algorithm in Section 3.2, we propose the robust clustered enhanced subset greedy (RC-ESG) multiuser scheduling method. We initiate this approach using the RGUS technique to schedule the first UE set. It first identifies a UE with the highest channel power by solving a robust extremum optimization problem (REOP) as follows:

$$\begin{aligned} k_1 = & \operatorname{argmax}_{k \in \mathcal{K}} \left(\min_{\tilde{\mathbf{g}}_k} \left(\mathbf{g}_k^H \mathbf{g}_k \right) \right) \\ & \text{subject to} \\ & \beta \leq \|\tilde{\mathbf{g}}_k\|^2 \leq \beta_0, \forall k \in \mathcal{K}, \end{aligned} \quad (5-7)$$

where $\mathcal{K} = \{1, \dots, K\}$ is set of all UEs. The robustification in this problem ensures that the solution is robust to variations within the channel constraints. Then, we select UEs to enhance the sum-rate. In each iteration, we identify and incorporate a UE that contributes to maximizing the channel power by solving a REOP problem similar to (5-7) as given by

$$\begin{aligned} k_1 = & \operatorname{argmax}_{k \in (\mathcal{K} \setminus \mathcal{U})} \left(\min_{\tilde{\mathbf{g}}_k} \left(\mathbf{g}_k^H \mathbf{g}_k \right) \right) \\ & \text{subject to} \\ & \beta \leq \|\tilde{\mathbf{g}}_k\|^2 \leq \beta_0, \forall k \in \mathcal{K} \setminus \mathcal{U}, \end{aligned} \quad (5-8)$$

where \mathcal{U} denotes the set of UEs selected in previous iterations. This process repeats until we find n UEs or it terminates when adding a new UE no longer improves the SR. The set of selected UEs is represented by S_n . Next, in an iterative manner, we utilize an RDUS technique for more possible EU set exploration. In this regard, in each iteration j , we identify a UE denoted as $k_r(j)$ within the current set $S_n(j)$ that under the worst-case channel conditions, exhibits the least channel power. Consequently, it is identified as the weakest link in terms of contributing to the SR. This is achieved through the solution of robust optimization problems as follows:

$$\begin{aligned} k_r(j) = & \operatorname{argmin}_{k \in S_n(j)} \left(\max_{\tilde{\mathbf{g}}_k} \left(\mathbf{g}_k^H \mathbf{g}_k \right) \right) \\ & \text{subject to} \\ & \beta \leq \|\tilde{\mathbf{g}}_k\|^2 \leq \beta_0, \forall k \in S_n(j). \end{aligned} \quad (5-9)$$

This optimization ensures the identification of the UE that could adversely affect the overall system performance under the worst estimation error. Next,

we select a UE from the current set of the remaining UEs $\mathcal{K}_{re}(j)$, those UEs not yet chosen in previous iterations, in a manner that is robust against imperfect CSI via an optimization problem as follows:

$$\begin{aligned} k_{su}(j) = & \underset{k \in \mathcal{K}_{re}(j)}{\operatorname{argmax}} \left(\min_{\tilde{\mathbf{g}}_k} \left(\mathbf{g}_k^H \mathbf{g}_k \right) \right) \\ & \text{subject to} \\ & \beta \leq \|\tilde{\mathbf{g}}_k\|^2 \leq \beta_0, \forall k \in \mathcal{K}_{re}(j). \end{aligned} \quad (5-10)$$

Note that $\mathcal{K}_{re}(1) = \mathcal{K} \setminus \mathcal{S}_n(1)$. Then, we replace $k_r(j)$ in the current UE set by $k_{su}(j)$, thereby obtaining the new UE set. Then, we can update the current set of selected UEs and the current set of the remaining UEs in each iteration as follows, respectively,

$$\mathcal{S}_n(j) = (\mathcal{S}_n(j-1) \setminus k_r(j-1)) \cup k_{su}(j-1), \quad (5-11)$$

$$\mathcal{K}_{re}(j) = \mathcal{K}_{re}(j-1) \setminus k_{su}(j-1). \quad (5-12)$$

This iteration is repeated and continued until we achieve a sufficient number of UE sets, allowing us to approximate the optimal set obtained through exhaustive search while substantially reducing computational complexity. Based on the given descriptions, we can detail the proposed RC-ESG method in Algorithm 8. This algorithm's selection criterion ensures robust, near-optimal convergence, with dynamic error bounds adapting to changing conditions. Its stopping criterion prevents overfitting, leading to a stable local optimum with reduced complexity, as validated by numerical results.

After obtaining the desired set based on the proposed RC-ESG algorithm, we update the sum-rate expression in (4-4) with $\tilde{\mathbf{G}}_a$. The updated sum-rate equation incorporates the expectation of \mathbf{R}_{UC} over $\tilde{\mathbf{G}}_a$, denoted as $\mathbf{R}_{UC_{\tilde{\mathbf{G}}_a}}$, which accounts for the dependency of the sum-rate on specific realizations of $\tilde{\mathbf{G}}_a$. Both $\hat{\mathbf{G}}_a$ and $\tilde{\mathbf{G}}_a$ are random variables. However, consistent with prior references such as [19], $\hat{\mathbf{G}}_a$ is treated as remaining constant within a coherence interval and is independent across different coherence intervals. Conversely, $\tilde{\mathbf{G}}_a$ is treated as a stochastic variable reflecting the channel error. By modeling $\tilde{\mathbf{G}}_a$ as a stochastic variable, we calculate an achievable rate that accounts for estimation errors, offering an upper bound on the sum-rate under imperfect channel knowledge. Since the transmitter only has access to the estimated channel $\hat{\mathbf{G}}_a$ and not the unknown estimation error $\tilde{\mathbf{G}}_a$, it is both practical and scientific to design the precoder \mathbf{P}_a solely based on $\hat{\mathbf{G}}_a$. This aligns with standard practice, as $\tilde{\mathbf{G}}_a$ is uncorrelated and independent of $\hat{\mathbf{G}}_a$ and cannot be included in the design without knowledge of the true channel, which is infeasible. Therefore, in our method, the precoder \mathbf{P}_a is designed only based

on $\hat{\mathbf{G}}_a$. Thus, the updated upper bound on the achievable sum-rate under imperfect channel knowledge is given by:

$$SR = \log_2 \left(\det \left[\mathbf{R}_{UC_{\hat{\mathbf{G}}_a}} + \mathbf{I}_K \right] \right), \quad (5-13)$$

where the expectation of \mathbf{R}_{UC} over $\tilde{\mathbf{G}}_a$ is:

$$\mathbf{R}_{UC_{\hat{\mathbf{G}}_a}} = \rho_f \hat{\mathbf{G}}_a^T \mathbf{P}_a \mathbf{P}_a^H \hat{\mathbf{G}}_a^* \left(\mathbf{R}_{\tilde{\mathbf{G}}_a} \right)^{-1}, \quad (5-14)$$

$$\mathbf{R}_{\tilde{\mathbf{G}}_a} = \mathbb{E}_{\tilde{\mathbf{G}}_a} \left[\rho_f \tilde{\mathbf{G}}_a^T \mathbf{P}_a \mathbf{P}_a^H \tilde{\mathbf{G}}_a^* \right] + \sigma_w^2 \mathbf{I}_K. \quad (5-15)$$

Algorithm 8: RC-ESG Multiuser Scheduling Algorithm with Worst-Case Scenario

```

1 Input: set  $\mathcal{K}$ , thresholds  $\beta, \beta_0$ , number of UEs  $n$ , system parameters
2 Output: scheduled UEs  $\mathcal{S}_n^d$ 
3 Initialize  $j = 1, l = 1$ 
4 Adjust  $\beta, \beta_0$  based on initial system state
5  $k_1 = \operatorname{argmax}_{k \in \mathcal{K}} \left( \min_{\tilde{\mathbf{g}}_k} \left( \mathbf{g}_k^H \mathbf{g}_k \right) \right)$ , s.t.  $\beta \leq \|\tilde{\mathbf{g}}_k\|^2 \leq \beta_0, \forall k \in \mathcal{K}$ 
6 Denote  $k_1$  as  $\mathcal{U}_1$  and the rate as  $SR(\mathcal{U}_1)$ 
7 while  $l < n$  do
8    $l = l + 1$ 
9   Dynamically adjust  $\beta, \beta_0$  based on current system performance
10   $k_l = \operatorname{argmax}_{k \in (\mathcal{K} \setminus \mathcal{U}_{l-1})} \left( \min_{\tilde{\mathbf{g}}_k} \left( \mathbf{g}_k^H \mathbf{g}_k \right) \right)$ , s.t.  $\beta \leq \|\tilde{\mathbf{g}}_k\|^2 \leq \beta_0$ 
11  Set  $\mathcal{U}_l = \mathcal{U}_{l-1} \cup \{k_l\}$  and denote the rate  $SR(\mathcal{U}_l)$ 
12  if  $SR(\mathcal{U}_l) \leq SR(\mathcal{U}_{l-1})$  then
13    Break,  $l = l - 1$ 
14  end
15 end
16 for  $j = 1$  to  $K - n + 1$  do
17   if  $j = 1$  then
18      $\mathcal{S}_n(j) = \mathcal{U}_l$ 
19      $\mathcal{K}_{\text{re}}(j) = \mathcal{K} \setminus \mathcal{S}_n(j)$ 
20   else
21      $\mathcal{S}_n(j) = (\mathcal{S}_n(j-1) \setminus k_r(j-1)) \cup k_{su}(j-1)$ 
22      $\mathcal{K}_{\text{re}}(j) = \mathcal{K}_{\text{re}}(j-1) \setminus k_{su}(j-1)$ 
23   end
24   Update  $\beta, \beta_0$  based on current system state
25    $k_r(j) = \operatorname{argmin}_{k \in \mathcal{S}_n(j)} \left( \max_{\tilde{\mathbf{g}}_k} \left( \mathbf{g}_k^H \mathbf{g}_k \right) \right)$ , s.t.  $\beta \leq \|\tilde{\mathbf{g}}_k\|^2 \leq \beta_0, \forall k \in \mathcal{S}_n(j)$ 
26    $k_{su}(j) = \operatorname{argmax}_{k \in \mathcal{K}_{\text{re}}(j)} \left( \min_{\tilde{\mathbf{g}}_k} \left( \mathbf{g}_k^H \mathbf{g}_k \right) \right)$ , s.t.  $\beta \leq \|\tilde{\mathbf{g}}_k\|^2 \leq \beta_0, \forall k \in \mathcal{K}_{\text{re}}(j)$ 
27   Compute:  $SR(\mathcal{S}_n(j))$ 
28 end
29  $\mathcal{S}_n^d = \operatorname{argmax}_{\mathcal{S}_n \in \mathcal{S}_n(m)} \{SR(\mathcal{S}_n)\}$ 

```

Within this algorithm, the primary focus is on addressing the REOP problems, exemplified by such a formulation as in (5-7)-(5-10). The analysis and the proposed solutions to these types of problems are discussed in Section 5.3.

5.2.2

Robust Power Allocation

Due to the computational cost and the difficulty to apply worst-case optimization for power allocation with the MMSE precoder, as discussed in Section 5.2.2.2, we devise an alternative approach based on the contribution of the channel estimation matrix. Next, we adopt the worst-case optimization strategy for a simpler precoder, i.e., ZF, which in this case offers a simpler analysis. Accordingly, we propose RGDPA and WRGDPA robust power allocation algorithms against the CSI errors which are used to determine the power allocation matrix \mathbf{D} . The proposed algorithms are based on gradient descent techniques, which are robust and cost-effective.

5.2.2.1

RGDPA approach

When faced with imperfect CSI, the RGDPA algorithm incorporates the channel estimation error and considers a robust optimization approach as follows:

$$\begin{aligned} & \min_{\mathbf{d}} \mathbb{E} [\varepsilon \mid \hat{\mathbf{G}}_a] \\ & \text{subject to} \end{aligned} \quad (5-16)$$

$$\|\mathbf{W}\text{diag}(\mathbf{d})\|^2 \leq P$$

This approach accounts for the uncertainty in the channel estimation, because by conditioning the expectation of the error ε on the estimated channel matrix $\hat{\mathbf{G}}_a$, the optimization problem acknowledges the presence of estimation errors leading to a power allocation strategy that is less sensitive to the inaccuracies in the CSI, and hence, is more robust.

In this context, we first obtain the error equation. Using (5-3) and (5-5), the error equation is expanded as

$$\begin{aligned} \varepsilon = & \mathbf{x}^H \mathbf{x} + \mathbf{w}^H \mathbf{w} + \\ & \rho_f \mathbf{x}^H \text{diag}(\mathbf{d}) \mathbf{W}^H \hat{\mathbf{G}}_a^* \hat{\mathbf{G}}_a^T \mathbf{W} \text{diag}(\mathbf{d}) \mathbf{x} + \\ & \rho_f \mathbf{x}^H \mathbf{P}_a^H \tilde{\mathbf{G}}_a^* \tilde{\mathbf{G}}_a^T \mathbf{P}_a \mathbf{x} - \\ & \sqrt{\rho_f} \mathbf{x}^H \hat{\mathbf{G}}_a^T \mathbf{W} \text{diag}(\mathbf{d}) \mathbf{x} - \sqrt{\rho_f} \mathbf{x}^H \text{diag}(\mathbf{d}) \mathbf{W}^H \hat{\mathbf{G}}_a^* \mathbf{x} - \\ & \sqrt{\rho_f} \mathbf{x}^H \tilde{\mathbf{G}}_a^T \mathbf{P}_a \mathbf{x} - \sqrt{\rho_f} \mathbf{x}^H \mathbf{P}_a^H \tilde{\mathbf{G}}_a^* \mathbf{x} - \\ & \mathbf{x}^H \mathbf{w} - \mathbf{w}^H \mathbf{x} + \rho_f \mathbf{x}^H \text{diag}(\mathbf{d}) \mathbf{W}^H \hat{\mathbf{G}}_a^* \tilde{\mathbf{G}}_a^T \mathbf{P}_a \mathbf{x} + \\ & \rho_f \mathbf{x}^H \mathbf{P}_a^H \tilde{\mathbf{G}}_a^* \hat{\mathbf{G}}_a^T \mathbf{W} \text{diag}(\mathbf{d}) \mathbf{x} + \\ & \sqrt{\rho_f} \mathbf{x}^H \text{diag}(\mathbf{d}) \mathbf{W}^H \hat{\mathbf{G}}_a^* \mathbf{w} + \sqrt{\rho_f} \mathbf{w}^H \hat{\mathbf{G}}_a^T \mathbf{W} \text{diag}(\mathbf{d}) \mathbf{x} + \\ & \sqrt{\rho_f} \mathbf{w}^H \tilde{\mathbf{G}}_a^T \mathbf{P}_a \mathbf{x} + \sqrt{\rho_f} \mathbf{x}^H \mathbf{P}_a^H \tilde{\mathbf{G}}_a^* \mathbf{w} \end{aligned} \quad (5-17)$$

Given that the trace operator retains a scalar unchanged, and employing the property that $Tr(\mathbf{A} + \mathbf{B}) = Tr(\mathbf{A}) + Tr(\mathbf{B})$, where \mathbf{A} and \mathbf{B} are matrices of the same dimensions, the error is reformulated as

$$\begin{aligned}
\varepsilon = & Tr(\mathbf{x}^H \mathbf{x}) - Tr(\mathbf{x}^H \mathbf{w}) - Tr(\mathbf{w}^H \mathbf{x}) + Tr(\mathbf{w}^H \mathbf{w}) + \\
& Tr(\rho_f \mathbf{x}^H \text{diag}(\mathbf{d}) \mathbf{W}^H \hat{\mathbf{G}}_a^* \hat{\mathbf{G}}_a^T \mathbf{W} \text{diag}(\mathbf{d}) \mathbf{x}) + \\
& Tr(\rho_f \mathbf{x}^H \mathbf{P}_a^H \tilde{\mathbf{G}}_a^* \tilde{\mathbf{G}}_a^T \mathbf{P}_a \mathbf{x}) - \\
& Tr(\sqrt{\rho_f} \mathbf{x}^H \hat{\mathbf{G}}_a^T \mathbf{W} \text{diag}(\mathbf{d}) \mathbf{x}) - \\
& Tr(\sqrt{\rho_f} \mathbf{x}^H \text{diag}(\mathbf{d}) \mathbf{W}^H \hat{\mathbf{G}}_a^* \mathbf{x}) - \\
& Tr(\sqrt{\rho_f} \mathbf{x}^H \tilde{\mathbf{G}}_a^T \mathbf{P}_a \mathbf{x}) - Tr(\sqrt{\rho_f} \mathbf{x}^H \mathbf{P}_a^H \tilde{\mathbf{G}}_a^* \mathbf{x}) + \\
& Tr(\rho_f \mathbf{x}^H \text{diag}(\mathbf{d}) \mathbf{W}^H \hat{\mathbf{G}}_a^* \hat{\mathbf{G}}_a^T \mathbf{P}_a \mathbf{x}) + \\
& Tr(\rho_f \mathbf{x}^H \mathbf{P}_a^H \tilde{\mathbf{G}}_a^* \hat{\mathbf{G}}_a^T \mathbf{W} \text{diag}(\mathbf{d}) \mathbf{x}) + \\
& Tr(\sqrt{\rho_f} \mathbf{x}^H \text{diag}(\mathbf{d}) \mathbf{W}^H \hat{\mathbf{G}}_a^* \mathbf{w}) + \\
& Tr(\sqrt{\rho_f} \mathbf{w}^H \hat{\mathbf{G}}_a^T \mathbf{W} \text{diag}(\mathbf{d}) \mathbf{x}) + \\
& Tr(\sqrt{\rho_f} \mathbf{w}^H \tilde{\mathbf{G}}_a^T \mathbf{P}_a \mathbf{x}) + Tr(\sqrt{\rho_f} \mathbf{x}^H \mathbf{P}_a^H \tilde{\mathbf{G}}_a^* \mathbf{w}).
\end{aligned} \tag{5-18}$$

where $\mathbf{x} \sim \mathcal{CN}(\mathbf{0}, \mathbf{I}_n)$ and \mathbf{w} similarly follows $\mathbf{w} \sim \mathcal{CN}(0, \sigma_w^2 \mathbf{I}_n)$, and we consider the elements of the error $\tilde{\mathbf{G}}_a$ as zero-mean random variables. Moreover, these elements are assumed to be mutually independent. Under these conditions, the expectation of the error given $\hat{\mathbf{G}}_a$ can be simplified as

$$\begin{aligned}
\mathbb{E}[\varepsilon | \hat{\mathbf{G}}_a] = & n + n\sigma_w^2 + \\
& Tr(\rho_f \text{diag}(\mathbf{d}) \mathbf{W}^H \hat{\mathbf{G}}_a^* \hat{\mathbf{G}}_a^T \mathbf{W} \text{diag}(\mathbf{d})) + \\
& Tr(\rho_f \mathbb{E}_{\tilde{\mathbf{G}}_a} [\mathbf{P}_a^H \tilde{\mathbf{G}}_a^* \tilde{\mathbf{G}}_a^T \mathbf{P}_a]) - \\
& Tr(\sqrt{\rho_f} \hat{\mathbf{G}}_a^T \mathbf{W} \text{diag}(\mathbf{d})) - \\
& Tr(\sqrt{\rho_f} \text{diag}(\mathbf{d}) \mathbf{W}^H \hat{\mathbf{G}}_a^*)
\end{aligned} \tag{5-19}$$

Accordingly, we first compute the derivative of the conditional error expectation with respect to the power allocation matrix. By employing $\frac{\partial Tr(\mathbf{A}\mathbf{B})}{\partial \mathbf{A}} = \mathbf{B} \odot \mathbf{I}$, where \mathbf{A} is a diagonal matrix and \odot is the Hadamard product [55], and the cyclic property of the trace operator, the first derivative of the objective function with respect to the power allocation factors is given by

$$\begin{aligned}
\frac{\partial \mathbb{E}[\varepsilon | \hat{\mathbf{G}}_a]}{\partial \mathbf{d}} = & 2\rho_f (\mathbf{W}^H \hat{\mathbf{G}}_a^* \hat{\mathbf{G}}_a^T \mathbf{W} \text{diag}(\mathbf{d})) \odot \mathbf{I} - \\
& 2\sqrt{\rho_f} Re \{ \mathbf{W}^H \hat{\mathbf{G}}_a^* \odot \mathbf{I} \}
\end{aligned} \tag{5-20}$$

Thus, as will be analyzed in Section 5.3.2, we consider the conditional error

expectation convex with respect to the power allocation matrix. Hence, we can use a gradient descent technique to solve the conditional MSE minimization with respect to the power allocation factors. Consequently, we update the power allocation coefficient in an iterative manner as follows:

$$\mathbf{d}(i) = \mathbf{d}(i-1) - \lambda \left. \frac{\partial \mathbb{E}[\varepsilon | \hat{\mathbf{G}}_a]}{\partial \mathbf{d}} \right|_{\mathbf{d}=\mathbf{d}(i-1)} \quad (5-21)$$

where i is the iteration index, and λ is the positive step size and $\frac{\partial \mathbb{E}[\varepsilon | \hat{\mathbf{G}}_a]}{\partial \mathbf{d}}$ is obtained as in (5-20). In order for the transmit power constraint to be satisfied as $\|\mathbf{W}\text{diag}(\mathbf{d})\|^2 = \|\mathbf{P}_a\|^2 \leq P$, after the iterations, we scale the power allocation coefficients as using the power scaling factor given by

$$\eta = \sqrt{\frac{\text{Tr}(\mathbf{P}_a \mathbf{P}_a^H)}{\text{Tr}(\mathbf{W}\text{diag}(\mathbf{d}, \mathbf{d}) \mathbf{W}^H)}} \quad (5-22)$$

A summary of the proposed RGDPA algorithm is presented in Algorithm 9.

Algorithm 9: Proposed RGDPA Power Allocation

```

1 Input:  $\mathbf{G}_a, \mathbf{P}_a, \mathbf{W}, \lambda, \mathbf{d}(1), I_D$ 
2 for  $i = 2$  to  $I_D$  do
3    $\left. \frac{\partial \mathbb{E}[\varepsilon | \hat{\mathbf{G}}_a]}{\partial \mathbf{d}} = 2\rho_f (\mathbf{W}^H \hat{\mathbf{G}}_a^* \hat{\mathbf{G}}_a^T \mathbf{W} \text{diag}(\mathbf{d})) \odot \mathbf{I} - 2\sqrt{\rho_f} \Re \{ \mathbf{W}^H \hat{\mathbf{G}}_a^* \odot \mathbf{I} \} \right|$ 
4    $\left. \mathbf{d}(i) = \mathbf{d}(i-1) - \lambda \frac{\partial \mathbb{E}[\varepsilon | \hat{\mathbf{G}}_a]}{\partial \mathbf{d}} \right|_{\mathbf{d}=\mathbf{d}(i-1)}$ 
5 end
6  $\mathbf{d}_d = \mathbf{d}(I_D)$ 
7 if  $\text{Tr}(\mathbf{W}\text{diag}(\mathbf{d}_d, \mathbf{d}_d) \mathbf{W}^H) \neq \text{Tr}(\mathbf{P}_a \mathbf{P}_a^H)$  then
8    $\eta = \sqrt{\frac{\text{Tr}(\mathbf{P}_a \mathbf{P}_a^H)}{\text{Tr}(\mathbf{W}\text{diag}(\mathbf{d}_d, \mathbf{d}_d) \mathbf{W}^H)}}$ 
9    $\mathbf{d}_d = \eta \mathbf{d}_d$ 
10 end
```

Note that when the error expectation is not conditioned, it gives rise to the gradient descent power allocation (GDPA) algorithm. In this case, we use the error equation in (5-18), where \mathbf{x} is assumed to follow a $\mathcal{CN}(\mathbf{0}, \mathbf{I}_n)$ distribution, \mathbf{w} follows a $\mathcal{CN}(0, \sigma_w^2 \mathbf{I}_n)$ distribution, and both $\hat{\mathbf{G}}_a$ and $\tilde{\mathbf{G}}_a$ are treated as zero-mean random variables. Furthermore, all these elements are considered to be mutually independent. Thus, the error expectation is expressed by

$$\begin{aligned} \mathbb{E}[\varepsilon] = & n + n\sigma_w^2 + \text{Tr} \left(\rho_f \mathbb{E}_{\tilde{\mathbf{G}}_a} \left[\mathbf{P}_a^H \tilde{\mathbf{G}}_a^* \tilde{\mathbf{G}}_a^T \mathbf{P}_a \right] \right) + \\ & \text{Tr} \left(\rho_f \text{diag}(\mathbf{d}) \mathbf{W}^H \hat{\mathbf{G}}_a^* \hat{\mathbf{G}}_a^T \mathbf{W} \text{diag}(\mathbf{d}) \right) \end{aligned} \quad (5-23)$$

Hence, we can obtain the first derivative of the error expectation with respect to the power allocation factors as follows:

$$\frac{\partial \mathbb{E}[\varepsilon]}{\partial \mathbf{d}} = 2\rho_f \left(\mathbf{W}^H \hat{\mathbf{G}}_a^* \hat{\mathbf{G}}_a^T \mathbf{W} \text{diag}(\mathbf{d}) \right) \odot \mathbf{I} \quad (5-24)$$

Accordingly, the GDPA algorithm is a special case of Algorithm 9, where the power allocation factors are updated in each iteration using $\frac{\partial \mathbb{E}[\varepsilon]}{\partial \mathbf{d}}$ as obtained in (5-24). The convexity of the conditional error expectation ensures that the GDPA algorithm converges to a global minimum, while the normalization step enforces the power constraint.

5.2.2.2

WRGDPA approach

In order to make the optimization problem given in (5-4) robust against imperfect CSI, a promising alternative is to define the worst-case robust optimization problem as follows:

$$\begin{aligned} & \min_{\mathbf{d}} \max_{\tilde{\mathbf{G}}_a} \mathbb{E}[\varepsilon] \\ & \text{subject to} \\ & \|\mathbf{W} \text{diag}(\mathbf{d})\|^2 \leq P, \\ & \beta_1 \leq \|\tilde{\mathbf{G}}_a\|^2 \leq \beta_2. \end{aligned} \quad (5-25)$$

In the optimization problem described in (5-25), the error expectation $\mathbb{E}[\varepsilon]$ is derived as (5-23) as described in Section 5.2.2.1. Based on the analysis in Section 5.3.3, in the objective function in (5-25), in order to obtain robustness against imperfect CSI, the CSI imperfection level parameter α should be optimized. Hence, for convexity analysis of the objective function with respect to CSI imperfection level α , we consider the following definitions:

$$\tilde{\mathbf{G}}_a = \sqrt{\alpha} \tilde{\mathbf{V}}, \tilde{\mathbf{V}}_{mk} = \sqrt{\beta_{mk}} \tilde{h}_{mk} \quad (5-26)$$

$$\hat{\mathbf{G}}_a = \sqrt{(1-\alpha)} \mathbf{V}, \mathbf{V}_{mk} = \sqrt{\beta_{mk}} h_{mk} \quad (5-27)$$

Thus, we rewrite (5-23) as

$$\begin{aligned} \mathbb{E}[\varepsilon] = & n + n\sigma_w^2 + \\ & \text{Tr} \left(\rho_f (1-\alpha) \text{diag}(\mathbf{d}) \mathbf{W}^H \mathbf{V}^* \mathbf{V}^T \mathbf{W} \text{diag}(\mathbf{d}) \right) + \\ & \text{Tr} \left(\rho_f \alpha \mathbb{E}_{\tilde{\mathbf{V}}} \left[\mathbf{P}_a^H \tilde{\mathbf{V}}^* \tilde{\mathbf{V}}^T \mathbf{P}_a \right] \right) \end{aligned} \quad (5-28)$$

We consider \mathbf{P}_a as the linear MMSE precoder given by

$$\mathbf{P}_a = \eta \mathbf{L}^{-1} \mathbf{G}_a^H \mathbf{F}^H \quad (5-29)$$

where

$$\eta = \sqrt{\frac{P}{\text{Tr}(\mathbf{L}^{-2} \mathbf{G}_a^H \mathbf{F}^H \mathbf{C}_x \mathbf{F} \mathbf{G}_a)}}, \quad (5-30)$$

$$\mathbf{L} = \mathbf{G}_a^H \mathbf{F}^H \mathbf{F} \mathbf{G}_a + \frac{\text{Tr}(\mathbf{F} \mathbf{C}_w \mathbf{F}^H)}{P} \mathbf{I}_n, \quad (5-31)$$

and \mathbf{F} is a linear equalizer matrix which we consider as $\mathbf{F} = \mathbf{I}_n$, $\mathbf{I}_n \in \mathbb{C}^{n \times n}$ is the identity matrix, $\mathbf{C}_x = \mathbf{I}_n$ is the signal covariance matrix, and $\mathbf{C}_w = \sigma_w^2 \mathbf{I}_n$ is the noise covariance matrix. Based on the given equations and expressions, the application of the MMSE linear precoder leads to intricate equations using the derivative rules, posing challenges for mathematical tractability regarding the first and the second derivatives of (5-28) with respect to α . Therefore, in order to be able to perform the worst-case optimization analysis, we employ a linear ZF precoder.

In this regard, the ZF precoder is described by

$$\mathbf{P}_a = (\mathbf{G}_a^H \mathbf{G}_a)^{-1} \mathbf{G}_a^H. \quad (5-32)$$

Using Equations (5-26) and (5-27), we can rewrite \mathbf{P}_a as

$$\mathbf{P}_a = (\mathbf{H})^{-1} \mathbf{Q}, \quad (5-33)$$

where

$$\begin{aligned} \mathbf{H} = & (1 - \alpha) \mathbf{V}^H \mathbf{V} + \sqrt{\alpha(1 - \alpha)} \mathbf{V}^H \tilde{\mathbf{V}} \\ & + \sqrt{\alpha(1 - \alpha)} \tilde{\mathbf{V}}^H \mathbf{V} + \alpha \tilde{\mathbf{V}}^H \tilde{\mathbf{V}}, \end{aligned} \quad (5-34)$$

$$\mathbf{Q} = \sqrt{\alpha} \tilde{\mathbf{V}}^H + \sqrt{(1 - \alpha)} \mathbf{V}^H. \quad (5-35)$$

Calculating the first derivatives of \mathbf{H} and \mathbf{Q} with respect to α , we obtain the following equations:

$$\begin{aligned} \mathbf{H}_{d1} = \frac{d\mathbf{H}}{d\alpha} = & -\mathbf{V}^H \mathbf{V} + \frac{1 - 2\alpha}{2\sqrt{\alpha(1 - \alpha)}} \mathbf{V}^H \tilde{\mathbf{V}} \\ & + \frac{1 - 2\alpha}{2\sqrt{\alpha(1 - \alpha)}} \tilde{\mathbf{V}}^H \mathbf{V} + \tilde{\mathbf{V}}^H \tilde{\mathbf{V}}, \end{aligned} \quad (5-36)$$

$$\mathbf{Q}_{d1} = \frac{d\mathbf{Q}}{d\alpha} = \frac{1}{2\sqrt{\alpha}} \tilde{\mathbf{V}}^H - \frac{1}{2\sqrt{(1 - \alpha)}} \mathbf{V}^H. \quad (5-37)$$

To obtain the first derivative of the objective function $\mathbb{E}[\varepsilon]$ given in (5-28) with respect to α , we use the chain rule for derivatives and $\frac{\partial \mathbf{A}^{-1}}{\partial x} = -\mathbf{A}^{-1} \frac{\partial \mathbf{A}}{\partial x} \mathbf{A}^{-1}$ where \mathbf{A} is a matrix and x is a scalar [55], and we take the derivative of \mathbf{P}_a as

$$\mathbf{P}_{ad1} = \frac{\partial \mathbf{P}_a}{\partial \alpha} = -\mathbf{H}^{-1} \mathbf{H}_{d1} \mathbf{H}^{-1} \mathbf{Q} + \mathbf{H}^{-1} \mathbf{Q}_{d1} \quad (5-38)$$

Consequently, we obtain the first derivative of the objective function with respect to α as follows:

$$\begin{aligned} \frac{\partial \mathbb{E}[\varepsilon]}{\partial \alpha} = & Tr \left(\rho_f \mathbb{E}_{\tilde{\mathbf{V}}} \left[\mathbf{P}_a^H \tilde{\mathbf{V}}^* \tilde{\mathbf{V}}^T \mathbf{P}_a \right] \right) + \\ & Tr \left(\rho_f \alpha \mathbb{E}_{\tilde{\mathbf{V}}} \left[\mathbf{P}_{ad1}^H \tilde{\mathbf{V}}^* \tilde{\mathbf{V}}^T \mathbf{P}_a \right] \right) + \\ & Tr \left(\rho_f \alpha \mathbb{E}_{\tilde{\mathbf{V}}} \left[\mathbf{P}_a^H \tilde{\mathbf{V}}^* \tilde{\mathbf{V}}^T \mathbf{P}_{ad1} \right] \right) - \\ & Tr \left(\rho_f \text{diag}(\mathbf{d}) \mathbf{W}^H \mathbf{V}^* \mathbf{V}^T \mathbf{W} \text{diag}(\mathbf{d}) \right) \end{aligned} \quad (5-39)$$

For the second derivative of the objective function with respect to α , we obtain derivatives of \mathbf{H}_{d1} , \mathbf{Q}_{d1} and \mathbf{P}_{ad1} as follows:

$$\mathbf{H}_{d2} = \frac{\partial \mathbf{H}_{d1}}{\partial \alpha} = \frac{-1}{4\alpha(1-\alpha)\sqrt{\alpha(1-\alpha)}} \left(\mathbf{V}^H \tilde{\mathbf{V}} + \tilde{\mathbf{V}}^H \mathbf{V} \right), \quad (5-40)$$

$$\mathbf{Q}_{d2} = \frac{\partial \mathbf{Q}_{d1}}{\partial \alpha} = -\frac{1}{4\sqrt{\alpha^3}} \tilde{\mathbf{V}}^H - \frac{1}{4\sqrt{(1-\alpha)^3}} \mathbf{V}^H, \quad (5-41)$$

$$\begin{aligned} \mathbf{P}_{ad2} = \frac{\partial \mathbf{P}_{ad1}}{\partial \alpha} = & -\mathbf{H}_{d1} \mathbf{H}_{d1} \mathbf{H}^{-1} \mathbf{Q} - \mathbf{H} \mathbf{H}_{d2} \mathbf{H}^{-1} \mathbf{Q} \\ & + \mathbf{H} \mathbf{H}_{d1} \mathbf{H} \mathbf{H}_{d1} \mathbf{H}^{-1} \mathbf{H}^{-1} \mathbf{Q} \\ & - \mathbf{H} \mathbf{H}_{d1} \mathbf{H}^{-1} \mathbf{Q}_{d1} - \mathbf{H} \mathbf{H}_{d1} \mathbf{H}^{-1} \mathbf{Q}_{d1} \\ & + \mathbf{H}^{-1} \mathbf{Q}_{d2}. \end{aligned} \quad (5-42)$$

Note that \mathbf{H}_{d1} is a square matrix. Accordingly, the second derivative of $\mathbb{E}[\varepsilon]$ with respect to α could be written as

$$\begin{aligned} \frac{\partial^2 \mathbb{E}[\varepsilon]}{\partial \alpha^2} = & Tr \left(\rho_f \mathbb{E}_{\tilde{\mathbf{V}}} \left[\mathbf{P}_{ad1}^H \tilde{\mathbf{V}}^* \tilde{\mathbf{V}}^T \mathbf{P}_a \right] \right) + Tr \left(\rho_f \mathbb{E}_{\tilde{\mathbf{V}}} \left[\mathbf{P}_a^H \tilde{\mathbf{V}}^* \tilde{\mathbf{V}}^T \mathbf{P}_{ad1} \right] \right) + \\ & Tr \left(\rho_f \mathbb{E}_{\tilde{\mathbf{V}}} \left[\mathbf{P}_{ad1}^H \tilde{\mathbf{V}}^* \tilde{\mathbf{V}}^T \mathbf{P}_a \right] \right) + Tr \left(\rho_f \alpha \mathbb{E}_{\tilde{\mathbf{V}}} \left[\mathbf{P}_{ad2}^H \tilde{\mathbf{V}}^* \tilde{\mathbf{V}}^T \mathbf{P}_a \right] \right) + \\ & Tr \left(\rho_f \alpha \mathbb{E}_{\tilde{\mathbf{V}}} \left[\mathbf{P}_{ad1}^H \tilde{\mathbf{V}}^* \tilde{\mathbf{V}}^T \mathbf{P}_{ad1} \right] \right) + Tr \left(\rho_f \mathbb{E}_{\tilde{\mathbf{V}}} \left[\mathbf{P}_a^H \tilde{\mathbf{V}}^* \tilde{\mathbf{V}}^T \mathbf{P}_{ad1} \right] \right) + \\ & Tr \left(\rho_f \alpha \mathbb{E}_{\tilde{\mathbf{V}}} \left[\mathbf{P}_{ad1}^H \tilde{\mathbf{V}}^* \tilde{\mathbf{V}}^T \mathbf{P}_{ad1} \right] \right) + Tr \left(\rho_f \alpha \mathbb{E}_{\tilde{\mathbf{V}}} \left[\mathbf{P}_a^H \tilde{\mathbf{V}}^* \tilde{\mathbf{V}}^T \mathbf{P}_{ad2} \right] \right). \end{aligned} \quad (5-43)$$

Now, in order to solve the maximization over channel estimation error in the optimization problem in (5-25), since we aim to solve the problem with respect to α , we resort to:

- $\frac{\partial^2 \mathbb{E}[\varepsilon]}{\partial \alpha^2} > 0$: In this case, since $\mathbb{E}[\varepsilon]$ is convex with respect to α , any local extremum (minimum or maximum) within the feasible region is also a global extremum. For maximization problems with a convex objective, the global maximum occurs at the boundary of the feasible region. This concept is illustrated in Fig. 5.2, where the convex function $f(x)$ is

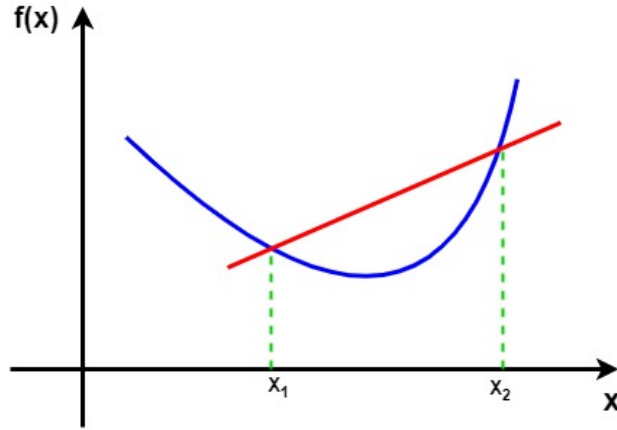


Figure 5.2: Boundary extremum illustration, convex case

examined within the interval $x_1 \leq x \leq x_2$, revealing that its maximum value occurs precisely at the endpoint x_2 . Thus, the maximum of the objective function will occur at the boundary of the feasible set and the desired α is given as follows:

$$\alpha = \begin{cases} \frac{\beta_1}{\|\mathbf{V}\|^2}, & \text{if } \mathbb{E}[\varepsilon] \Big|_{\alpha=\frac{\beta_1}{\|\mathbf{V}\|^2}} > \mathbb{E}[\varepsilon] \Big|_{\alpha=\frac{\beta_2}{\|\mathbf{V}\|^2}} \\ \frac{\beta_2}{\|\mathbf{V}\|^2}, & \text{if } \mathbb{E}[\varepsilon] \Big|_{\alpha=\frac{\beta_2}{\|\mathbf{V}\|^2}} > \mathbb{E}[\varepsilon] \Big|_{\alpha=\frac{\beta_1}{\|\mathbf{V}\|^2}} \end{cases} \quad (5-44)$$

- $\frac{\partial^2 \mathbb{E}[\varepsilon]}{\partial \alpha^2} < 0$: In this case, $\mathbb{E}[\varepsilon]$ is concave with respect to α . Thus we use a gradient ascent technique to find the desired α which maximizes the objective $\mathbb{E}[\varepsilon]$. In this regard, the imperfection parameter is updated as

$$\alpha(t) = \alpha(t-1) + \gamma \frac{\partial \mathbb{E}[\varepsilon]}{\partial \alpha} \Big|_{\alpha=\alpha(t-1)} \quad (5-45)$$

where t is the iteration index, γ is the positive step size and $\frac{\partial \mathbb{E}[\varepsilon]}{\partial \alpha}$ is obtained using (5-39). After obtaining the desired channel estimation error parameter as α_d , if the feasible set is not met, the following update is done to make sure that it lies in the feasible set $\beta_1 \leq \|\tilde{\mathbf{G}}_a\|^2 \leq \beta_2$:

$$\alpha_d = \begin{cases} \frac{\beta_1}{\|\mathbf{V}\|^2}, & \text{if } \alpha < \frac{\beta_1}{\|\mathbf{V}\|^2} \\ \frac{\beta_2}{\|\mathbf{V}\|^2}, & \text{if } \alpha > \frac{\beta_2}{\|\mathbf{V}\|^2} \end{cases} \quad (5-46)$$

Next, we should solve the minimization of the MSE over the power loading matrix \mathbf{D} . We first investigate the convexity of $\mathbb{E}[\varepsilon]$ given in (5-23). Thus, we derive the first derivative with respect to \mathbf{d} as (5-24). However, as Equations (5-20) and (5-24) are the same with respect to the power allocation factors \mathbf{d} , the

convexity analysis of the error expectation over \mathbf{d} is the same as the described analysis in Section 5.3.2. Thus, we conclude that the objective $\mathbb{E}[\varepsilon]$ is convex with respect to the power allocation factors. Therefore, in order to obtain the MSE minimization solution with respect to the power allocation factors, we use the same gradient descent technique developed in Section 5.2.2.1, while $\frac{\partial \mathbb{E}[\varepsilon]}{\partial \mathbf{d}}$ is calculated using Equation (5-24) to update the power allocation coefficients.

We can now summarize the proposed worst-case robust gradient descent power allocation (WRGDPA) algorithm in Algorithm 10, where I_G and I_D show the numbers of iterations in the iterative maximization and iterative minimization in the solution to the problem in (5-25), respectively. The WRGDPA algorithm ensures optimality by identifying the worst-case α based on convexity and then minimizing the error over \mathbf{d} using gradient descent, while enforcing power constraints.

Algorithm 10: Proposed WRGDPA Power Allocation

```

1 Input:  $\mathbf{G}_a, \mathbf{P}_a, \mathbf{W}, \tilde{\mathbf{V}}, \mathbf{V}, \lambda, \gamma, \beta_1, \beta_2, \mathbf{I}_D, \mathbf{I}_G, \alpha(1), \mathbf{d}(1)$ 
2 Calculate  $\frac{\partial \mathbb{E}[\varepsilon]}{\partial \alpha}$  using Eq. (5-39) and  $\frac{\partial^2 \mathbb{E}[\varepsilon]}{\partial \alpha^2}$  as Eq. (5-43)
3 if  $\frac{\partial^2 \mathbb{E}[\varepsilon]}{\partial \alpha^2} > 0$  then
4   | Derive  $\alpha$  as Eq. (5-44)
5   |  $\tilde{\mathbf{G}}_a = \sqrt{\alpha} \tilde{\mathbf{V}}$ 
6   |  $\hat{\mathbf{G}}_a = \sqrt{1 - \alpha} \mathbf{V}$ 
7 else
8   | for  $t = 2$  to  $\mathbf{I}_G$  do
9     |  $\alpha(t) = \alpha(t-1) + \gamma \frac{\partial \mathbb{E}[\varepsilon]}{\partial \alpha} \Big|_{\alpha=\alpha(t-1)}$ 
10  | end
11  |  $\alpha_d = \alpha(\mathbf{I}_G)$ 
12  | if  $\alpha_d < \frac{\beta_1}{\|\tilde{\mathbf{V}}\|^2}$  then
13  |   |  $\alpha_d = \frac{\beta_1}{\|\tilde{\mathbf{V}}\|^2}$ 
14  | else if  $\alpha_d > \frac{\beta_2}{\|\tilde{\mathbf{V}}\|^2}$  then
15  |   |  $\alpha_d = \frac{\beta_2}{\|\tilde{\mathbf{V}}\|^2}$ 
16  |   |  $\tilde{\mathbf{G}}_a = \sqrt{\alpha_d} \tilde{\mathbf{V}}$ 
17  |   |  $\hat{\mathbf{G}}_a = \sqrt{1 - \alpha_d} \mathbf{V}$ 
18  | end
19  | for  $i = 2$  to  $\mathbf{I}_D$  do
20  |   |  $\frac{\partial \mathbb{E}(\varepsilon)}{\partial \mathbf{d}} = 2\rho_f \left( \mathbf{W}^H \hat{\mathbf{G}}_a^* \hat{\mathbf{G}}_a^T \mathbf{W} \text{diag}(\mathbf{d}(i-1)) \right) \odot \mathbf{I}$ 
21  |   |  $\mathbf{d}(i) = \mathbf{d}(i-1) - \lambda \frac{\partial \mathbb{E}(\varepsilon)}{\partial \mathbf{d}} \Big|_{\mathbf{d}=\mathbf{d}(i-1)}$ 
22  | end
23  |  $\mathbf{d}_d = \mathbf{d}(\mathbf{I}_D)$ 
24  | if  $\text{Tr} \left( \mathbf{W} \text{diag}(\mathbf{d}_d, \mathbf{d}_d) \mathbf{W}^H \right) \neq \text{Tr} \left( \mathbf{P}_a \mathbf{P}_a^H \right)$  then
25  |   |  $\eta = \sqrt{\frac{\text{Tr}(\mathbf{P}_a \mathbf{P}_a^H)}{\text{Tr}(\mathbf{W} \text{diag}(\mathbf{d}_d, \mathbf{d}_d) \mathbf{W}^H)}}$ 
26  |   |  $\mathbf{d}_d = \eta \mathbf{d}_d$ 
27  | end

```

5.3**Analysis**

This section presents an analysis of convexity and introduces solutions for the REOP problems ((5-7) - (5-10)) in Algorithm 8. It then examines the convexity of the objective function of the robust power allocation problem in (5-16), and the convexity analysis of the error expectation with respect to the

channel estimation error $\tilde{\mathbf{G}}_a$. An analysis of complexity of the proposed and existing approaches are provided.

5.3.1

Analysis and Proposed Solutions to REOP Problems

5.3.1.1

Convexity analysis of the objective function J with respect to the channel estimation error

For user k , the channel from AP m is denoted as g_{mk} as specified in (5-1). Consequently, the channel vector for user k is defined as follows:

$$\mathbf{g}_k = [g_{1k}, \dots, g_{Mk}]^T, \quad (5-47)$$

where \mathbf{g}_k contains the channel coefficients from all M APs to user k . Using (5-1), we rewrite \mathbf{g}_k as follows:

$$\mathbf{g}_k = \hat{\mathbf{g}}_k + \tilde{\mathbf{g}}_k, \quad (5-48)$$

where $\hat{\mathbf{g}}_k$ is the channel estimation vector and $\tilde{\mathbf{g}}_k$ is the channel estimation error vector for UE k .

Next, we rewrite the objective function J :

$$\begin{aligned} J = \mathbf{g}_k^H \mathbf{g}_k &= \hat{\mathbf{g}}_k^H \hat{\mathbf{g}}_k + \hat{\mathbf{g}}_k^H \tilde{\mathbf{g}}_k + \tilde{\mathbf{g}}_k^H \hat{\mathbf{g}}_k + \tilde{\mathbf{g}}_k^H \tilde{\mathbf{g}}_k = \\ &= \hat{\mathbf{g}}_k^H \hat{\mathbf{g}}_k + 2 \operatorname{Re} \left(\hat{\mathbf{g}}_k^H \tilde{\mathbf{g}}_k \right) + \tilde{\mathbf{g}}_k^H \tilde{\mathbf{g}}_k. \end{aligned} \quad (5-49)$$

Given that J is scalar, it can be equated to its trace. Consequently, to compute the first derivative of J with respect to $\tilde{\mathbf{g}}_k$, we employ the following equation [55]:

$$\frac{df(z)}{dz} = \frac{1}{2} \left(\frac{\partial f(z)}{\partial \operatorname{Re}(z)} - j \frac{\partial f(z)}{\partial \operatorname{Im}(z)} \right), \quad (5-50)$$

where z is a complex variable, $\operatorname{Re}(\cdot)$ and $\operatorname{Im}(\cdot)$ are the real and imaginary parts, respectively, and j is the imaginary unit. The vector differentiation rule is then adopted [56]:

$$\frac{\partial \mathbf{a}}{\partial \mathbf{b}} = \begin{bmatrix} \frac{\partial a_1}{\partial b_1} & \dots & \frac{\partial a_m}{\partial b_1} \\ \vdots & \ddots & \vdots \\ \frac{\partial a_1}{\partial b_n} & \dots & \frac{\partial a_m}{\partial b_n} \end{bmatrix}, \quad (5-51)$$

where \mathbf{a} is an m -element vector, and \mathbf{b} is an n -element vector. Consequently, we deduce that

$$\frac{\partial a}{\partial \mathbf{b}} = \begin{bmatrix} \frac{\partial a}{\partial b_1} \\ \vdots \\ \frac{\partial a}{\partial b_n} \end{bmatrix}, \quad (5-52)$$

where a is a scalar. As such, $\frac{\partial \hat{\mathbf{g}}_k^H \hat{\mathbf{g}}_k}{\partial \tilde{\mathbf{g}}_k} = 0$, and by applying (5-50) and (5-52), it can be demonstrated that

$$\frac{\partial \left(2 \operatorname{Re} \left(\hat{\mathbf{g}}_k^H \tilde{\mathbf{g}}_k \right) \right)}{\partial \tilde{\mathbf{g}}_k} = \hat{\mathbf{g}}_k^H. \quad (5-53)$$

Moreover, by invoking $\frac{\partial \mathbf{x}^H \mathbf{x}}{\partial \mathbf{x}} = \mathbf{x}^H$, as per [57], we obtain

$$\frac{\partial \left(\tilde{\mathbf{g}}_k^H \tilde{\mathbf{g}}_k \right)}{\partial \tilde{\mathbf{g}}_k} = \tilde{\mathbf{g}}_k^H. \quad (5-54)$$

Therefore, the first derivative of the objective function in relation to $\tilde{\mathbf{g}}_k$ is

$$\frac{\partial J}{\partial \tilde{\mathbf{g}}_k} = \hat{\mathbf{g}}_k^H + \tilde{\mathbf{g}}_k^H. \quad (5-55)$$

Upon computing the second derivative in respect to $\tilde{\mathbf{g}}_k$ and considering $\mathbf{0}$ as the zero matrix, we have

$$\frac{\partial^2 J}{\partial \tilde{\mathbf{g}}_k^2} = \mathbf{0}, \quad (5-56)$$

indicating that the objective function is affine with respect to $\tilde{\mathbf{g}}_k$. This assertion holds true even when the derivative is taken with respect to $\hat{\mathbf{g}}_k$. Furthermore, for calculation of the derivative of the objective with respect to the small scale fading error vector $\tilde{\mathbf{h}}_k = [\tilde{h}_{1k}, \dots, \tilde{h}_{Mk}]^T$, we write the objective function as follows:

$$J = \sum_{m=1}^M g_{mk} g_{mk}^* = \sum_{m=1}^M \beta_{mk} f_{mk}, \quad (5-57)$$

$$f_{mk} = \left[(1 - \alpha) h_{mk} h_{mk}^* + \alpha \tilde{h}_{mk} \tilde{h}_{mk}^* + \sqrt{\alpha(1 - \alpha)} (h_{mk} \tilde{h}_{mk}^* + h_{mk}^* \tilde{h}_{mk}) \right] \quad (5-58)$$

Using Equation (5-50), we obtain

$$\frac{\partial f_{mk}}{\partial \tilde{h}_{mk}} = \alpha \tilde{h}_{mk}^* + \sqrt{\alpha(1 - \alpha)} h_{mk}^* \quad (5-59)$$

Thus, the first derivative with respect to \tilde{h}_{mk} is given as follows:

$$\frac{\partial J}{\partial \tilde{\mathbf{h}}_k} = \begin{bmatrix} \beta_{1k} \left(\alpha \tilde{h}_{1k}^* + \sqrt{\alpha(1 - \alpha)} h_{1k}^* \right) \\ \vdots \\ \beta_{Mk} \left(\alpha \tilde{h}_{Mk}^* + \sqrt{\alpha(1 - \alpha)} h_{Mk}^* \right) \end{bmatrix} \quad (5-60)$$

Since $\frac{\partial^2 f_{mk}}{\partial \tilde{h}_{mk}^2} = 0$, the second derivative is obtained as

$$\frac{\partial^2 J}{\partial \tilde{\mathbf{h}}_k^2} = \mathbf{0}, \quad (5-61)$$

which shows that the objective function is also affine with respect to $\tilde{\mathbf{h}}_k$. Thus, in order to obtain robustness against imperfect CSI, the CSI imperfection level parameter should be optimized.

5.3.1.2

Convexity analysis of the objective function with respect to CSI imperfection parameter

Here, we once more examine the objective function in terms of α as follows:

$$J = \sum_{m=1}^M |g_{mk}|^2 = \sum_{m=1}^M \beta_{mk} f_{mk}(\alpha), \quad (5-62)$$

where

$$\begin{aligned} f_{mk}(\alpha) &= (1-\alpha)|h_{mk}|^2 + \alpha|\tilde{h}_{mk}|^2 + \\ &\quad \sqrt{\alpha(1-\alpha)}(h_{mk}\tilde{h}_{mk}^* + h_{mk}^*\tilde{h}_{mk}) = \\ &= (1-\alpha)|h_{mk}|^2 + \alpha|\tilde{h}_{mk}|^2 + \\ &\quad \sqrt{\alpha(1-\alpha)}2\text{Re}\{h_{mk}\tilde{h}_{mk}^*\}. \end{aligned} \quad (5-63)$$

Taking the first derivative with respect to α , we obtain

$$\begin{aligned} \frac{\partial f_{mk}(\alpha)}{\partial \alpha} &= -|h_{mk}|^2 + |\tilde{h}_{mk}|^2 + \\ &\quad \frac{1-2\alpha}{\sqrt{\alpha(1-\alpha)}}2\text{Re}\{h_{mk}\tilde{h}_{mk}^*\}. \end{aligned} \quad (5-64)$$

Thus, the second derivative with respect to α is obtained as

$$\frac{\partial^2 f_{mk}(\alpha)}{\partial \alpha^2} = \frac{-\text{Re}\{h_{mk}\tilde{h}_{mk}^*\}}{\alpha(1-\alpha)\sqrt{\alpha(1-\alpha)}}. \quad (5-65)$$

Accordingly, we obtain

$$\frac{\partial J}{\partial \alpha} = \sum_{m=1}^M \beta_{mk} q_{mk}(\alpha), \quad (5-66)$$

where $q_{mk}(\alpha)$ is given as

$$q_{mk}(\alpha) = -|h_{mk}|^2 + |\tilde{h}_{mk}|^2 + \frac{1-2\alpha}{\sqrt{\alpha(1-\alpha)}}2\text{Re}\{h_{mk}\tilde{h}_{mk}^*\}. \quad (5-67)$$

Following that, the second derivative of the objective function with respect to α is

$$\frac{\partial^2 J}{\partial \alpha^2} = -\sum_{m=1}^M \beta_{mk} \frac{\text{Re}\{h_{mk}\tilde{h}_{mk}^*\}}{\alpha(1-\alpha)\sqrt{\alpha(1-\alpha)}} = r(\alpha). \quad (5-68)$$

To discuss the convexity of the function J , we need to consider the sign of the second derivative of the function $f_{mk}(\alpha)$. Given that h_{mk} and \tilde{h}_{mk} are independent Gaussian random variables representing small-scale fading, their product $h_{mk}\tilde{h}_{mk}^*$ and consequently its real part, $\text{Re}\{h_{mk}\tilde{h}_{mk}^*\}$, are also random. This randomness affects the sign of the second derivative and, therefore, the convexity of J . The denominator $\alpha(1-\alpha)\sqrt{\alpha(1-\alpha)}$ is always positive for $\alpha \in (0, 1)$, as it represents a product and square root of positive terms within this interval. The sign of the numerator, $-\text{Re}\{h_{mk}\tilde{h}_{mk}^*\}$, depends on the real

part of the product of the random variables which could be positive or negative.

5.3.1.3

Problem Solution

- Case 1, $r(\alpha) > 0$:

In this case, the objective function J would be convex for all $\alpha \in (0, 1)$.

- Max-min problems: For solution of the max-min problems such as what we have in (5-7) and (5-10), where J is the objective function defined as (5-62), we utilize a gradient descent technique where the channel estimation error parameter α is updated as

$$\alpha(i) = \alpha(i-1) - \mu \left. \frac{\partial J}{\partial \alpha} \right|_{\alpha=\alpha(i-1)}, \quad (5-69)$$

where i is the iteration index, μ is the positive step size and $\frac{\partial J}{\partial \alpha}$ is obtained using (5-66). Next, we will project the result to the feasible region defined by $\beta \leq \|\tilde{\mathbf{g}}_k\|^2 \leq \beta_0$ such that if the constraint is not satisfied, α is updated. In order to update α , we first rewrite $\tilde{\mathbf{g}}_k$ in (5-48) as

$$\tilde{\mathbf{g}}_k = \sqrt{\alpha} \left[\sqrt{\beta_{1k}} \tilde{h}_{1k}, \dots, \sqrt{\beta_{Mk}} \tilde{h}_{Mk} \right]^T = \sqrt{\alpha} \mathbf{\Gamma}_k. \quad (5-70)$$

Then, α is updated as

$$\alpha(i) = \begin{cases} \frac{\beta}{\|\mathbf{\Gamma}_k\|^2}, & \text{if } \alpha < \frac{\beta}{\|\mathbf{\Gamma}_k\|^2} \\ \frac{\beta_0}{\|\mathbf{\Gamma}_k\|^2}, & \text{if } \alpha > \frac{\beta_0}{\|\mathbf{\Gamma}_k\|^2} \end{cases} \quad (5-71)$$

After finding the given α and calculation of the objective function for every UE, the UE for which the objective function is maximized is selected as the solution to (5-7) or (5-10).

- Min-max problems: In order to solve the min-max problems such as what we have in (5-9), using the objective function given in (5-62) is convex, similar to the explanations in Section 5.2.2.2, we evaluate the objective function at the constraint boundaries $\|\tilde{\mathbf{g}}_k\|^2 = \beta$ and $\|\tilde{\mathbf{g}}_k\|^2 = \beta_0$. Thus, α is obtained by

$$\alpha = \begin{cases} \frac{\beta}{\|\mathbf{\Gamma}_k\|^2}, & \text{if } J \Big|_{\alpha=\frac{\beta}{\|\mathbf{\Gamma}_k\|^2}} > J \Big|_{\alpha=\frac{\beta_0}{\|\mathbf{\Gamma}_k\|^2}} \\ \frac{\beta_0}{\|\mathbf{\Gamma}_k\|^2}, & \text{if } J \Big|_{\alpha=\frac{\beta_0}{\|\mathbf{\Gamma}_k\|^2}} > J \Big|_{\alpha=\frac{\beta}{\|\mathbf{\Gamma}_k\|^2}} \end{cases} \quad (5-72)$$

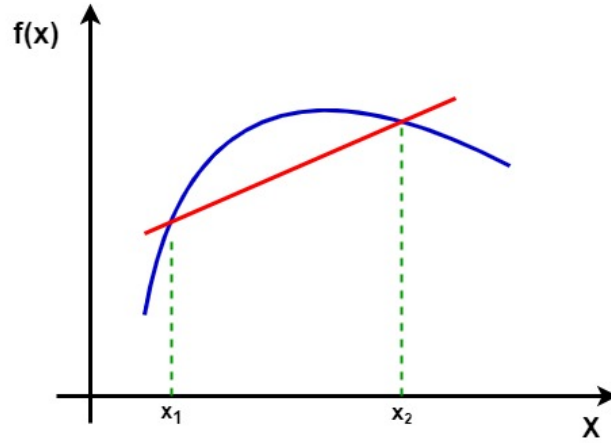


Figure 5.3: Boundary extremum illustration, concave case.

After finding α for UEs in the set $\mathcal{S}_n(j)$, we select the UE which minimizes the objective function as the solution to (5-9).

- Case 2, $r(\alpha) < 0$:

In this case, the objective J is concave for all $\alpha \in (0, 1)$.

- Max-min problems: To solve the minimization in the problems such as (5-7) and (5-10), since the objective is concave, the global minimum will occur at the boundary of the feasible region as shown in Fig. 5.3, where the concave function $f(x)$ is examined within the interval $x_1 \leq x \leq x_2$, and its minimum value occurs precisely at the endpoint x_1 . Thus, desired α is obtained as

$$\alpha = \begin{cases} \frac{\beta}{\|\mathbf{\Gamma}_k\|^2}, & \text{if } J \Big|_{\alpha=\frac{\beta}{\|\mathbf{\Gamma}_k\|^2}} < J \Big|_{\alpha=\frac{\beta_0}{\|\mathbf{\Gamma}_k\|^2}} \\ \frac{\beta_0}{\|\mathbf{\Gamma}_k\|^2}, & \text{if } J \Big|_{\alpha=\frac{\beta_0}{\|\mathbf{\Gamma}_k\|^2}} < J \Big|_{\alpha=\frac{\beta}{\|\mathbf{\Gamma}_k\|^2}} \end{cases} \quad (5-73)$$

Given α for every UE, the one with highest objective is the desired UE.

- Min-max problems: To solve the maximization in the problems such as (5-9), we use a gradient ascent technique in which the channel estimation error parameter is updated using the following equation,

$$\alpha(j) = \alpha(j-1) + \eta \frac{\partial J}{\partial \alpha} \Big|_{\alpha=\alpha(j-1)}, \quad (5-74)$$

where j is the iteration index, η is the positive step size and $\frac{\partial J}{\partial \alpha}$ is obtained using (5-66). Subsequently, if the obtained parameter does

not satisfy the constraint $\beta \leq \|\tilde{\mathbf{g}}_k\|^2 \leq \beta_0$, we will project the result to the feasible region using the same method as in (5-71).

After obtaining α for every UE in the given set of UEs, the UE with the smallest objective J is selected as the solution to min-max problems.

5.3.2

Convexity Analysis of the Conditioned Error Expectation

For convexity analysis of the objective function with respect to the power allocation factors, in (5-19), the first derivative is obtained as (5-20) as described in Section 5.2.2.1. To take the second derivative with respect to \mathbf{d} , the only focus is on the term $2\rho_f \left(\mathbf{W}^H \hat{\mathbf{G}}_a^* \hat{\mathbf{G}}_a^T \mathbf{W} \text{diag}(\mathbf{d}) \right) \odot \mathbf{I}$ which includes the power allocation matrix. Since $\mathbf{W}^H \hat{\mathbf{G}}_a^* \hat{\mathbf{G}}_a^T \mathbf{W}$ is positive semi-definite and elements of \mathbf{d} are positive, we can consider the $\mathbf{W}^H \hat{\mathbf{G}}_a^* \hat{\mathbf{G}}_a^T \mathbf{W} \text{diag}(\mathbf{d})$ as positive semi-definite. Equation (5-20) keeps the main diagonal of a positive semi-definite matrix which are non-negative. In matrix derivative rules, the derivative of a matrix with respect to a matrix as $\frac{d\mathbf{A}}{d\mathbf{B}}$, we should calculate derivative of \mathbf{A} with respect to every element of \mathbf{B} each one results in a matrix. Thus, if we take the second derivative of the objective function with respect to \mathbf{D} , it will result in a set of n matrices. Using (5-50) shows that each matrix will be a matrix with one non-negative element on the main diagonal and other element are zero which is also positive semi-definite. Thus, we conclude that the objective $\mathbb{E}[\varepsilon | \hat{\mathbf{G}}_a]$ is convex with respect to the power allocation matrix.

5.3.3

Analysis of the error with respect to $\tilde{\mathbf{G}}_a$

Since $\mathbb{E}[\varepsilon]$ as given in (5-23) incorporates the expectation $\mathbb{E}_{\tilde{\mathbf{G}}_a}$ over the channel estimation errors, the objective function no longer explicitly depends on the instantaneous realization of $\tilde{\mathbf{G}}_a$. As a result, any derivatives of the expected objective $\mathbb{E}[\varepsilon]$ with respect to $\tilde{\mathbf{G}}_a$ become zero, i.e., $\frac{\partial \mathbb{E}[\varepsilon]}{\partial \tilde{\mathbf{G}}_a} = 0$, and thus there is no direct way to optimize $\mathbb{E}[\varepsilon]$ with respect to $\tilde{\mathbf{G}}_a$. Therefore, to address imperfect CSI, we introduce and optimize the parameter α , treating it as a deterministic design variable that can be tuned to improve performance under channel uncertainty.

5.3.4

Computational complexity

For complexity comparison of the C-ESG and RC-ESG, we note that for calculation of the $\mathbf{g}_k^H \mathbf{g}_k$ of all UEs, the required complexity is of order $\mathcal{O}(KNL)$. For sum-rate calculation, considering the matrix inversion based on Equation (4-4), we consider the complexity of order $\mathcal{O}((NL)^3)$, and considering scheduled UEs, we need $\mathcal{O}(n(NL)^3)$ calculations. Thus, for C-ESG, the complexity is of order $\mathcal{O}(n(NL)^3) + \mathcal{O}(KNL)$. For RC-ESG, considering I_R iterations in solution of the REOP optimization problems and the same complexity for sum-rate expressions, the complexity is of the order $\mathcal{O}((NL)^3) + \mathcal{O}(I_R KNL)$. Depending on the number of iterations I_R , the complexity of the RC-ESG, is larger than C-ESG due to the inclusion of channel estimation errors and worst-case scenario optimization. For GDPA and RGDPA algorithms, the complexities are of orders $\mathcal{O}(4(NL)^2 n I_D)$ and $\mathcal{O}(3(NL)^2 n I_D)$, respectively. The additional complexity in the RGDPA algorithm arises from computing the extra term specified in (5-20), as compared to (5-24). About WRGDPA, calculation of (5-43) imposes the complexity of order $\mathcal{O}(24(NL)^2 n)$. Next, we need $\mathcal{O}(9(NL)^2 n I_G)$ calculations to obtain the desired α using (5-39), and $\mathcal{O}(3(NL)^2 n I_D)$ calculations to obtain desired power allocation factors. Thus, WRGDPA is with the complexity of order $\mathcal{O}(24(NL)^2 n) + \mathcal{O}(9(NL)^2 n I_G) + \mathcal{O}(3(NL)^2 n I_D)$.

5.4

Simulation Results

In this section, we consider a user centric cell-free network including $L = 16$ APs each equipped with $N = 4$ antennas, $K = 32$ UEs, and we use the C-ESG multiuser scheduling technique to select $n = 16$ UEs. The network area, path loss and shadowing parameters are based on the network used in Section 4.4. We consider the systems with perfect CSI and imperfect CSI with a levels of CSI uncertainty. In all cases of the robust resource allocation, we set the channel estimation error power bounds (including β , β_0 , β_1 and β_2) such that a range of $0.05 \leq \alpha \leq 0.3$ is resulted for imperfect channel factor. It is important to highlight that this interval is determined to ensure the channel remains within a balanced range - neither deviating significantly towards an unreliable state nor approaching too closely to an ideal, perfect channel. In all simulation results, the sum-rate is averaged over multiple independent channel realizations to mitigate the randomness and ensure reliable performance evaluation.

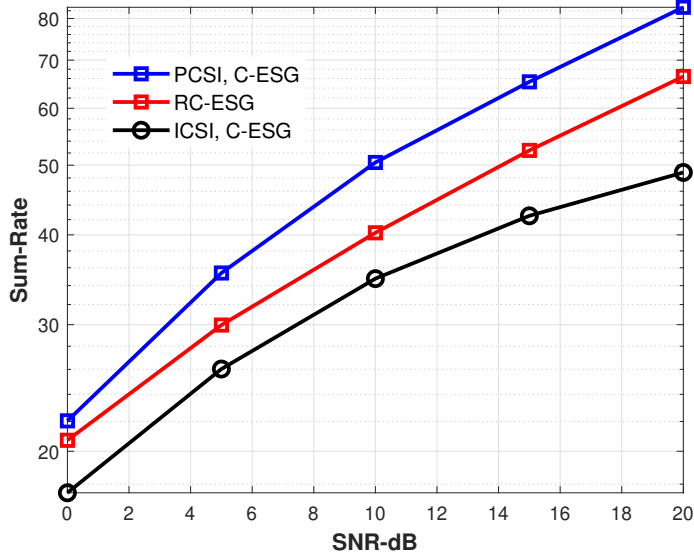


Figure 5.4: Comparison of the C-ESG multiuser scheduling in perfect CSI and imperfect CSI UCCF networks and the RC-ESG for MMSE precoder and EPL power loading, when $\alpha = 0.15$ for imperfect CSI case, $L = 16$, $N = 4$, $K = 32$ and $n = 16$.

Subsequently, the robust multiuser scheduling approach we propose is implemented. To compare the performance of C-ESG under perfect CSI (PCSI) and imperfect CSI (ICSI), as well as RC-ESG with EPL, we set $\alpha = 0.15$ for the ICSI network, and the results are as shown in Fig. 5.4. It is evident that RC-ESG surpasses C-ESG in the context of ICSI, approaching the performance seen in networks with PCSI. Quantitatively, the RC-ESG improves the sum-rate by approximately 10%-20% across different SNR levels, highlighting its robustness in handling imperfect CSI.

In Fig. 5.5, we have compared the proposed GDPA and RGDPA power allocation algorithms where we used the C-ESG user scheduling algorithm. It is evident that RGDPA provides better performance, with a sum-rate increase of 15%-25% compared to GDPA under ICSI, and approaches the performance of PCSI. The uncertainty level was set to $\alpha = 0.15$ for ICSI.

In solution of the worst-case robust power allocation Equation (5-25), for maximization of the objective function with respect to the CSI error, equal power loading has been considered. After simulation of the second derivative with respect to α , we found out that it is always negative ($\frac{\partial^2 \mathbb{E}[\epsilon]}{\partial \alpha^2} < 0$) for the given range. Accordingly, in Fig. 5.6, considering ZF precoder for the given network and after user scheduling using C-ESG, the proposed WRGDPA and RGDPA power allocation techniques are compared with the GDPA power allocation for both PCSI and ICSI cases when the imperfection CSI factor $\alpha = 0.15$ is considered in ICSI. As we can see, the proposed WRGDPA

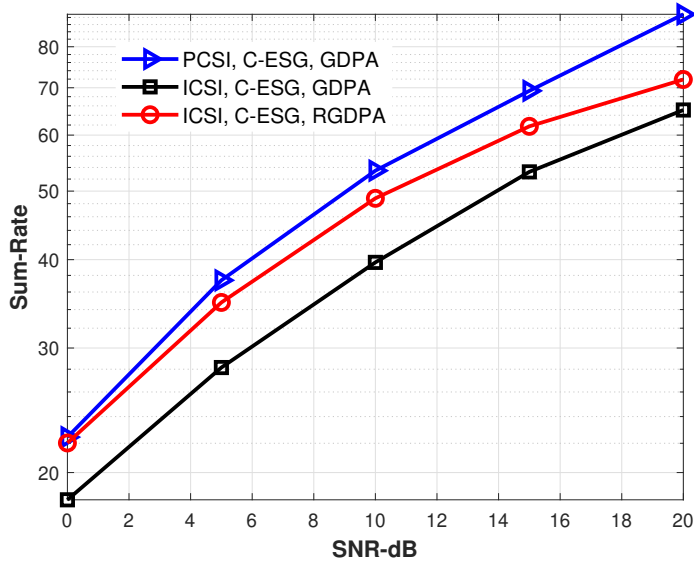


Figure 5.5: Comparison of the RGDPA power allocation, GDPA with ICSI and GDPA with PCSI, when $\alpha = 0.15$ for imperfect CSI case, $L = 16$, $N = 4$, $K = 32$, $n = 16$ and MMSE precoder.

and RGDPA has significantly outperformed the GDPA with ICSI and has approached the PCSI case. As comparison of the WRGDPA and RGDPA, RGDPA has shown a better performance for lower SNRs. However, as SNR increases, WRGDPA outperforms RGDPA.

In Fig. 5.7, we combined RC-ESG with RGDPA to assess the performance of the proposed robust resource allocation techniques. In this case, the imperfection level for the ICSI scenario has been reduced from $\alpha = 0.15$ to $\alpha = 0.1$. This adjustment demonstrates the effect of reduced CSI imperfection on the performance of the proposed resource allocation techniques. The results show that even with different levels of imperfection, the proposed techniques consistently yield a sum-rate improvement of up to 20% compared to existing approaches under ICSI, further validating the effectiveness of the proposed techniques.

5.5 Summary

In this chapter, we used the sum-rate expression for the downlink of a UCCF network under conditions of imperfect CSI and introduced a robust resource allocation framework designed to significantly enhance network performance. Our approach encompasses a robust user scheduling algorithm grounded in worst-case optimization techniques and two distinct power allocation strategies: One according to the worst-case robust optimization and another based on conditional MSE minimization. These approaches have been

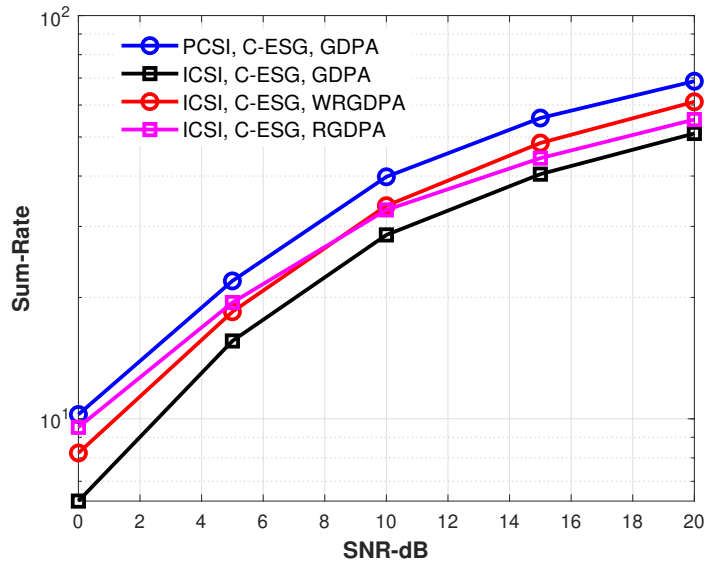


Figure 5.6: Comparison of WRGDPA and RGDPDA power allocation, GDPA with ICSI and GDPA with PCSI, when $\alpha = 0.15$ for imperfect CSI case, $L = 16$, $N = 4$, $K = 32$, $n = 16$ and ZF precoder.

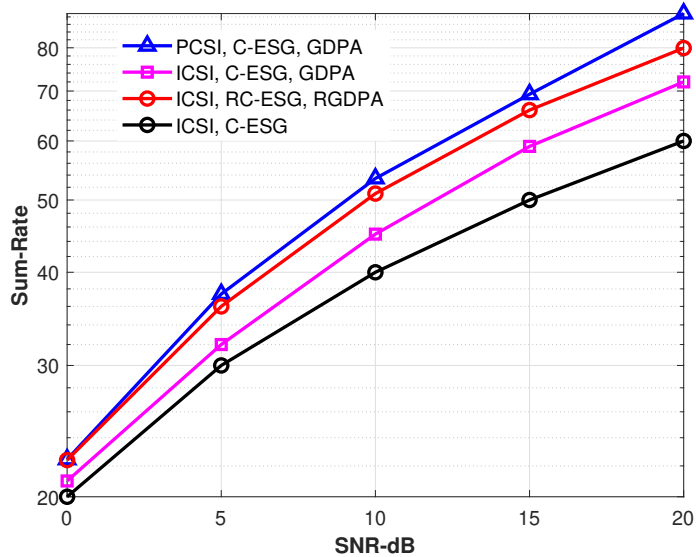


Figure 5.7: Performance of the proposed resource allocation technique, when $\alpha = 0.1$ for imperfect CSI case, $L = 16$, $N = 4$, $K = 32$, $n = 16$ and MMSE precoder.

analyzed analytically and their effectiveness is demonstrated through simulation results, which show a sum-rate improvement of up to 30% under various SNR levels and CSI conditions, approaching the performance of systems with perfect CSI. These findings confirm that our proposed framework effectively mitigates the adverse effects of imperfect CSI and leads to substantial enhancements in network performance.

6

Conclusions and Future Works

This thesis has investigated various aspects of resource allocation, including precoding, multiuser scheduling, and power allocation techniques within cellular, CF and CLCF massive MIMO networks. It has also examined UCCF networks, focusing on AP selection techniques and robust resource allocation strategies in such networks. Through both mathematical evaluations and simulation-based studies, the computational costs and signaling loads of the explored and proposed methodologies have been quantified. Moreover, the merits and limitations of these investigated approaches have been thoroughly scrutinized and documented. The main conclusions of this thesis can be summarized as follows:

- The deployment of the enhanced greedy algorithm, an extension of the search procedure for optimal UE set identification, has shown efficacy in both cell-free and multicell MIMO systems. This effectiveness is magnified when paired with linear MMSE and ZF precoders, thus leading to significant performance advancements.
 - ★ The sum-rate criterion employed by the proposed algorithm outstrips the performance of the channel-correlation criterion. However, this superior performance comes with a slight increase in computational complexity.
 - ★ The performance of the proposed method has been investigated under both perfect and imperfect CSI conditions.
- We investigated the C-ESG multiuser scheduling algorithm and assessed its effectiveness across different scenarios. When applied to both network-wide and clustered CF systems, the C-ESG algorithm exhibited substantial performance improvements over competing techniques.
 - ★ When the C-ESG algorithm is employed alongside network clustering, the computational cost and signaling load are greatly reduced. This demonstrates that network clustering can be a vital element in efficient system design.

- The development of an SMSPA resource allocation technique for downlink CLCF massive MIMO networks is another major accomplishment. This technique integrates the C-ESG multiuser scheduling algorithm and a power allocation algorithm based on the GD and GA methods.
 - ★ Simulation results confirm that MMSE precoders outdo ZF precoders in performance when used with the GD power allocation technique. Furthermore, the SMSPA technique significantly enhances sum-rates, even under imperfect CSI conditions.
- We developed and assessed the F-Gr resource allocation algorithm across CF and UCCF networks using BSR and LSF criteria for AP clustering.
 - ★ The F-Gr algorithm notably improves performance in UCCF networks compared to those using LSF.
 - ★ UCCF networks, particularly those utilizing BSR, prove to be scalable and efficient, making them suitable for high-density network environments.
- Another accomplishment is the introduction of a robust resource allocation framework designed to significantly enhance network performance for the downlink of UCCF networks under conditions of imperfect CSI, which are often encountered in wireless networks.
 - ★ A robust user scheduling algorithm grounded in worst-case optimization techniques and two distinct power allocation strategies, one adhering to worst-case robust optimization and the other centered on conditional MSE minimization were investigated.
 - ★ Through thorough analysis and simulation, we demonstrated the effectiveness of these methodologies in enhancing the robustness and efficiency of UCCF networks against CSI uncertainties.
 - ★ The results confirm that the proposed framework not only mitigates the adverse effects of imperfect CSI but also leads to substantial improvements in overall network performance.

Suggestions for future works include:

1. To assess the impact of different channel estimation error models on the proposed robust resource allocation framework to identify potential areas for refinement and enhancement.

2. To investigate the integration of robust precoding techniques specifically designed to handle imperfect CSI at the transmitter, which could further enhance system performance in practical scenarios.
3. To develop and evaluate machine learning-based approaches for resource allocation, encompassing precoding, user scheduling, and power allocation, to optimize system performance and reduce computational complexity.
4. To investigate the application of machine learning techniques for AP selection in UCCF networks to improve network efficiency and adaptability in dynamic environments.

Bibliography

- [1] NGO, H. Q.; ASHIKHMIN, A.; YANG, H.; LARSSON, E. G. ; MARZETTA, T. L., **Cell-free massive mimo versus small cells**, IEEE Transactions on Wireless Communications, vol. 16, no. 3, pp. 1834–1850, 2017.
- [2] BJÖRNSON, E.; SANGUINETTI, L., **Scalable cell-free massive mimo systems**, IEEE Transactions on Communications, vol. 68, no. 7, pp. 4247–4261, 2020.
- [3] CHENG, H. V.; BJÖRNSON, E. ; LARSSON, E. G., **Optimal pilot and payload power control in single-cell massive mimo systems**, IEEE Transactions on Signal Processing, vol. 65, no. 9, pp. 2363–2378, 2016.
- [4] NAYEBI, E.; ASHIKHMIN, A.; MARZETTA, T. L. ; RAO, B. D., **Performance of cell-free massive mimo systems with mmse and lsfd receivers**, In: 2016 50TH ASILOMAR CONFERENCE ON SIGNALS, SYSTEMS AND COMPUTERS, pp. 203–207. IEEE, 2016.
- [5] DENIS, J.; ASSAAD, M., **Improving cell-free massive mimo networks performance: A user scheduling approach**, IEEE Transactions on Wireless Communications, vol. 20, no. 11, pp. 7360–7374, 2021.
- [6] PALHARES, V. M.; FLORES, A. R. ; DE LAMARE, R. C., **Robust mmse precoding and power allocation for cell-free massive mimo systems**, IEEE Transactions on Vehicular Technology, vol. 70, no. 5, pp. 5115–5120, 2021.
- [7] GONG, X.; WU, G., **Dynamic user scheduling with user satisfaction rate in cell-free massive mimo**, In: 2022 IEEE/CIC INTERNATIONAL CONFERENCE ON COMMUNICATIONS IN CHINA (ICCC WORKSHOPS), pp. 100–105. IEEE, 2022.
- [8] RIERA-PALOU, F.; FEMENIAS, G., **Trade-offs in cell-free massive mimo networks: Precoding, power allocation and scheduling**, In: 2019 14TH INTERNATIONAL CONFERENCE ON ADVANCED TECHNOLOGIES, SYSTEMS AND SERVICES IN TELECOMMUNICATIONS (TELSIKS), pp. 158–165. IEEE, 2019.

- [9] AMMAR, H. A.; ADVE, R.; SHAHBAZPANAHI, S.; BOUDREAU, G. ; SRINIVAS, K. V., **Downlink resource allocation in multiuser cell-free mimo networks with user-centric clustering**, *IEEE Transactions on Wireless Communications*, vol. 21, no. 3, pp. 1482–1497, 2021.
- [10] HAMDY, R.; QARAQE, M., **Power allocation and cooperation in cell-free massive mimo systems with energy exchange capabilities**, In: 2020 IEEE 91ST VEHICULAR TECHNOLOGY CONFERENCE (VTC2020-SPRING), pp. 1–5. IEEE, 2020.
- [11] MING, Y.; SHA, Z.; DONG, Y. ; WANG, Z., **Downlink resource allocation with pilot length optimization for user-centric cell-free mimo networks**, *IEEE Communications Letters*, vol. 26, no. 11, pp. 2705–2709, 2022.
- [12] DIMIC, G.; SIDIROPOULOS, N. D., **On downlink beamforming with greedy user selection: performance analysis and a simple new algorithm**, *IEEE Transactions on Signal Processing*, vol. 53, no. 10, pp. 3857–3868, 2005.
- [13] CHEN, W.; HSIEH, P. ; CHEN, B., **Multi-objective power minimization design for energy efficiency in multicell multiuser mimo beamforming system**, *IEEE Transactions on Green Communications and Networkings*, vol. 4, no. 1, pp. 31–45, 2020.
- [14] NGUYEN, X.; KHA, H. H., **Energy efficient full-duplex multicell multi-user mimo networks**, *International Conference on Advanced Technologies for Communications (ATC)*, pp. 163–167, 2018.
- [15] WONG, K. K.; LIU, G.; CUN, W.; ZHANG, W.; ZHAO, M. ; ZHENG, Z., **Truly distributed multicell multi-band multiuser mimo by synergizing game theory and deep learning**, *IEEE Access*, vol. 9, pp. 30347–30358, 2021.
- [16] HAJRI, S. E.; ASSAAD, M. ; CAIRE, G., **Scheduling in massive mimo: User clustering and pilot assignment**, *54th Annual Allerton Conference on Communication, Control, and Computing*, pp. 107–114, 2016.
- [17] MARZETTA, T. L., **Noncooperative cellular wireless with unlimited numbers of base station antennas**, *IEEE Transactions on Wireless Communications*, vol. 9, no. 11, pp. 590–600, 2010.
- [18] NGO, H. Q.; ASHIKHMINEV, A.; YANG, H.; LARSSON, E. G. ; MARZETTA, T. L., **Cell-free massive mimo: Uniformly great service for**

- everyone, pp. 201–205. presented at the IEEE 16th international workshop on SPAWC, Stockholm, Sweden, 2015.
- [19] NAYEBI, E.; ASHIKHMIN, A.; MARZETTA, T. L.; YANG, H. ; RAO, B. D., **Precoding and power optimization in cell-free massive MIMO systems**, IEEE Transactions on Wireless Communications, vol. 16, no. 7, pp. 4445–4459, 2017.
- [20] TANG, A.; SUN, J. ; GONG, K., **Mobile propagation loss with a low base station antenna for nlos street microcells in urban area**, In: IEEE VTS 53RD VEHICULAR TECHNOLOGY CONFERENCE, SPRING 2001. PROCEEDINGS (CAT. NO. 01CH37202), vol. 1, pp. 333–336. IEEE, 2001.
- [21] SHEN, Z.; CHEN, R.; ANDREWS, J. G.; HEATH, R. W. ; EVANS, B. L., **Low complexity user selection algorithms for multiuser mimo systems with block diagonalization**, IEEE Transactions on Signal Processing, vol. 54, no. 9, pp. 3658–3663, 2006.
- [22] ZHANG, X.; LEE, J., **Low complexity mimo scheduling with channel decomposition using capacity upperbound**, IEEE Transactions on Communications, vol. 56, no. 6, pp. 871–876, 2008.
- [23] SIGDEL, S.; KRZYMIEN, W. A., **Simplified fair scheduling and antenna selection algorithms for multiuser mimo orthogonal space-division multiplexing downlink**, IEEE Transactions on Vehicular Technology, vol. 58, no. 3, pp. 1329–1344, 2009.
- [24] FLORES, A. R.; DE LAMARE, R. C. ; CLERCKX, B., **Linear precoding and stream combining for rate splitting in multiuser mimo systems**, IEEE Communications Letters, vol. 24, no. 4, pp. 890–894, 2020.
- [25] MASHDOUR, S.; DE LAMARE, R. C. ; LIMA, J. P., **Multiuser scheduling with enhanced greedy techniques for multicell and cell-free massive mimo systems**, In: 2022 IEEE 95TH VEHICULAR TECHNOLOGY CONFERENCE:(VTC2022-SPRING), pp. 1–5. IEEE, 2022.
- [26] ZHANG, J.; CHEN, R.; ANDREWS, J. G.; GHOSH, A. ; HEATH, R. W., **Networked mimo with clustered linear precoding**, IEEE transactions on wireless communications, vol. 8, no. 4, pp. 1910–1921, 2009.
- [27] HUANG, H.; TRIVELLATO, M.; HOTTINEN, A.; SHAFI, M.; SMITH, P. J. ; VALENZUELA, R., **Increasing downlink cellular throughput with**

- limited network mimo coordination**, IEEE Transactions on Wireless Communications, vol. 8, no. 6, pp. 2983–2989, 2009.
- [28] FLORES, A. R.; DE LAMARE, R. C. ; MISHRA, K. V., **Clustered cell-free multi-user multiple-antenna systems with rate-splitting: Precoder design and power allocation**, IEEE Transactions on Communications, 2023.
- [29] MISHRA, A.; MAO, Y.; SANGUINETTI, L. ; CLERCKX, B., **Rate-splitting assisted massive machine-type communications in cell-free massive MIMO**, IEEE Communications Letters, vol. 26, no. 6, pp. 1358–1362, 2022.
- [30] VERDU, S.; OTHERS, *Multiuser detection*, Cambridge university press, 1998.
- [31] TSE, D.; VISWANATH, P., *Fundamentals of wireless communication*, Cambridge university press, 2005.
- [32] BOYD, S. P.; VANDENBERGHE, L., *Convex optimization*, Cambridge University Press, 2004.
- [33] WANG, T.; DE LAMARE, R. C. ; SCHMEINK, A., **Joint linear receiver design and power allocation using alternating optimization algorithms for wireless sensor networks**, IEEE transactions on vehicular technology, vol. 61, no. 9, pp. 4129–4141, 2012.
- [34] MASHDOUR, S.; DE LAMARE, R. C.; SCHMEINK, A. ; LIMA, J. P. S. H., **MMSE-based resource allocation for clustered cell-free massive MIMO networks**, pp. 149–154. presented at the IEEE 13th SCC, Braunschweig, Germany, February. 27- March. 3, 2023.
- [35] MASHDOUR, S.; DE LAMARE, R. C. ; LIMA, J. P. S. H., **Enhanced subset greedy multiuser scheduling in clustered cell-free massive mimo systems**, IEEE Commun. Lett., 2022, doi: 10.1109/LCOMM.2022.3230641.
- [36] AMMAR, H. A.; ADVE, R.; SHAHBAZPANAHI, S.; BOUDREAU, G. ; SRINIVAS, K. V., **User-centric cell-free massive mimo networks: A survey of opportunities, challenges and solutions**, IEEE Communications Surveys & Tutorials, vol. 24, no. 1, pp. 611–652, 2021.
- [37] GUEVARA, A. P.; CHEN, C. M.; CHIUMENTO, A. ; POLLIN, S., **Partial interference suppression in massive mimo systems: Taxonomy**

- and experimental analysis, *IEEE Access*, vol. 9, pp. 128925–128937, 2021.
- [38] TENTU, V.; SHARMA, E.; AMUDALA, D. N. ; BUDHIRAJA, R., **Uav-enabled hardware-impaired spatially correlated cell-free massive mimo systems: Analysis and energy efficiency optimization**, *IEEE Trans. Commun.*, vol. 70, no. 4, pp. 2722–2741, April 2022.
- [39] WEI, C.; XU, K.; XIA, X.; SU, Q.; SHEN, M.; XIE, W. ; LI, C., **User-centric access point selection in cell-free massive mimo systems: a game-theoretic approach**, *IEEE Commun. Lett.*, vol. 26, no. 9, pp. 2225–2229, Sept. 2022, doi: 10.1109/LCOMM.2022.3186350.
- [40] ZHOU, X.; XIA, H. ; WU, S., **A successful transmission probability based ap clustering scheme in user-centric cell-free networks**, *China Communications*, vol. 19, no. 12, pp. 118–128, 2022.
- [41] BANERJEE, B.; ELLIOTT, R. C.; KRZYRNIEŃ, W. A. ; FARMANBAR, H., **Access point clustering in cell-free massive mimo using multi-agent reinforcement learning**, In: 2022 IEEE 33RD ANNUAL INTERNATIONAL SYMPOSIUM ON PERSONAL, INDOOR AND MOBILE RADIO COMMUNICATIONS (PIMRC), pp. 1086–1092. IEEE, 2022.
- [42] VAN CHIEN, T.; BJÖRNSSON, E. ; LARSSON, E. G., **Joint power allocation and load balancing optimization for energy-efficient cell-free massive mimo networks**, *IEEE Transactions on Wireless Communications*, vol. 19, no. 10, pp. 6798–6812, 2020.
- [43] WU, S.; LIU, L.; ZHANG, W.; MENG, W.; YE, Q. ; MA, Y., **Revenue-maximizing resource allocation for multitenant cell-free massive mimo networks**, *IEEE Systems Journal*, vol. 16, no. 2, June 2022.
- [44] D'ANDREA, C.; LARSSON, E. G., **User association in scalable cell-free massive mimo systems**, In: 2020 54TH ASILOMAR CONFERENCE ON SIGNALS, SYSTEMS, AND COMPUTERS, pp. 826–830. IEEE, 2020.
- [45] DIMIC, G.; SIDIROPOULOS, N. D., **On downlink beamforming with greedy user selection: performance analysis and a simple new algorithm**, *IEEE Trans. Sig. Proc.*, vol. 53, no. 10, pp. 3857–3868, Oct. 2005.
- [46] DEMIR, T.; BJÖRNSSON, E. ; SANGUINETTI, L., **Foundations of user-centric cell-free massive MIMO**, *Foundations and Trends in Signal Processing*, vol. 14, no. 3-4, pp. 162–472, 2021.

- [47] BUZZI, S.; D'ANDREA, C., **Cell-free massive MIMO: User-centric approach**, *IEEE Wireless Communications Letters*, vol. 6, no. 6, pp. 706–709, 2017.
- [48] INTERDONATO, G.; BJÖRNSON, E.; NGO, H. Q.; FRENGER, P. ; LARSSON, E. G., **Ubiquitous cell-free massive MIMO communications**, *EURASIP Journal on Wireless Communications and Networking*, vol. 2019, no. 1, pp. 1–13, 2019.
- [49] FLORES, A. R.; DE LAMARE, R. C., **Robust and adaptive power allocation techniques for rate splitting based MU-MIMO systems**, *IEEE Transactions on Communications*, vol. 70, no. 7, pp. 4656–4670, 2022.
- [50] RONG, Y.; SHAHBAZPANAHI, S. ; GERSHMAN, A. B., **Robust linear receivers for space-time block coded multiaccess MIMO systems with imperfect channel state information**, *IEEE Transactions on Signal Processing*, vol. 53, no. 8, pp. 3081–3090, 2005.
- [51] BASHAR, M.; BURR, A.; HANEDA, K. ; CUMANAN, K., **Robust user scheduling with COST 2100 channel model for massive MIMO networks**, *IET Microwaves, Antennas Propagation*, vol. 12, no. 11, pp. 1786–1792, 2018.
- [52] VAEZY, H.; OMIDI, M. J. ; YANIKOMEROGLU, H., **Energy efficient precoder in multi-user MIMO systems with imperfect channel state information**, *IEEE Wireless Communications Letters*, vol. 8, no. 3, pp. 669–672, 2018.
- [53] WANG, J.; PALOMAR, D. P., **Worst-case robust MIMO transmission with imperfect channel knowledge**, *IEEE Transactions on Signal Processing*, vol. 57, no. 8, pp. 3086–3100, 2009.
- [54] CHANG, Z.; WANG, Z.; GUO, X.; HAN, Z. ; RISTANIEMI, T., **Energy-efficient resource allocation for wireless powered massive MIMO system with imperfect CSI**, *IEEE Transactions on Green Communications and Networking*, vol. 1, no. 2, pp. 121–130, 2017.
- [55] PETERSEN, K. B.; PEDERSEN, M. S., **The matrix cookbook**, Technical University of Denmark, vol. 7, no. 15, pp. 510, 2008.
- [56] BARNES, R. J., **Matrix differentiation**, *Springs Journal*, pp. 1–9, 2006.
- [57] HAYKIN, S. S., *Adaptive filter theory*, Pearson Education India, 2002.